

## Lincoln University Digital Thesis

### Copyright Statement

The digital copy of this thesis is protected by the Copyright Act 1994 (New Zealand).

This thesis may be consulted by you, provided you comply with the provisions of the Act and the following conditions of use:

- you will use the copy only for the purposes of research or private study
- you will recognise the author's right to be identified as the author of the thesis and due acknowledgement will be made to the author where appropriate
- you will obtain the author's permission before publishing any material from the thesis.

# Upscaling of point-scale groundwater recharge measurements using machine learning: A case study in New Zealand and Colombia

A thesis  
submitted in partial fulfilment  
of the requirements for the Degree of  
Master of Water Resource Management

At  
Lincoln University  
by  
Manuel Alejandro Rios Rivera

Dr. Markus Pahlow<sup>1</sup> (Primary supervisor)  
Dr. MS Srinivasan<sup>2</sup> (Co-supervisor)  
Prof. Jenny Webster-Brown<sup>3</sup> (Associate Supervisor)

<sup>1</sup>Department of Civil and Natural Resources Engineering, University of Canterbury

<sup>2</sup>Applied Hydrology, National Institute of Water & Atmospheric Research

<sup>3</sup>Faculty of Environment, Society and Design, Department of Environmental Management, Lincoln University

Lincoln University  
2019

Abstract of a thesis submitted in partial fulfilment of the  
Requirements for the degree of M.W.R.M.

Upscaling of point-scale groundwater recharge measurements using machine learning: A case study in  
New Zealand and Colombia

By  
Manuel Alejandro Ríos Rivera

Estimating groundwater (GW) recharge rates is essential for water resources decision-making, in particular for dynamic regional-scale allocation. Typically, recharge has been estimated either based on models that require observed historic climatic and soil data for calibration or through measurements at a lysimeter monitoring site. Lysimeters are known as the most direct method of measuring drainage, yet utilization for decision making in regional water management is limited as merely point-scale measures of recharge are provided. In the past, machine learning techniques such as artificial neural networks (ANNs) have been found robust for modelling nonlinear hydrologic processes in relation to groundwater management. For this study, an ANN was selected in order to evaluate whether decision making in groundwater allocation can be improved by upscaling lysimeter-measured recharge. Model uncertainty for the ANN scheme was estimated employing a “Dropout” Monte Carlo (MC) technique. The ANN was trained and assessed in terms of its predictive performance to match lysimeter-measured recharge. The ANN was trained on daily time scale, employing recharge data recorded at three lysimeter stations in the Canterbury plains of New Zealand i.e. Dorie, Dunsandel and Methven sites. The best model in terms of accuracy and parsimony, provided  $R^2$  values ranging from 0.65 up to 0.86 and a mean absolute error ranging from 0.41 to 0.99 when tested at the three lysimeter locations, with a model uncertainty of 6%. The model was implemented in a geographic information system (GIS) environment, in order to predict the spatial variability of land surface recharge, but also to calculate GW allocation for three of the groundwater allocation zones of the Canterbury Region (i.e. Rakaia-Selwyn, Ashburton and Chertsey). GW available for allocation was estimated to be approximately  $650 * 10^6$   $m^3$   $year^{-1}$  for the Rakaia-Selwyn allocation zone; whereas allocation limits of  $284.41 * 10^6$   $m^3$   $year^{-1}$  and  $332.45 * 10^6$   $m^3$   $year^{-1}$  were estimated for Ashburton and Chertsey respectively. The suitability of applying an ANN to estimate LSR in a comparably data scarce region in Colombia was also tested. The results support how the inclusion of lysimeter data into the analysis, improves our confidence regarding the estimation of groundwater recharge.

The methodology developed in this study couples a supervised machine learning technique i.e. ANNs with a visualisation tool in a GIS to predict land surface recharge employing rainfall, potential evapotranspiration and dominant soil texture data as inputs. The tool developed here can be utilised to provide support to water managers in order to identify sustainable dynamic regional groundwater allocation strategies.

Keywords: Water allocation, Groundwater recharge, Artificial Neural Networks, GIS, Upscaling, Supervised Machine Learning

## **Acknowledgements**

First, I would like to thank the NZ Ministry of Foreign Affairs and Trade for providing me with the opportunity to come and study in New Zealand. Second, I would like to thank my supervisors Dr Markus Pahlow and Dr MS Srinivasan. Thank you for always answering my questions, and for all the guidance and support provided over the last year. Thanks to NIWA for providing the data for this project, especially to MS and Dr Shailesh Singh.

Last but not least many thanks must be given to my parents, sisters and friends for providing me with unfailing support throughout the process of writing this thesis. Without your help and continuous encouragement I wouldn't have been able to do this. Thanks to Fernan, Ramiro, Rosie and all the Latin American community at Lincoln for being my family away from home.

Thank you very much, everyone!

## Contents

1.	INTRODUCTION .....	1
2.	LITERATURE REVIEW.....	3
2.1	Background information .....	3
2.2	Uncertainty in groundwater modelling .....	3
2.3	An overview of lysimeter studies .....	4
2.3.1	Application in groundwater recharge studies .....	5
2.3.2	Applications in evapotranspiration and soil water balance studies.....	5
2.3.3	Soil moisture content as a proxy to estimate groundwater recharge .....	6
2.4	Regionalisation case studies.....	7
2.4.1	Geostatistical Techniques .....	7
2.4.2	Regression Methods .....	8
2.4.3	Artificial Neural Networks (ANNs).....	8
2.5	Regionalising recharge estimations .....	10
3.	RESEARCH QUESTION and RESEARCH OBJECTIVES .....	11
3.1	Research Question .....	11
3.2	Research Objectives.....	11
4.	METHODOLOGY.....	12
4.1	Case Study I - Canterbury, New Zealand (Three GW allocation zones) .....	12
4.1.1	Sites Description .....	12
4.1.2	Data quality control .....	16
4.1.3	Time series analysis and Model (ANN) Development.....	16
4.1.4	Model Uncertainty .....	21
4.1.5	Upscaling (Spatial analysis) .....	22
4.1.6	Estimating Groundwater allocation.....	22
4.1.7	Flowchart Case Study I.....	23
4.2	Case Study II – Patia Valley, Cauca, Colombia.....	23
4.2.1	Site Description.....	24
4.2.2	Data Analysis.....	25
4.2.3	Model development.....	26
4.2.4	Model Uncertainty .....	27
5.	RESULTS .....	27
5.1	Canterbury, New Zealand (Case Study I).....	27

5.1.1	Data Quality Control.....	27
5.1.2	Time series analysis .....	30
5.1.3	Model development.....	35
5.1.3.1	Approach 1 .....	35
5.1.3.2	Approach 2: Step (i) .....	42
5.1.3.3	Approach 2: Step (ii) .....	45
5.1.4	Neural Network Uncertainty .....	46
5.1.5	Spatial analysis - Upscaling .....	49
5.1.6	Groundwater allocation limits calculated employing the NN model.....	53
5.2	Patia Valley, Cauca, Colombia (Case Study II) .....	55
5.2.1	Overview of available data .....	55
5.2.2	Model Development .....	58
5.2.1	Model Uncertainty .....	61
6.	DISCUSSION .....	62
6.1	Canterbury, New Zealand – Case study I.....	62
6.1.1	Data quality control .....	62
6.1.2	Time Series analysis.....	63
6.1.3	Model development.....	66
6.1.4	Neural Network Uncertainty .....	68
6.1.5	Upscaling and Groundwater allocation.....	69
6.2	Patia Valley, Cauca, Colombia – Case study II .....	71
6.2.1	Model development.....	71
6.2.2	Model Uncertainty .....	72
7.	CONCLUSIONS AND RECOMMENDATIONS.....	72
8.	APPENDIX .....	74
8.1	Appendix A.....	74
8.2	Appendix B.....	75
8.3	Appendix C.....	75
8.4	Appendix D.....	79
8.5	Appendix E.....	80
8.1	Appendix F .....	81
8.2	Appendix G.....	85

8.3	Appendix H.....	96
9.	REFERENCES .....	99

## List of Figures

Figure 1.	Areas of interest for regionalization of lysimeter-measured recharge and location of lysimeter sites.....	13
Figure 2.	Schematic layout of a lysimeter site (Source: Duncan et al., 2016) .....	14
Figure 3.	Soil dominant texture class for the three GW allocation zones. ....	15
Figure 4.	Architecture of a (4-5-1) feed-forward neural network. (i.e. 4 neurons on the input layer, 5 neurons in the hidden layer and one output).....	17
Figure 5.	Combined dataset for training a single NN. The timeseries were aggregated with the assistance of Pandas (McKinney, 2010). ....	20
Figure 6.	(Left) Standard neural network, (Right) The same NN after applying dropout. Source: (Srivastava et al., 2014) .....	20
Figure 7.	Screenshot of the tool for predicting LSR on a given area.....	22
Figure 8.	Flowchart of steps to work out the research objectives and to answer the research question .....	23
Figure 9.	Study area for case study II. Shown are the Patia Valley and the flow direction towards the Patia River.....	24
Figure 10.	Rainfall and ET stations in the area .....	26
Figure 11.	Example showing the gaps observed in the volumetric water content data at Dorie, “NaN” represents gaps.....	28
Figure 12.	NaN (i.e. missing) values detected in the recharge dataset at Methven. ....	28
Figure 13.	VWC outliers recorded by one of the soil moisture sensors at Dunsandel.....	29
Figure 14.	Dataset after the QC procedure at Dorie.....	31
Figure 15.	Dataset utilised in the analysis at Dunsandel .....	32
Figure 16.	Dataset utilised in the analysis at Methven .....	33
Figure 17.	The behaviour of mean daily recharge uncertainty, plotted on two axes: [1] In $\text{mm d}^{-1}$ (left axis, red); and [2] as a percentage of recharge (right axis, blue). ....	47
Figure 18.	Rainfall/irrigation plotted against daily recharge (left, red) and daily uncertainty (right, blue). ....	48
Figure 19.	Potential Evapotranspiration plotted against daily recharge (left, red) and daily uncertainty (right, blue). ....	48
Figure 20.	Soil particle dominant size plotted against daily recharge (Left axis, red) and daily uncertainty (right axis, blue). ....	49
Figure 21.	GIS tool for predicting land surface recharge in a larger area. ....	50
Figure 22.	Sample model output. The NN trained on point scale data now transferred into a GIS software calculates land surface recharge for the three GW allocation zones on a daily basis (here recharge was calculated for 11 July 2017 as an example). Data Source: NIWA, grid size: 280 m x 280 m pixels. ....	52
Figure 23.	Land surface recharge predicted with the NN model for three GW allocation zones.....	54
Figure 24.	Evapotranspiration patterns in a small region of Colombia, units are in $\text{mm year}^{-1}$ . ....	56
Figure 25.	Yearly rainfall patterns in the area of interest inside Colombia, units are in $\text{mm year}^{-1}$ . ....	57
Figure 26.	Mean flow measured upstream (La Fonda) and downstream (Loma Alta).....	58

Figure 27. Overview of a portion of the data employed for training and testing a NN in the Patia Valley. Runoff represents river flow in the python code. ....	58
Figure 28. The behaviour of mean monthly recharge uncertainty, plotted on two axes: [1] In mm month <sup>-1</sup> (left axis, red); and [2] as a percentage of recharge (right axis, blue). ....	62
Figure 29. Recharge behaviour - Dorie 2017 .....	63
Figure 30. Recharge behaviour - Methven 2017 .....	64
Figure 31. Recharge behaviour - Dunsandel 2017 .....	65
Figure 32. Groundwater allocation limits in three allocation zones in the Canterbury region. The blue bars show the limits registered in the regional plan, and the red bars show the limits calculated employing the NN model. The black error bars overlapping the NN predictions represent the uncertainty. ....	71

## List of Tables

Table 1. Overview of the lysimeter stations and their corresponding location within a GW allocation zone. 12	12
Table 2. Data available at each lysimeter location .....	14
Table 3. Overview of the gaps and outliers observed in the dataset. ....	29
Table 4. Descriptive statistics of the data measured at Dorie. ....	30
Table 5. Descriptive statistics of the data measured at Dunsandel. ....	31
Table 6. Descriptive statistics of the data measured at Methven .....	32
Table 7. Cumulated values of recharge, rainfall/irrigation and PET across the lysimeter locations for the entire study period. ....	34
Table 8. Results of developing a feed forward neural network employing data collected at Methven only. .	35
Table 9. Results of developing a feed forward neural network employing data collected at Dunsandel only .....	37
Table 10. Results of developing a feed forward neural network employing data collected at Dorie only .....	38
Table 11. Results of testing the NN on a seasonal basis .....	40
Table 12. Results of checking whether a NN developed with data from one location was able to predict recharge at a different location. ....	41
Table 13. Results of checking whether a NN developed with data from one location was able to predict recharge at a different location, after switching the training and testing datasets. ....	42
Table 14. Results of testing one NN on a monthly basis, the dataset employed for training included information from the three locations. ....	43
Table 15. Results of testing one NN on a daily basis, the dataset employed for training included information from the three locations. ....	44
Table 16. Results of testing different architectures of a NN with 3 inputs, and an increased training dataset on a daily basis. ....	46
Table 17. LSR predicted for each allocation zone (*Rakaia –Selwyn and Little Rakaia comprehend the same allocation zone).....	53
Table 18. Results of testing a NN on a monthly basis, employing a ratio of 60% of data for training and 40% for testing. ....	59
Table 19. Results of testing a NN on a monthly basis, employing a ratio of 70% of data for training and 30% for testing. ....	60
Table 20. NN trained with 70% of data, on a Keras environment (employing dropout) .....	61
Table 21. Seasonal recharge behaviour across locations in 2017. ....	66

## 1. INTRODUCTION

Climate change, population growth and the uncertainty associated with rainfall distribution are -to name a few- of the challenges faced by water managers, science and regional councils in terms of water allocation decisions (Carroll et al., 2015; Guerra, et al., 2016). Nowadays, one of the main measures to increase food production is irrigation, thus the necessity to actively manage water use and improve efficiency (Zhang et al., 2013). Generally, surface water resources are scarce and highly unreliable, which has led to an increased use of groundwater (Duncan et al., 2016). The aquifers are considered as the primary solution to droughts for both human requirements and crop production, since they provide a higher reliability in access to water that surface resources can hardly match (Siebert et al., 2010). The world's groundwater abstraction as per 2013 was estimated to be 1000 km<sup>3</sup> per year (IGRAC, 2017), and although the significance of groundwater withdrawals from the global freshwater supply is well recognised (Siebert et al., 2010), there is still a lot of uncertainty regarding groundwater recharge and distribution (Westerhoff et al., 2018).

Groundwater recharge is a process highly variable in space and time (Scanlon et al., 2005), as a function of rainfall, irrigation, soil type, geology and land use (Lovett & Payne, 2014). Recharge derives partially from rivers and from the land surface (i.e. land surface recharge). In places where the land is used for irrigated agriculture (e.g. dairy), recharge volumes can be potentially altered by irrigation (Duncan et al., 2016). However, there are not many studies evaluating recharge on irrigated land. This may be attributed to the high uncertainty on recharge estimations under irrigated conditions, which depend on the numerous water and land management decisions taking place at a farm scale (Crosbie et al., 2010). In New Zealand, Canterbury Plains alone account for 58% of total water allocated across the country which highlights the importance of efficient irrigation practices in this region (Weaver et al., 2016). It is therefore important to evaluate the effects of irrigation on recharge to enable informed water management and allocation (Duncan et al., 2016).

Land surface recharge (LSR) occurs when water (coming either from rainfall or irrigation) infiltrates through the soil column into an aquifer. LSR can be estimated employing numerical models, or through direct measurements at a lysimeter monitoring site (Lovett & Payne, 2014). Lysimeters are monitoring devices used in hydrogeology for the quantification of the dynamics of soil moisture change (Augenstein et al., 2015), and are recognised as the most direct method of observing recharge rates (Stoffregen et al., 2002). However, such facilities are expensive to install and manage, which is perhaps the main drawback for their implementation. According to Bastola et al. (2008), hydrological data have always been fundamental in policy making for sustainable water management, though the extent to which a point-scale measure can be “up-scaled” is a common point of discussion in environmental sciences.

The varying scales to which a catchment process can be represented is perhaps one of the main challenges in hydrogeology. As mentioned by Zirlwagen & Wilpert (2004), observations on a point scale level are often not sufficient as a basis for management activities at the regional scale. Similarly, Sophocleous (1992) mentioned that direct measurement of hydrologic variables (e.g. recharge) only provide point estimates, and consequently, the problem of areal representation of point-scale measures exists. It is therefore essential to

find ways by which an environmental process can be represented at the landscape level to evaluate the effect of management activities (Zirlewagen & Von Wilpert, 2010).

Upscaling techniques (i.e. regionalisation) mentioned by Healy (2010), have become popular in recent years as an intent to predict the general behaviour of hydrological processes based on point estimations at a few locations within a catchment. Delin et al. (2007) define regionalisation as the process by which a local-scale estimation can be extrapolated to a regional scale. It may concern different variables, from characteristic discharges and meteorological descriptors, to the parameters of a given model. When regionalising a specific process such as recharge, it is required to develop a model at a larger scale capable of explaining its behaviour (Hingray et al., 2014).

According to Heuvelmans et al. (2006), regionalisation could be performed in either a discontinuous or continuous way. The latter consists of building a numerical model that estimates approximate parameter values given a set of catchment descriptors. This can be done in different ways, one example is regression models, which are used to establish a linear relationship between the output and output predictors (Refsgaard et al., 2016). A different approach is artificial neural networks (ANNs), which consists of a network of input units, a set of output units and a set of hidden units, which mathematically transform the inputs and link them to the output (Heuvelmans et al., 2006). For regionalising LSR, the mentioned methods require recharge data (either measured or estimated), in order to model the “empirical” relationship between output and catchment descriptors (e.g. climate data). Therefore, the combination of regionalisation techniques and lysimeter-measured data may open new possibilities for modelling in hydrogeology, and assist decision-making for water allocation.

Groundwater recharge volumes are considered as a key input to set allocation limits, particularly in places where policy is managed at a regional scale. This parameter is typically evaluated employing numerical models based on climatic and hydrologic data, however, due to the complexity of directly measuring recharge volumes, not much is known about the uncertainty of model outputs (Westerhoff et al., 2018). According to Muthusamy et al. (2017), when modelling any hydrologic parameter, robust interpretation of results is directly associated with uncertainty quantification, though there is not a “universal framework” for uncertainty assessment (Zeng et al., 2016). It is therefore essential to: (1) Improve uncertainty assessment which would highly benefit groundwater recharge models, and, (2) collect hydrogeological data (e.g. lysimeter-measured recharge) to provide stochastic models with additional information in order to reduce prediction uncertainty (Leube et al., 2012). In general, the estimation of effective soil hydraulic properties at a regional scale is challenging (Zhu & Mohanty.,2002), however, groundwater management is improved as our understanding of the drivers, scales and spatial distribution of recharge develops (Wohling et al., 2012).

The problem that this work aims to address is: Given that a few point-scale recharge measurements covering a large area and a short time frame are available in the Canterbury Plains, how can we make the best use of these data to establish regionalised recharge patterns in order to assist water allocation decisions? And, assuming the availability of data, would be possible to estimate regional recharge employing an artificial neural network in a region of south-west Colombia to assist groundwater allocation decisions?

## **2. LITERATURE REVIEW**

### **2.1 Background information**

Groundwater recharge rates are considered essential to set allocation limits in water management. According to White et al. (2003), the estimation of recharge has been generally done employing uncalibrated models. Although numerical models are essentially the “standard tools” for planning and decision making at a regional scale, there is still improvement required for actually representing the general behaviour of recharge (Sophocleous, 2012). Previously, lysimeter-measured estimations have been used to calibrate models predicting recharge in Canterbury (Duncan et al., 2016; White et al., 2003), and though previous studies have shown approaches to regionalise point-scale recharge measures (These studies are reviewed in 2.5), it is a field that is still under research.

Regionalisation is complex, and its effectiveness for upscaling local-scale recharge measurements is still uncertain. This review will provide an overview of the application of lysimeter data in different studies. Also, a review of different papers employing the upscaling techniques mentioned by Healy (2010) is presented. The methodologies included here are: (a) Geostatistical techniques, which have been used for the interpolation of climatic variables (e.g. kriging for interpolating rainfall data); (b) Regression models; which consist in constructing a linear relationship between the variable to be explained and different variables capable of explaining a maximum amount of the variance; and (c) Artificial neural networks, which according to Sun et al (2016), are capable of simulating the nonlinear dynamics of hydrological processes.

### **2.2 Uncertainty in groundwater modelling**

Modelling is a process subject to uncertainty from various sources, associated to the conceptual framework, the model parameters, model calibration and the predictive uncertainties (Brewer et al., 2003). Hill & Tiedeman (2007) suggest inferential statistics and random sampling (Monte Carlo) methods for quantifying prediction uncertainty. For both methods the mechanism for communicating uncertainty is often some type of interval around the prediction. Bastola et al. (2008) recognised that for regionalisation schemes, and for achieving reliable results, uncertainty assessment is essential. Different studies predicting modelling uncertainties will be mentioned later on.

Models are useful tools for the assessment of environmental impacts of a certain agricultural practice, or to simulate the outcome of a given change (Groenendijk et al., 2014). They provide a basis to increase the understanding of pedological and hydrological factors that have an effect on hydrogeological processes. According to Delin et al. (2007), recharge is the variable that modellers usually know the least about- due to the complexity of direct recharge observations- but to which the models are most sensitive to. Lubczynski & Gurwin (2005) recognized modelling as the best tool to support groundwater management and highlight the rapid development of numerical coding to increase the ability of models to predict values efficiently. Molz (2017) support this trend by mentioning the change that the introduction of MODFLOW in 1984 generated in

hydrogeology. Although it has been used widely, problems with boundary conditions, discretisation and convergence arise when dealing with complex aquifer conditions (Zaidel et al., 2010). The mentioned problems affect the ability of a given model to predict reliable values, therefore, calibration procedures are necessary (Josset et al., 2015). Bastola et al. (2008) concluded that the parameters of hydrological models exhibit uncertainty, and is therefore essential to consider uncertainty assessment as an integral part of regionalisation schemes. In the same way, Kasiviswanathan & Sudheer (2017) mentioned that the lack of uncertainty quantification in hydrologic models, may produce misleading results, which limits the practical application of modelled outputs in water management decision-making processes.

As stated by Josset et al. (2015), the major challenge in modelled hydrogeology is to deal with the uncertainty of complex aquifer properties. Poeter & Anderson (2005) support this by mentioning the relevance of considering different approaches to predict reliable estimations with “reasonable definition” of uncertainty. However, the absence of “real” measurements, makes it impossible to address hydrogeological issues on a deterministic basis. Dagan (2002) explained how uncertainty on aquifer properties are usually propagated by employing a stochastic framework and Monte Carlo simulations, which are discussed later on within this review. Hill & Tiedeman (2007), mentioned how uncertainty assessment employing the methods mentioned by Dagan (2002) may improve the reliability of modelled recharge estimations, however, in countries such as New Zealand, groundwater recharge models hardly ever report uncertainty values (Westerhoff et al., 2018). Kasiviswanathan & Sudheer (2017) showed a review of the methodologies employed to quantify uncertainty of ANN-based hydrologic models in different studies published between 2002 and 2015. The most common ways of quantifying uncertainty include bootstrap, fuzzy, Bayesian and Monte Carlo simulation techniques. Fuzzy and Bayesian methods have been evaluated on a very limited number of studies and there is still development required for further application, also, Bayesian approaches require huge sampling and a high computational effort which limit their use. The authors reviewed different studies employing bootstrap sampling and Monte Carlo simulations successfully, and mentioned the high robustness of uncertainty estimations. These techniques, are based on simulating the distribution of the model output, however, none of them compare the model output to local-scale observed data. For this reason, lysimeter-measured recharge may provide a “direct” basis to assess whether the predictions of a given recharge model - considering uncertainty- are reliable or not.

### **2.3 An overview of lysimeter studies**

According to Meissner et al. (2000), lysimeters have become an accepted tool for studying water and solute movement in soil. There is an evident increase of lysimeter-based investigations to assess water balance components and hydrogeologic parameters all over the world, and though evaluating all the areas that could develop lysimeter-based research are out of the scope of this review, an overview of their application in hydrology and hydrogeology is presented.

### **2.3.1 Application in groundwater recharge studies**

White et al. (2003) evaluated three rainfall recharge models (a soil water balance model, the SOILMOD model and a neural-network) and compared them in relation to their ability to estimate rainfall recharge measured by 4 dryland lysimeters in the Canterbury plains. The root-mean-square-error (RMSE) of the neural network predictions were lower compared to the other two models at all of the four sites. Also, the maximum and minimum weekly differences between the neural network and lysimeter-observed recharge were the lowest of the three models at all the sites as well. Therefore, it was observed that the trained neural network predicted more accurate results than the other two models when compared to the recharge values observed by the lysimeters. Similarly, Duncan et al. (2016) characterised recharge seasonal patterns on irrigated dairy farms employing three sets of drainage lysimeters in Canterbury, New Zealand. The authors highlight the importance of recharge evaluations under irrigation conditions, and similarly to Crosbie et al. (2010), they mentioned how irrigation management (scheduling, timing and so forth) could either increase or reduce infiltration volumes. Reszler & Fank (2016) tested the different modules of the “MIKE SHE” model to represent evapotranspiration and the flow in the unsaturated zone in Austria. They compared the model response with lysimeter-measured recharge rates, volumetric water content and soil tension data. These studies describe how the identification of inaccuracies in groundwater models, are only detectable if direct recharge measurements are available.

### **2.3.2 Applications in evapotranspiration and soil water balance studies**

Xu & Chen (2005) evaluated seven evapotranspiration models and their performance in water balance studies at a meteorological station in Germany. Three models calculated actual evapotranspiration (AE) directly employing different equations (i.e. the CRAE model of Morton, the advection–aridity (AA) model of Brutsaert and Stricker, and the GG model of Granger and Gray), and the other four models calculated potential evapotranspiration (PET) first and then AE based on soil moisture condition. Model performance was tested in terms of the models’ ability to predict actual evapotranspiration, recharge and soil moisture content (SMC). It was observed that the mean annual error of the predictions of the AA, GG, Priestley-Taylor and Makkink models was less than 5% when compared with lysimeter-measured evapotranspiration. In terms of recharge, the GG and the AA models performed better with mean annual errors of 4.4% and 5.7% respectively. Regarding soil moisture content, all seven models simulated the mean annual SMC successfully, with a mean annual error of less than 5%. Similarly, Wegehenkel et al. (2008) tested two soil-water balance models by comparing simulated with daily rates of evapotranspiration, soil water storage, recharge and capillary rise measured in twelve weighable lysimeters. Precipitation, evapotranspiration and capillary rise were measured with a set of two weighing systems installed underneath each lysimeter. The results were presented with a calibration of the model parameters and without such procedure. In some cases, the calibration of model parameters resulted in a better fit between observed and cumulative rates of recharge, however, the simulation quality decreased in terms of RMSE for some lysimeters. In this study, they also found that the uncalibrated models led to an underestimation of groundwater recharge at some lysimeters, however, the uncalibrated application of both water balance models also presented an acceptable

fit among measured and simulated results in terms of the modelling-efficiency index (IA) and the RMSE. For instance, in 4 of the lysimeters the IA varied between 0.45 and 0.68 whereas the RMSE varied between 1.3 and 1.6 mm d<sup>-1</sup> for one of the uncalibrated models. For the same model but after the calibration procedure, the IA ranged between 0.41 and 0.68 and the RMSE between 1.5 and 2.1 mm d<sup>-1</sup>. Similar results on a different area of science were reported by Groenendijk et al. (2014). They conducted a performance assessment of 6 different models to simulate nitrate leaching against lysimeter data. None of the models performed well throughout the statistical analysis, consequently, the authors mentioned that an accurate model calibration may not guarantee a good predictive capacity of the model.

### **2.3.3 Soil moisture content as a proxy to estimate groundwater recharge**

Lysimeters are the most direct way of measuring recharge rates, however, such devices are very expensive to manage. As a response to this, Jackson (2002) mentioned how remote sensing techniques can be employed to infer variables such as soil moisture, and how these data may be useful to complement monitoring and modelling of groundwater recharge. Consequently, the usefulness of soil moisture content data as a proxy to estimate groundwater recharge is evaluated by Sorensen et al. (2014). They compared four models (Penman–Grindley -PG, UN Food and Agricultural Organization -FAO, spatial Distributed Evaporation-SPADE and Joint UK Land Environment simulator -JULES) that estimate potential recharge at four different sites with different land covers (2 woodland sites and 2 grassland sites). The models were validated against soil moisture observations. The PG model -being the simplest one-, performed better than the others at simulating the changes in soil moisture content (i.e. presented the lowest root mean square deviation (RMSD) value) in one of the woodland sites and one of the grassland sites when compared to the other models. Overall, all the models performed well when simulating SMC at all the sites (i.e. RMSD ranging between 27 and 66 mm). On the other hand, a high variation was observed in the modelled recharge values. For instance, in 2007 at one of the woodland sites, the mean annual recharge was 81, 20, 215 and 57 mm employing the PG, FAO, SPADE and JULES models respectively. In the same year, at one of the grassland sites, recharge estimations were 23, 7, 269 and 291 mm using the PG, FAO, SPADE and JULES respectively. They also found that simulated recharge beneath woodland using JULES and the SPADE model is around 20% less than under grassland on the same soil type. This was attributed to greater woodland evaporation, thus the significance of models characterizing evaporation appropriately. In conclusion, the authors observed that although the four models performed well when comparing modelled SMC to observed data, significant differences were noticed in how the models modelled groundwater recharge. This differences were attributed to: (a) the way by which each model apportioned precipitation through the hydrological cycle, (b) the inaccurate simulation of evaporation, and (c) differences in model structure and parameter selection. More recently, Mathias et al. (2017) performed a Monte Carlo simulation using the same SMC data (same 4 locations) previously analysed by Sorensen et al. (2014) in conjunction with daily net rainfall, PE data and soil texture data in a model (SMAP) capable of simulating SMC and recharge. Given that precipitation and actual evapotranspiration were monitored, the SMC was used in a water balance to estimate vertical percolation rates. They observed a great sensitivity of recharge to soil texture, and given the nonlinear function of SMC described by the SMAP model to calculate recharge, any minor variability in SMC led to a

greater recharge variability. The SMAP model was calibrated against observed SMC data, however, they found that the value of SMC observations as the primary diagnostic for recharge modelling is rather questionable due to the insensitivity of SMC to soil texture.

## **2.4 Regionalisation case studies**

### **2.4.1 Geostatistical Techniques**

Zirlewagen & Von Wilpert (2010) upscaled soil chemical properties to the landscape scale, with the aim of evaluating the effect of land use changes on soil carbon storage. They employed a multiple, linear regression to predict soil carbon storage, and regionalised the results employing a kriging technique based on soil chemical properties measured at 56 sampling points. Upscaling problems mentioned by them include a relatively low sampling intensity and the strong local fluctuations of soil chemical parameters, which produce great uncertainty. Similarly, Muthusamy et al. (2017) scaled up rainfall observations measured in eight paired rain gauges in a 400m x 200m urban catchment using block kriging. They used the coefficient of variation as an estimate of uncertainty due to both spatial variability of rainfall and “errors” of the tipping buckets. The two main challenges addressed by them were the low quantity of rainfall measurement locations and non-normality of the data, which has to be considered on geostatistical techniques. Also, it’s uncertain to assess whether the number of sampling points presented in Zirlewagen & Wilpert (2004) and Muthusamy et al. (2017) can produce an efficient and meaningful result. Webster & Oliver (2007) mentioned that approximately 100 measurement points are needed to calibrate a geostatistical model, though there is no universal rule for it. Problems with sample size are also mentioned in Dewandel et al., (2012). They aimed to regionalise hydraulic-conductivity and effective porosity values at the catchment scale. The approach was tested on an unconfined granitic aquifer, considered a highly heterogeneous system. Hydraulic conductivity regionalisation was not possible due to a low density of measures compared to aquifer heterogeneity. McKenzie & Ryan (1999) mentioned that the development of reliable kriging models is difficult when the sampling size is low compared to the heterogeneity of aquifer properties. One of the key assumptions mentioned by Dewandel et al. (2012) for upscaling employing geostatistical techniques, is that the number of sampling locations is assumed to describe the amplitude and frequency of the aquifer properties to which they belong, which is also highly uncertain.

Carmichael & Ailleres (2016) presented the results of stochastic sub-sampling, grid cell averaging and spherical statistics for upscaling orientation data in 3D geology models. Orientation data was successfully upscaled with the three methods and the level of uncertainty inherent to the process was quantified as well. In a different study, grid cell averaging is discussed by Dewandel et al. (2012), they mentioned that cell size on geostatistical computations is critical, specifically when a model is trying to recreate the general pattern of aquifer properties. In general, geographical proximity does not guarantee a similar hydrological behaviour (Bastola et al., 2008), and that is perhaps one of the reasons why geostatistical techniques may not be the best option to regionalise recharge measurements.

### **2.4.2 Regression Methods**

Most studies aim to establish regionalisation schemes based on linear regression models, though the linearity of the relationship between catchment descriptors and model parameters is often obviated (Heuvelmans et al., 2006). Moreover, Zhang & Qi (2005) mentioned that the particular linear relationship assumed in these models limits their ability to model complex and nonlinear problems that are closer to reality.

Heuvelmans et al. (2006) compared the performance of a linear regression analysis and an artificial neural network (ANN) for regionalising the parameters of the hydrological model “SWAT”. They employed climatic, soil and land use data for the analysis, and consequently, a correlation analysis was performed to identify the correlations that the regionalisation scheme should reflect. An uncertainty assessment was also performed employing bootstrap sampling. Generally, the ANN delivered more accurate parameter estimates than the linear regression, with the exception of sites with catchment descriptors outside the range of descriptor values employed for the training process of the ANN. The performance of the regression was also affected under these conditions, however, the resulting error remained smaller for the regression approach. Regarding the uncertainty analysis, the ANN-based scheme presented larger uncertainties, a consequence of the greater amount of free parameters for the ANN structure compared to the regression model. Similar results were reported by Bastola et al. (2008). In their study, they aimed to regionalised parameters of hydrological models at a daily time scale, employing a new multi-objective regional calibration method (MORC), an ANN, a linear regression and a multiple polynomial regression. The higher uncertainty (assessed employing bootstrap sampling) was observed in the MORC, and compared to multiple regression-based schemes, the ANN resulted in considerable uncertainty. They noticed that ANNs and MLR have only limited capability to extrapolate outside the range over which they are trained or calibrated, however, the error employing a MLR is comparatively small.

Camarero et al. (2009) successfully upscaled site-specific soil properties to the regional scale. The methodology relied on a multiple regression model, used to model soil parameters as a function of diverse environmental parameters such as land cover, climatic data, lithology and geographic data. The resulting regionalised parameters were used as input in a model to simulate water chemistry (e.g. pH). The method was tested comparing the model output employing the regionalised soil properties against field measures of water chemistry. Though, there was some uncertainty in estimating the soil properties based on the regression, the effect on water chemistry simulations was small. The use of regression models for upscaling is discussed by Zirlwagen & Von Wilpert (2010). They concluded that despite the recent development of modern techniques, it is still recommended to use regression techniques as accurate spatial predictors of environmental parameters, which enable the study of cause-effect relationships and the analysis of different management scenarios.

### **2.4.3 Artificial Neural Networks (ANNs)**

Artificial neural networks are defined as “data-driven” structures capable of modelling any relationship for both linear and nonlinear processes with high accuracy (G. P. Zhang & Qi, 2005). When constructing an ANN

model, one presents the network with input patterns and their associated outputs. Then, the network organizes itself to represent the relationship among inputs and outputs (Jain et al., 2001). The network is interconnected through many processing units called “neurons” which receive input from an external source, compute the output, and transmit the computed output to a neuron in the following layer. Although many types of neural network models have been proposed, the feed-forward network model with one input layer, one hidden layer and an output layer is the most popular one (G. P. Zhang & Qi, 2005). One of the key concepts related to the use of ANNs is how they are trained to predict more accurate outputs. Given a known output, the error at the output layer (predicted value) can be computed based on the difference with the real output value. Then, the computed error is back propagated from the output layer through the network and the “connection weights or strengths” are updated using the “back-propagation algorithm” (BPA) introduced by Rumelhart et al. (1986), so the network ends up predicting values closer to reality. In hydrology, the ANN models have been applied to predict nonlinear processes such as rainfall runoff, stream flow, precipitation, and water quality modelling (ASCE, 2000b)

Jain et al. (2001) compared ANN models, regression models and time series models in terms of their performance when predicting water demand in one region of India. The input data for the models consisted of weekly water demand, total weekly rainfall and weekly average maximum air temperature. Consistently, the ANN outperformed the regression and time series models. Six different neural networks were developed for the study, and an absolute error in forecasting of 2.41% was achieved by the best one. They mentioned ANNs’ ability to learn from the input data and the resulting output data, and how this is considered by many researchers as one of the advantages that ANNs have over different methods. Though there is a disagreement with this theory as mentioned by Maier & Dandy (2000); they mentioned that ANN’s ability to learn from examples has no difference with the parameter estimation phase in conventional statistical models (e.g. regression models), therefore, this data-driven learning procedure is not an advantage over regression techniques.

Krishna et al. (2008) and Nayak et al. (2006) successfully predicted the groundwater level (GWL) fluctuation in coastal aquifers in India employing ANN models with input variables such as meteorological information and GWL data. Both studies used the same architecture for the models, consisting of a feed-forward network, with an input layer, output and one hidden layer, and according to Maier & Dandy (2000) one hidden layer is sufficient for most water resources problems. Nayak et al. (2006) reported a good performance of the ANN when forecasting water level up to 6 months in advance, however, Krishna et al. (2008) mentioned that ANNs are effective in forecasting groundwater level only for making short term-predictions (i.e. one month lead prediction). Similarly, Yoon et al. (2011) employed an ANN and support vector machines (SVMs) to predict groundwater level in two wells at a coastal aquifer in Korea. Past groundwater level, precipitation and tide level were considered as the input parameters to develop the models. The result showed a better performance of the neural network in training and testing stages, but a better overall performance of the SVM. An uncertainty analysis was also performed, showing a higher degree of uncertainty for the network model, which seems to be the overall outcome when employing ANNs.

The complexity of ANNs varies simply by changing the transfer function on each neuron or the network architecture (Maier & Dandy, 2000). Minns & Hall (1996) employed an ANNs as a predictor for a rainfall-runoff model. They investigated to which extent a more complex architecture (i.e. more hidden layers in the network) improves performance. It was found that an extra hidden layer, does not appear to justify the computational effort especially for nonlinear problems. In the same manner, Wong et al. (2010) mentioned under-fitting and over-fitting as problems with neural networks, and how they are directly related to the network complexity. Both over and under-fitting could lead to poor predictive performance and hence the importance of determining an optimal architecture. However, there is no unified rule for the determination of an optimal network (ASCE, 2000a).

Beck et al. (2013) trained a multilayer feed-forward neural network with one hidden layer and 30 hidden neurons to estimate base flow and the baseflow recession constant ( $k$ ) based on streamflow observations from 3394 catchment around the world. Since a nonlinear relationship was observed between climatic and physiographic characteristics of the catchments, the use of a neural network was justified and it proved effectiveness on predicting both baseflow and ( $k$ ). More recently, Beck et al. (2015) performed a regression analysis to evaluate the relationship among catchment descriptors and physiographic characteristics of stream flow. Also, 20 different neural networks were designed to estimate stream flow characteristics (e.g. base flow) at the catchment and global scale. The data set was partitioned into 3 subsets: training (80%), validation (15%) – to prevent overfitting-, and testing (5%). The process of subdivision was performed randomly. For training, they used the Levenberd-Marquardt algorithm in combination with the mean-square error performance function. The neural networks' performance was tested against the estimated stream flow values from two land surface models and two global hydrological models obtaining  $R^2$  values ranging from 0.65 up to 0.93. Employing the same training procedure, Krishna et al. (2008) found that a feed-forward neural network with Levenberd-Marquardt (LM) algorithm performed better than a network trained with Bayesian Regularization (BR) when predicting groundwater level.

## **2.5 Regionalising recharge estimations**

Sophocleous (1992) presented a first attempt of how to regionalise site-specific recharge measurements in the United States. The analysis was performed combining a linear regression (based on precipitation, soil water storage, depth to water table and spring rainfall rate) and a GIS overlay technique. So, the region was zoned according to the regression coefficients (representing the parameters that could explain most of the variance of the recharge) and one GIS layer was created representing each of the variables previously mentioned. Consequently, all the layers were combined to create a recharge layer. They concluded this approach as powerful and practical, however, due to its simplicity, should not be used for management purposes. Similarly, Lorenz & Delin (2007) aimed to calculate regional recharge for an aquifer in Minnesota. The model was based on a regression of recharge estimates (derived from analysis of stream base flow), precipitation, growing degree days and specific yield, since these were the parameters that presented a higher correlation with recharge estimates. Unexpectedly, land use was not considered, since the residuals did not show any relation to any of the dominant land covers on the study area. They mentioned this model

to be helpful for water managers to obtain recharge estimates for management plans at local scales. Though, the model is not applicable in areas where perennial streams do not occur.

As mentioned by Maier & Dandy (2000), different techniques such as Monte Carlo simulations (e.g. bootstrap sampling) have been considered to deal with uncertainty in the development of neural networks. Westerhoff et al. (2018) developed a model based on satellite data (NGRM) to estimate rainfall recharge at the national scale in New Zealand. The results include an uncertainty analysis of the model, and comparisons of simulated results with observed recharge values (i.e. lysimeter drainage) and a recharge model developed for the Waimakariri zone and one model developed for Southland. Uncertainty was calculated based on variance and covariance analyses and sensitivity of the input components (i.e. propagation of error). The simulated recharge values (and their uncertainty) compared well against the lysimeters in Canterbury. For instance, the NGRM model estimated a mean annual rainfall recharge of  $163 \pm 23$  mm year<sup>-1</sup> and  $67 \pm 33$  mm year<sup>-1</sup> at the airport and Lincoln sites respectively whereas the observed mean annual rainfall recharge values at the same locations were 156 mm year<sup>-1</sup> at the airport and 68 mm year<sup>-1</sup> at Lincoln. The NGRM model also performed well compared to the MIKE-SHE model developed by Environment Canterbury for the Waimakariri Zone. The NGRM presented a standard deviation of 110 mm year<sup>-1</sup> compared to approximately 125 mm year<sup>-1</sup> for the ECAN model. The differences were also minimum when comparing the results against the recharge model for the mid-Mataura catchment (Southland). The effect of irrigation was not considered directly for the national recharge model, and it's one of the points that the authors mentioned as future research towards improvements in recharge modelling, however, the model uncertainty calculation is a valuable addition to the area, since it has not been typically assessed on previous research.

### **3. RESEARCH QUESTION and RESEARCH OBJECTIVES**

#### **3.1 Research Question**

- Can decision making regarding dynamic regional groundwater allocation be improved by analysis and upscaling of point-scale lysimeters measurements?

#### **3.2 Research Objectives**

1. To establish a quality control procedure in order to assess lysimeter-measured recharge data.
2. To build an artificial neural network capable of predicting recharge under irrigated conditions in the Canterbury Plains.
3. To perform an uncertainty assessment related to estimated recharge values predicted with the ANN.
4. To evaluate the performance of an artificial neural network on regionalising recharge at the regional scale in the Canterbury Plains.
5. To identify key climatic, soil, irrigation management and soil moisture parameters that are critical for the prediction of lysimeter recharge across Canterbury Plains.

6. To investigate the availability of key input parameters for an artificial neural network capable of predicting groundwater recharge in a region of South-West Colombia.

## 4. METHODOLOGY

This research was comprised of two different case studies, guided by the objectives outlined above. The first case study (Objectives 1 to 5) involved the regionalisation of lysimeter-measured recharge at three groundwater allocation zones in the Canterbury region, employing a supervised machine learning technique (i.e. artificial neural networks). The second case study (Objective 6) involved a small region in South-West Colombia, where the usefulness of employing a neural network for estimating land surface recharge was evaluated.

### 4.1 Case Study I - Canterbury, New Zealand (Three GW allocation zones)

#### 4.1.1 Sites Description

This study aims to regionalise (Objective 4) the recharge measurements recorded at three lysimeter stations to a larger scale (i.e. to the groundwater allocation zone scale). The data collected at three different lysimeter stations was employed for analysis i.e. Dorie, Dunsandel and Methven stations. The Dorie Lysimeter station is located in the Chertsey allocation zone, whereas the Dunsandel and Methven lysimeters are installed in the Rakaia-Selwyn and Ashburton allocation zones respectively (Table 1).

Table 1. Overview of the lysimeter stations and their corresponding location within a GW allocation zone.

Lysimeter Station	Located in: GW allocation zone	Area [ha]
Dorie	Chertsey	69328.8
Dunsandel	Rakaia – Selwyn	120189.7
Methven	Ashburton/Lyndhurst	63196.8

Figure 1 presents the location of the three lysimeter stations utilised for analysis. As observed, each lysimeter station is installed on a different allocation zone. The study area was selected based on the groundwater allocation zones defined by Environment Canterbury in the land and water regional plan (ECan, 2017). All the lysimeters were installed on farmland, mainly covered by ryegrass/white clover pasture, typical of actively irrigated grasslands in the Canterbury Plains of New Zealand. In terms of irrigation, Dorie and Methven lysimeters are irrigated using a centre pivot, whereas at Dunsandel, irrigation is applied using a travelling irrigator, therefore irrigation at the latter is much higher in comparison with the other two sites.

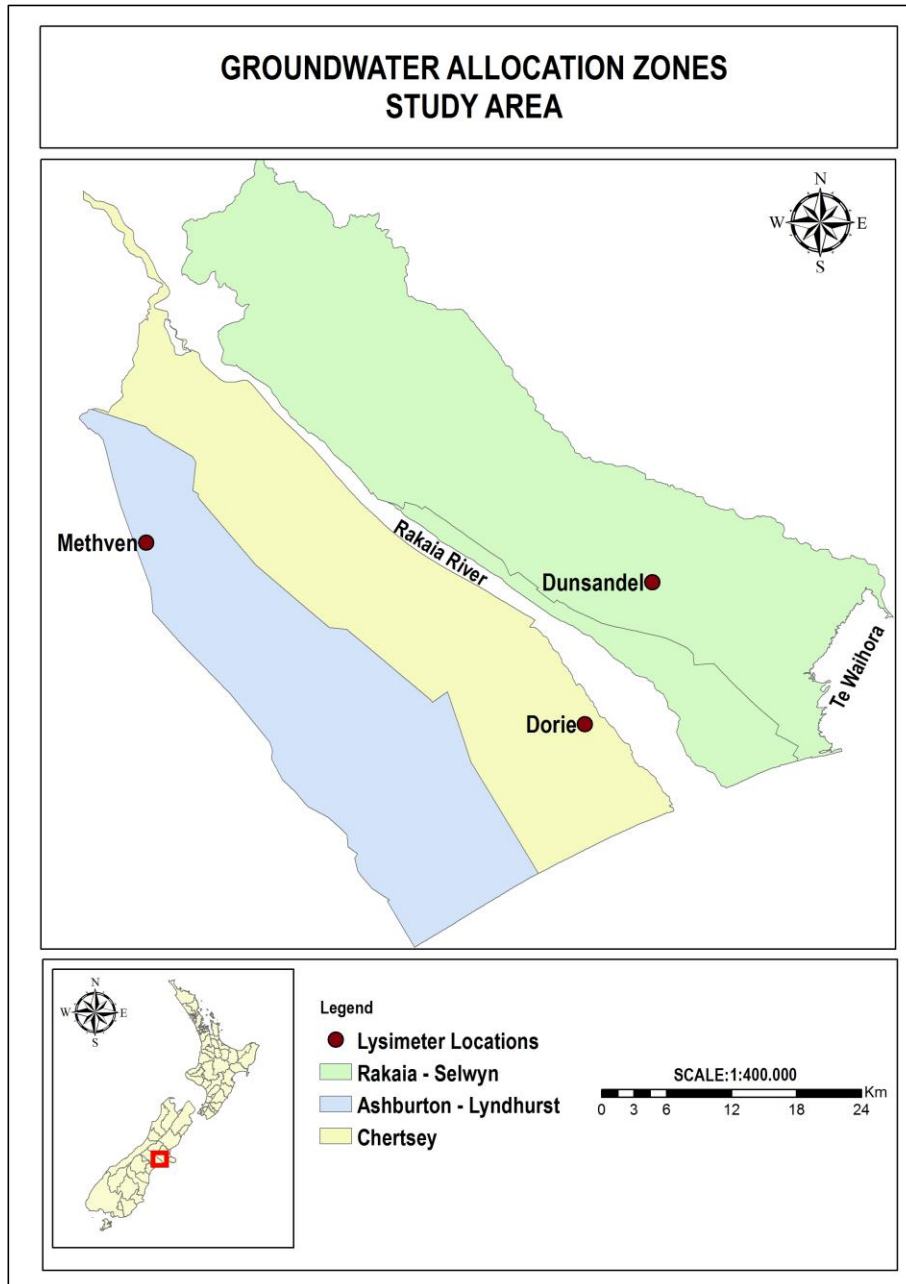


Figure 1. Areas of interest for regionalization of lysimeter-measured recharge and location of lysimeter sites.

Drainage lysimeter systems are in operation at each lysimeter station, maintained and operated by the National Institute of Water and Atmospheric Research (NIWA), Environment Canterbury (ECan), Aqualinc and HydroServices. At each site, three drainage lysimeters 0.5m in diameter and 0.7m in depth were installed (Duncan et al., 2016). Recharge was measured by a tipping bucket gauge (0.2 mm cup size), each tip of the bucket representing 0.032 mm of recharge with respect to the lysimeter diameter. The lysimeters at each location were aligned so that they were irrigated by the same spray nozzles of the centre pivot irrigators. This was also done to ensure that the tipping bucket rain gauge, the lysimeters and check gauge received the same input. Figure 2 shows a schematic layout of a lysimeter site.

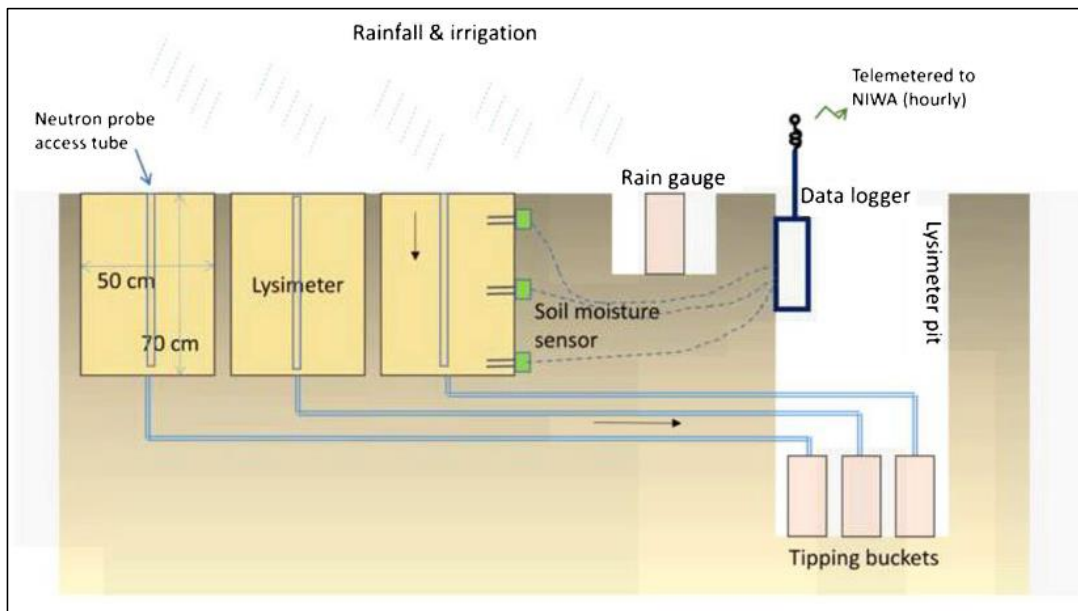


Figure 2. Schematic layout of a lysimeter site (Source: Duncan et al., 2016)

At each station, rainfall, irrigation, potential evapotranspiration (PET), and volumetric water content data were recorded. However, the amount of data available for analysis varied across sites as shown in Table 2. Firstly, Dorie lysimeters records start on July 2010, whereas Methven and Dunsandel lysimeters start on January 2011 and May 2016 respectively. Also, volumetric water content was only recorded at 10 cm depth for the Dunsandel and Methven lysimeters, whereas at Dorie, 30 cm and 54 cm depth soil moisture data was recorded. In New Zealand, seasons go as follows: Spring is from September to November, summer goes from December through February, autumn is March to May, with winter being June through August.

Table 2. Data available at each lysimeter location

Location	Parameter						Period:	
	Recharge [mm d <sup>-1</sup> ]	R + I [mm d <sup>-1</sup> ]	PET [mm d <sup>-1</sup> ]	VWC_10cm(%)	VWC_30cm(%)	VWC_54cm(%)	From	To
Dorie	✓	✓	✓	✓	✓	✓	09/07/2010	31/12/2017
Dunsandel	✓	✓	✓	✓	N/A	N/A	28/05/2016	11/05/2018
Methven	✓	✓	✓	✓	N/A	N/A	11/01/2011	31/05/2018

R + I: Rainfall and Irrigation, VWC: Volumetric water content at X depth, PET: Potential Evapotranspiration,  
N/A: Not available

White et al. (2003) describe the Canterbury plains as a series of coalescing major Pleistocene alluvial fans consisting of greywacke gravels, cobbles and boulders in a highly variable matrix of sand and silt. Most of the soils in Canterbury are also shallow, with stones in the topsoil. The Methven lysimeters are located on shallow, silty, stony soils overlying coarse sandy gravels (Duncan et al., 2016), with a profile available water (PAW) ranging from 53 mm up to 80 mm (Newsome et al., 2008). At Dorie, soils are moderately deep (55 – 100 cm) above sand over a sandy gravel (Duncan et al., 2016), presenting a moderately well drained silty

profile, with a PAW ranging from 55 mm to 144 mm (Newsome et al., 2008). The Dunsandel lysimeters are installed on shallow (20 – 40 cm depth) well drained (loamy-like) soils. At this location, the PAW is classified by Newsome et al. (2008) as moderate to low, with values ranging from 53 mm to 80 mm. Figure 3 shows the spatial distribution of texture profile in the three zones of interest.

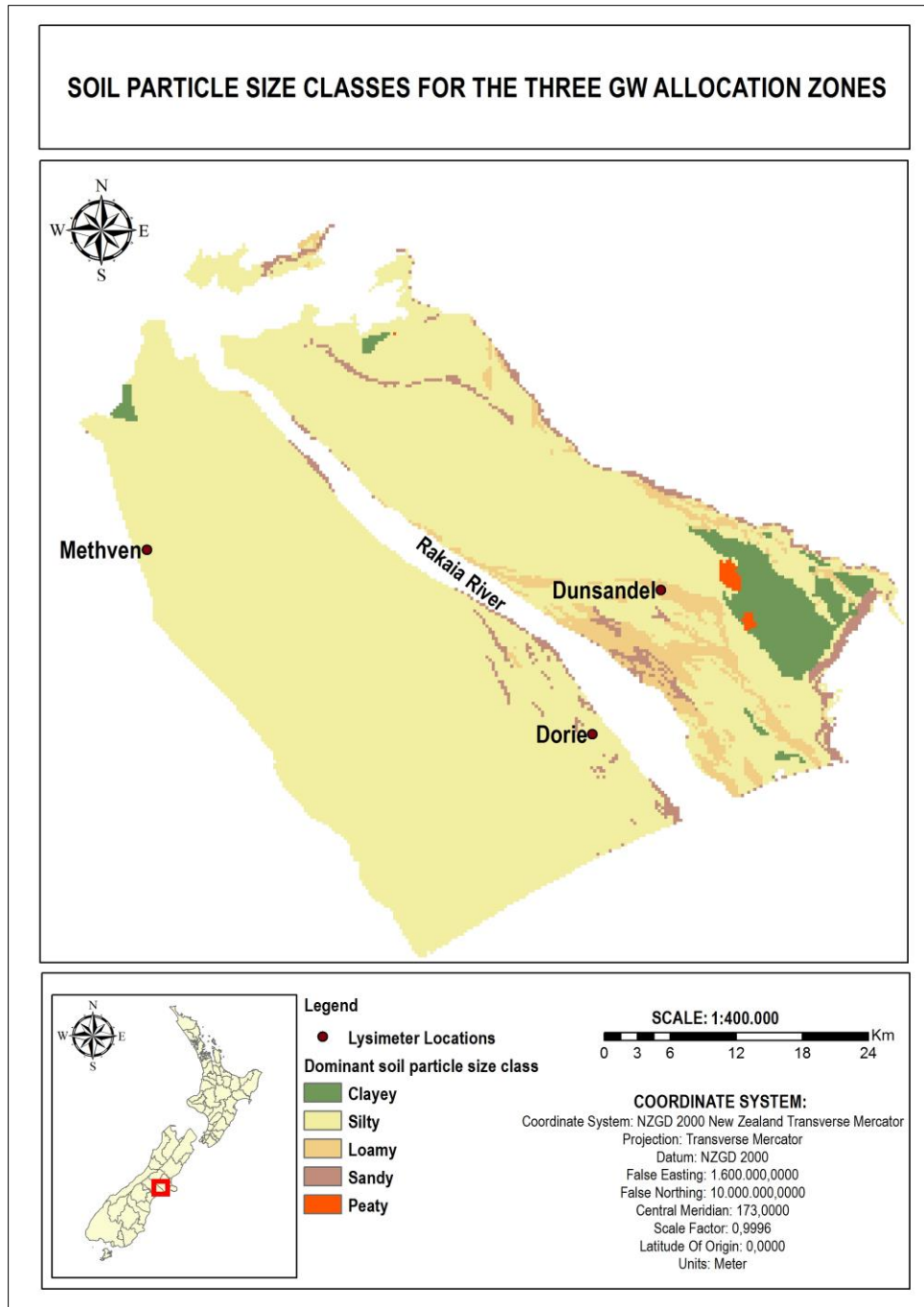


Figure 3. Soil dominant texture class for the three GW allocation zones.

### 4.1.2 Data quality control

The current work was based on available data, therefore, quality associated to calibration and installation of the lysimeters was out of scope. However, Duncan et al. (2016) mentioned that at the Methven and Dorie lysimeters, all tipping buckets were field-calibrated annually. In general, all datasets were recorded daily, at 15 minutes intervals. Following the procedure by Muthusamy et al. (2017), the quality control procedure applied to the collected recharge observations was performed prior to model development as follows:

- (a) Assembly of a daily recharge dataset (i.e. midnight to midnight): In the process of assembling a daily dataset based on daily recharge measures, gaps in the 15-minute records occurred. If the daily gaps did not exceed 10% of the total measurements per day, the gaps were ignored. When this was not the case, the day was flagged as an outlier for further review. Where nothing unusual was noticed, the gap was filled by averaging the recharge value measured by the other two lysimeters at the same location.
- (b) Outlier Detection: For each variable collected at each location, visual inspection of each time series was carried out, and unusual values were marked as potential outliers.
- (c) Gap Filling: If a gap was observed in the recharge dataset at one lysimeter of a specific location, that value was replaced by the average of the two remaining values measured (On the other two lysimeters) on the same day. Also, a few gaps were observed in the volumetric water content dataset. Where gaps were detected, the missing value was replaced by the result of a multiple linear regressor (MLR) developed based on previous complete data from the same season where the gap was observed (e.g. If a gap was detected in the winter, a MLR trained on complete data from previous winters was employed to estimate and filled that missing value). Basically, the calculation of missing values was carried out as a function of rainfall, irrigation and volumetric water content at deeper depths (only where VWC data at deeper depths was available).

### 4.1.3 Time series analysis and Model (ANN) Development

The time series analysis consisted of two steps: (1) Descriptive statistics of the quality-controlled datasets generated based on the procedure outlined in section 4.1.2, and (2) Analysing the seasonal variability of lysimeter-measured recharge across the three locations.

For regionalising recharge measures within the three GW allocation zones, it was crucial to develop a model capable of explaining LSR behaviour. An ANN model was selected for this study, given its demonstrated power in prediction of a wide range of hydrological processes including: transport processes in coastal aquifers (Bhattacharjya & Datta, 2005), aquifer parameter estimation (Karahan & Ayvaz, 2008) and groundwater level forecasting (Nayak et al., 2006). Furthermore, an ANN was used by White et al. (2003) to predict lysimeter-measured recharge on dryland conditions in Canterbury. The theory behind neural networks is described here in brief: The neural network consists of an input layer, one (or more) hidden layers, and an

output layer (Figure 4). Each layer consist of “neurons” (circles in Figure 4); all the neurons are connected to all neurons in the following layers by a set of “weights” ( $W_1, W_2..$  in Figure 4). Each neuron basically executes two processes: (1<sup>st</sup>) they perform a weighted combination of its inputs: As shown in Figure 4, the first neuron receives all the inputs from the input layer. Each input is multiplied by its corresponding weight  $W_i$ . Then, the products are summed up and this is the result of the first step ((1) in Figure 4); (2<sup>nd</sup>) the second process consist of a transformation of the result of the previous step through an “activation function”. There are many activation functions available, however, the Rectified Linear Unit (“ReLU”) function, is perhaps the most commonly used in machine learning. Eq. (1) shows the way the “ReLU” function mathematically transforms the results of the 1<sup>st</sup> step. Basically, ReLU returns a value of zero is the summation of the 1<sup>st</sup> step is less than zero, or returns the value of the summation is the summation is above or equal to zero.

$$ReLU(x) = \max(0, x) \text{ Eq. (1)}$$

As shown in Figure 4, the summation of the 1<sup>st</sup> step for the first neuron is greater than zero (Sum=5.3), therefore the activation function i.e. “ReLU”, returns the same value. The result of this step is finally pass forward into the output layer. The same process occurs in every neuron of the network.

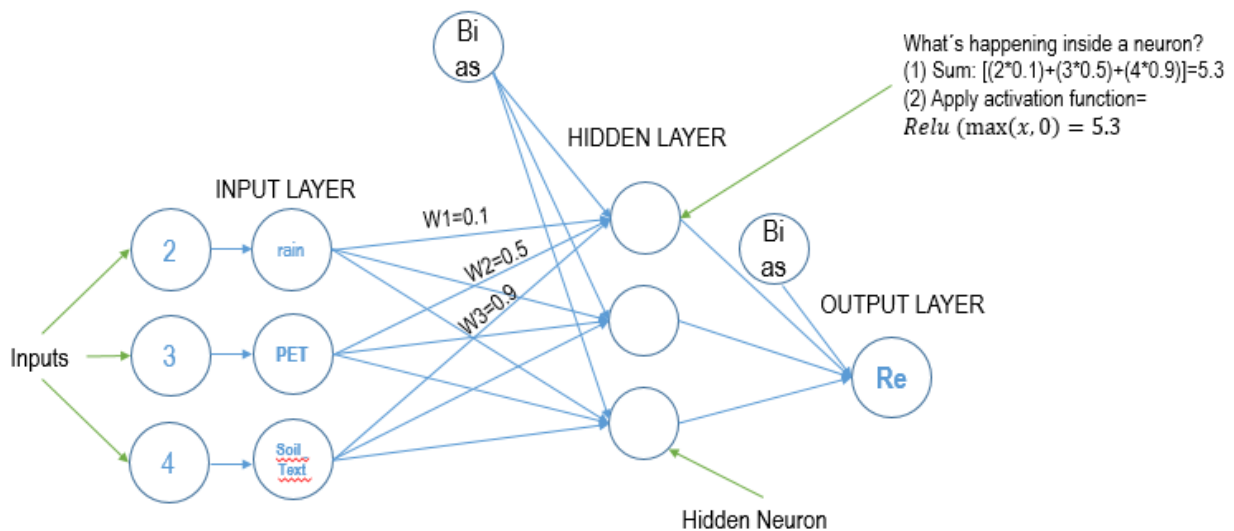


Figure 4. Architecture of a (4-5-1) feed-forward neural network. (i.e. 4 neurons on the input layer, 5 neurons in the hidden layer and one output).

The application of ANNs consists of two phases (training and testing). The training is an iterative process that aims to adapt the network internally (i.e. the weights are updated) in such a way that the calculated results from the network are as close as possible to the expected results (van Leeuwen, 2012). Updating the model parameters such as “Weights” and “biases” is basically performed through an optimization algorithm such as the commonly known “ADAM” (Kingma & Ba, 2015), a method for stochastic optimization. The result of the training phase is a trained network. This network is then used during the testing phase to generate new output results based on new input data (which was not used for training). The new input data used for testing is different from the training input data but covers the same problem domain (van Leeuwen, 2012).

### - **General NN architecture and Internal design**

For the construction of the ANN, the design procedure introduced by Karahan & Ayvaz (2008) was followed. The dataset used for developing the model was split into two sets: training and testing. Though different approaches were considered in order to find the best NN architecture and are described later on. In all cases, the number of neurons in the hidden layer was defined by trial and error i.e. different numbers of neurons were tested and the one presenting the best performance during the testing stage was selected (Karahan & Ayvaz, 2008). The model performance (Testing stage) was evaluated by employing two parameters: (a) The coefficient of determination ( $R^2$ ) and the Mean Absolute Error (MAE), thereby following Mathias et al. (2017) and Adamowski & Chan (2011). Also, for every case the adaptive momentum (“ADAM”) was defined as the optimizer, since it is straightforward to implement, it is computationally efficient, has little memory requirements, and is well suited for problems that are large in terms of data and/or parameters (Kingma & Ba, 2015). On the hidden layer the Rectified Linear Unit (“ReLU” – Eq. 1) was used as the activation function, since it presented an improvement in convergence when compared to the commonly used Hyperbolic tangent function in the landmark ImageNET classification paper by Krizhevsky et al. (2012).

The inputs for the NN model development were defined based on the information that was available at each lysimeter location (Table 2), but also by considering the information that was available in the region. Crop evapotranspiration was not considered as an input, since Graham et al. (2016) have proven that potential evapotranspiration provides an accurate means of predicting evapotranspirative losses for irrigated grasslands in New Zealand i.e. it is assumed that irrigated pastures in the region evaporate-transpire at potential rates. In the output layer of the NN, the goal was to match the average recharge at each location (i.e. mean recharge of the three lysimeters at each location). The methodology for finding the best NN consisted on trying two different approaches:

#### Approach 1 (2 steps):

- Step (i) - One neural network for each location: A single neural network was developed at each site for a total of three NN (1 NN per lysimeter location). 80% of the dataset was considered just for training, whereas the remaining 20% was used for testing. However, the training dataset was split in 5 different ways in order to check whether data collected at different seasons would have an effect on NN performance. The assumption when splitting the data was that records collected at different seasons, may influence the performance of the model differently. Therefore, the NNs were trained with different datasets defined as follows: (1) The whole training dataset was employed, (2) Only previous summers’ data from the training dataset was employed in training, (3) Only data from previous autumns, (4) Previous winters’ data only, and (5) Previous springs’ data only. Consequently, model performance was evaluated
  
- Step (ii) – Transfer to other locations: The best NN developed at each location was tested with data collected at the other two locations (following White et al. (2003)), in order to evaluate whether a NN was able to predict measured recharge at a different location. Also, the training and testing datasets were swapped as a measure to avoid bias.

## Approach 2 – One single NN for upscaling

- Step (i): Up to this point only three inputs had been considered (rainfall/irrigation, PET and soil moisture). The volumetric water content (VWC) was considered as an input for the NN due to its significant correlation to lysimeter-recharge ( $P < 0.05$ ). Although VWC at 10 cm depth was recorded at all locations, this parameter shows a high variability, mainly associated to rainfall events, irrigation management and soil type, which were different for all the farms where the lysimeters are installed. Also, keeping in mind the upscaling aspect of the analysis, it is necessary to collect data that are available for the three GW allocation zones i.e. outside the lysimeter sites, which is not the case for VMC. For these reasons, VWC was removed from further analysis.

Therefore, this approach consisted of developing a single neural network trained on data from all locations considered here. The aim was to generate a fairly large training dataset by aggregating the information collected at the three locations as observed in Figure 5. Given that the larger dataset now included information from the three sites, it was necessary to include soil parameters that provide the model with the examples to characterise the soil differences that influence recharge processes. For this reason, additional inputs were included during training in order to represent the soil differences across the sites. The dominant soil texture (particle\_size in Figure 5), drainage class, topsoil stoniness and the profile available water were considered for further analysis due to their influence on land surface recharge, which has been reported for in Canterbury (Duncan et al., 2016; White et al., 2003). The soil data were derived from the “New Zealand Land Resource Inventory” (NZLRI) (Newsome et al., 2008), a national database that comprises several physical resource themes. Since this data is based on a classification according to the New Zealand soil classification, it was necessary to reclassify and assign an integer value for each class, so the NN could recognise the input as a value and not as a class. The reclassified values are shown in Appendix A and were defined according to the logic presented by Singh et al. (2018). Here, each factor was reclassified into different classes ranging from 1 and up to 7, with the highest value assigned for attributes that favour groundwater recharge. For instance, Clayey soils were assigned a reclassified value of 1 because they have a higher tendency to restrict infiltration (USDA, 2014). After this, different NN architectures were tested in order to find the best model with the highest predictive performance employing fewer inputs (i.e. the most parsimonious model). In this step, the time scale for training the model was set up on two different scales: monthly (inspired on the model developed by Westerhoff et al. (2018)) and daily (based on findings from approach 1).

	rainplusirri	vwc_10	PET(mm)	L	rain	irri	location	particle_size	topsoil_stoniness	PAW	drainage_class
2017-12-29	0.0	40.065208	4.7	0.704000	0.0	0.0	Dorie	2.0	1.0	3	4.0
2017-12-29	0.0	14.875000	4.7	0.000000	0.0	0.0	Dunsandel	3.0	3.0	5	5.0
2017-12-29	0.0	32.600694	4.2	0.032000	0.0	0.0	Methven	2.0	3.0	5	5.0
2017-12-30	0.0	14.538194	5.2	0.000000	0.0	0.0	Dunsandel	3.0	3.0	5	5.0
2017-12-30	0.0	39.589097	5.2	0.544000	0.0	0.0	Dorie	2.0	1.0	3	4.0
2017-12-30	0.0	31.617222	4.6	0.000000	0.0	0.0	Methven	2.0	3.0	5	5.0
2017-12-31	0.0	14.024306	4.2	0.010667	0.0	0.0	Dunsandel	3.0	3.0	5	5.0
2017-12-31	0.0	38.896181	4.1	0.405333	0.0	0.0	Dorie	2.0	1.0	3	4.0
2017-12-31	9.0	31.148333	3.3	0.000000	9.0	0.0	Methven	2.0	3.0	5	5.0

Figure 5. Combined dataset for training a single NN. The timeseries were aggregated with the assistance of Pandas (McKinney, 2010).

- Step (ii): In this step an approximate Bayesian Neural network was developed in order to check whether performance could be improved. This was achieved by employing “Dropout”, a popular empirical technique to avoid overfitting in NNs developed by Srivastava et al. (2014), which has been successfully used in the past by Huang & Weinberger (2018) and Lecun et al. (2015). Generally, when Dropout is applied, the weights' matrix of a NN is multiplied by a binary vector of zeros and ones, whereby the probability that an entry is 1 is given by a random parameter (P) drawn from a Bernoulli distribution. Where the binary vector is 0, that hidden unit in a particular layer is switched off or dropped out (Figure 6). In this step a dropout layer was added before the hidden layer. Three dropout rate probability (P) were considered i.e. 10%, 15% and 20% thereby following Ioffe & Szegedy (2015). The intention here was to evaluate which (P) value was more beneficial in order to increase NN performance. Consequently, the final dropout probability was set as 10%.

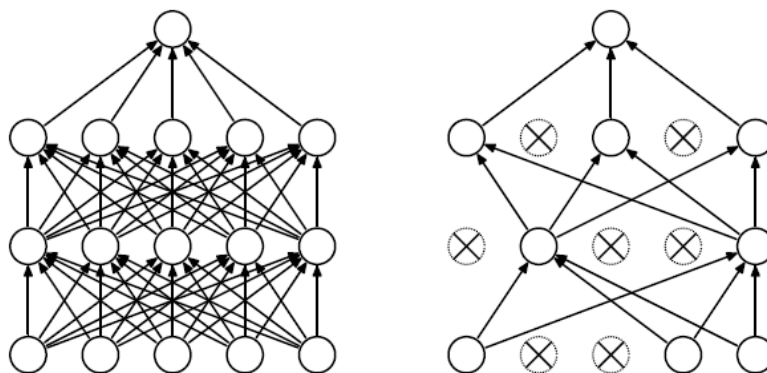


Figure 6. (Left) Standard neural network, (Right) The same NN after applying dropout. Source: (Srivastava et al., 2014)

Finally, the parsimonious configuration that resulted in both maximum efficiency and minimum error during testing was selected and applied in the upscaling.

## - Programming Language Libraries

Keras (Chollet, 2015) with Google TensorFlow (Abadi et al., 2015) backend was used to implement the deep learning algorithms in IPython (Pérez & Granger, 2007). The fundamental numerical operations were performed with the aid of NumPy (van der Walt et al., 2011). Data analysis and mining was done with the assistance of Pandas (McKinney, 2010) and Scikit-learn (F. Pedregosa et al., 2011), python libraries which provide integrated and intuitive mechanisms for performing data manipulation and analysis on structured datasets. Additionally, the integration of Matplotlib (Hunter, 2007) with IPython provided an interactive environment for data visualisation.

### 4.1.4 Model Uncertainty

Deep learning methods represent the state-of-the-art for many forecasting applications in water resource engineering. The key to estimating model uncertainty in deep learning models (e.g. NNs), is the posterior distribution, also referred to as Bayesian inference (Rowan, 2017). The latter can be approximated through “Monte Carlo (MC) Dropout”, a technique developed by Gal & Ghahramani (2016b). MC Dropout has been successfully applied in a wide range of different NN architectures to get state of the art results in convolutional and recurrent neural networks (Gal & Ghahramani, 2016a; Gal et al., 2016). This algorithm works as follows: Given a new set of data  $X^*$  (i.e. data not used for training), one computes the neural network output  $\widehat{Y}^*$  with stochastic dropout at each layer, in other words, randomly dropout each hidden unit during testing time with a certain probability (P) (similar to the process described in Figure 6). Then, one can collect the results of the  $t$  stochastic passes and get a sample predictive mean and variance (uncertainty). Since MC Dropout randomly switches off some units during testing, the testing dataset is passing through slightly different networks every time. According to Der Kiureghian & Ditlevsen (2007) there are two main uncertainties one can model. Aleatoric uncertainty, which captures the noise inherent in the observations that cannot be reduced even if more data are collected. Secondly, epistemic uncertainty, which accounts for uncertainty in the model parameters – uncertainty that captures our ignorance about the “real” model which generated our collected data. This is captured by the predictive variance and can be approximated as:

$$Var(y) \approx \sigma^2 + \frac{1}{T} \sum_{t=1}^T f^{\widehat{W}_t}(x)^T f^{\widehat{W}_t}(x_t) - E(y)^T E(y) \quad Eq. (2)$$

One can see that the variance is decomposed into two terms: The first term on the right hand side,  $\sigma^2$ , corresponds to the amount of noise inherent in the data, which captures the uncertainty in the data generation process and is irreducible (Kendall & Gal, 2017). The calculation of this parameter within this study was out of scope. The second term on the right hand side, reflects our ignorance regarding the specifications of model parameters, and is referred to as the model uncertainty. To capture model uncertainty 10,000 stochastic passes were carried out in order to capture predictive variability with a Dropout probability of 10%. The Python code for this step is given in Appendix E. The uncertainty is reported here as one standard deviation, after running the stochastic passes through the network.

#### 4.1.5 Upscaling (Spatial analysis)

Firstly, raster grids of rainfall, PET and soil dominant texture were created. Secondly, the matrix of weights and biases which describe the best neural network selected in 4.1.3 were extracted from the Keras environment (Chollet, 2015). Then, similar to Lee et al. (2014), a toolbox was created within a GIS for GW recharge prediction, which allows GIS users to perform spatial analysis and predict land surface recharge on a daily basis. In essence the toolbox predicts LSR in the same way as the NN would, but with the difference that it calculates an estimation for each cell of a raster grid. Consequently, it produces a map describing the spatial pattern of land surface recharge. Figure 7 shows a screenshot of the tool to upscale lysimeter-measured recharge for the three GW allocation zones considered here.

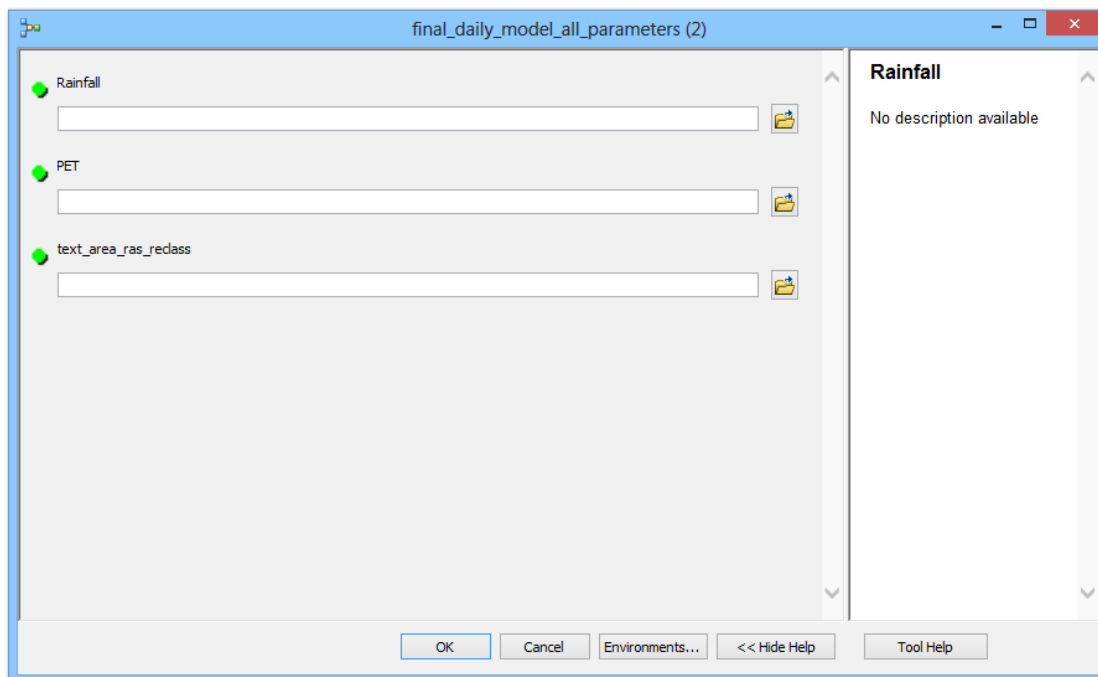


Figure 7. Screenshot of the tool for predicting LSR on a given area.

#### 4.1.6 Estimating Groundwater allocation

The research question of this work refers to evaluate whether lysimeter data could assist decision-making processes in groundwater allocation. Therefore, an estimate of how much groundwater can potentially be allocated per allocation zone was computed i.e. volumetric allocation on a seasonal scale. Assuming that water allocation in Canterbury was set under an adaptive framework, it would most likely be based on total recharge over the preceding winter (i.e. 1<sup>st</sup> April to 1<sup>st</sup> September), since that is when most GW recharge occurs (Zeb Etheridge, ECan, personal communication, 12 November 2018). Consequently, the model was run daily from 1<sup>st</sup> April 2017 to 1<sup>st</sup> September 2017 in order to (supposedly) calculate water allocation for 2018. Since running the model every day was highly time consuming, a Python script with the assistance of the ArcPy module was created in order to automatize the process (Appendix C and D). For the calculation of

LSR in the three allocation zones, the inputs from irrigation were not incorporated, since this information is not available region-wide. However, most of recharge is occurring during the winter when the inputs from irrigation are either very low or zero, therefore the underestimation of recharge for the allocation zones is negligible.

#### 4.1.7 Flowchart Case Study I

Figure 8 shows an overview of the steps to work out research objectives 1 to 5.

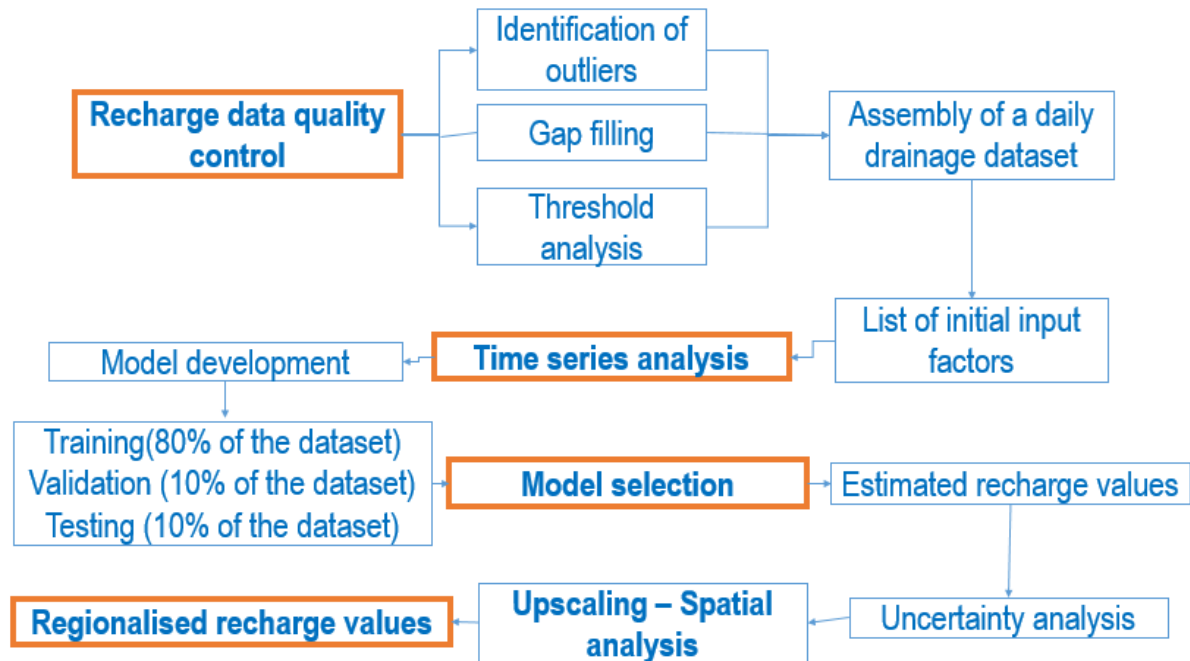


Figure 8. Flowchart of steps to work out the research objectives and to answer the research question

#### 4.2 Case Study II – Patia Valley, Cauca, Colombia

To reach objective 6, the suitability of employing an artificial neural network to estimate regional recharge was assessed in a small region (13000 hectares) of Southwest Colombia (Patia Valley). Similarly to Canterbury, the land cover in Patia Valley is mainly composed of crops and irrigated grasslands (Vergara Varela, 2015), and groundwater is the primary source for irrigation (CRC, 2017). Groundwater allocation is based on land surface recharge calculated employing a water balance i.e. groundwater recharge volumes are calculated as the inputs from rainfall minus the outputs from evapotranspiration and runoff. Given that Colombia is a developing country, the availability of data is a big constraint when assessing new approaches. The methodology involved the estimation of LSR based on data that is available region-wide i.e. Rainfall, ET and River Flow data. Although lysimeter-measured infiltration data is available in the region, access to those data was not granted this study. Therefore the procedure consisted of training a NN to predict LSR based on monthly LSR estimated previously by the regional council through water balance calculations (CRC, 2017).

#### 4.2.1 Site Description

The Patia Valley is located at 1° 15' N, 77° W and 2° 15' N, 77° 20' W between the Western and Central Andes of Colombia (Figure 9), with a mean annual rainfall of 1,600 mm (Vergara Varela, 2015). The Patia Valley is approximately 120 km long and 20 km wide. The Patia River, flows south along the eastern base of the Western Andes, and discharges into the Pacific Ocean (Ramirez et al., 2018). Low lying open plains form the centre of the upper Patia Valley. Those plains are about 4 to 5 km wide and located at 550 to 600 m above sea level. The higher parts of the plains are located at 1,000 – 1,200 m above sea level and are formed by layers of tuff and gravel covering the steeply dipping Tertiary rock formations beneath. Land cover in the area has been changing over the last few years from a dry forest ecosystem to crops and irrigated grasslands for livestock development (Vergara Varela, 2015).

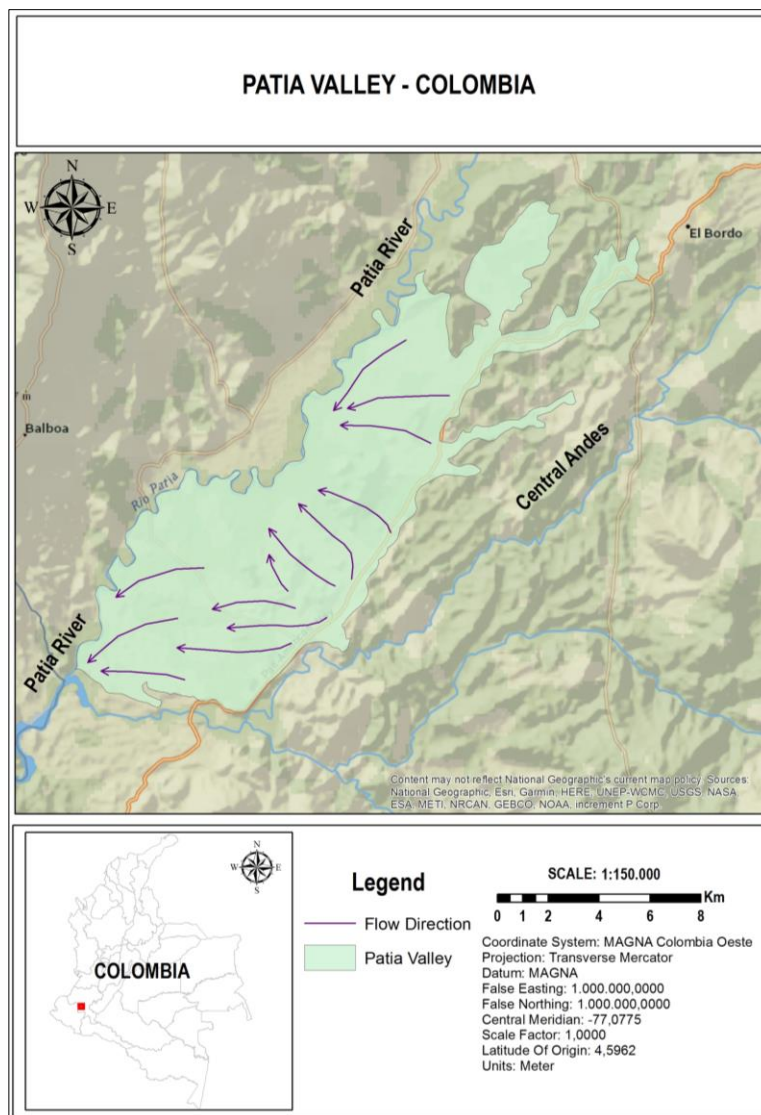


Figure 9. Study area for case study II. Shown are the Patia Valley and the flow direction towards the Patia River.

## 4.2.2 Data Analysis

Rainfall, evapotranspiration and river flow data were available for analysis in this study and were provided by the regional council, which manages water allocation in the area. The regional council has estimated land surface recharge for the Patia region employing a water balance, whereby the amount of water that infiltrates through the soil column equals the rainfall minus evapotranspiration losses and runoff (CRC, 2017). As opposed to the methodology for the Canterbury region, river flow was considered here as an input for the NN given its inclusion on previous LSR estimations reported by the regional council.

Because of the strong variability of rainfall in time, the regional council plans water allocation based on what an average scenario of recharge would be. This average scenario of recharge is calculated based on what an average scenario of rainfall, evapotranspiration and runoff would also be. By average, the council refers to rainfall depths which present a 50% probability of exceedance. The latter refers to the probability of occurrence of e.g. a rainfall event greater than some given value  $P$  drawn from a Weibull distribution (Weibull, 1939) which ranges from 0 to 100%. In general, as the rainfall amount increases, its probability of exceedance (occurrence) decreases. These rainfall depths can only be obtained by a thoroughly analysis of long time series of historic rainfall data. Through a long term time series analysis, the council defines an average scenario employing rainfall, ET and runoff depth with a 50% probability of exceedance.

An analysis of the long-term records of climate data was performed. 30 years of monthly data were recorded by the rainfall, ET and river flow stations located in the area (Figure 10). Surrounding the valley, there are 4 ET stations i.e. open pan evaporation sites, 10 rainfall stations and two stations to measure flow in the Patia River, one located in the upper reaches of the catchment and one in the lowest part of the catchment. After defining the average scenarios (i.e. the events that presented a 50% probability of occurrence), a spatial mapping of rainfall and ET was performed. Kriging interpolation was used as the method to map the spatial behaviour of the variables that were used later for training the NN. Álvarez-Villa et al. (2011) have shown that kriging interpolation is able to capture the main physical characteristics of rainfall in Colombia.

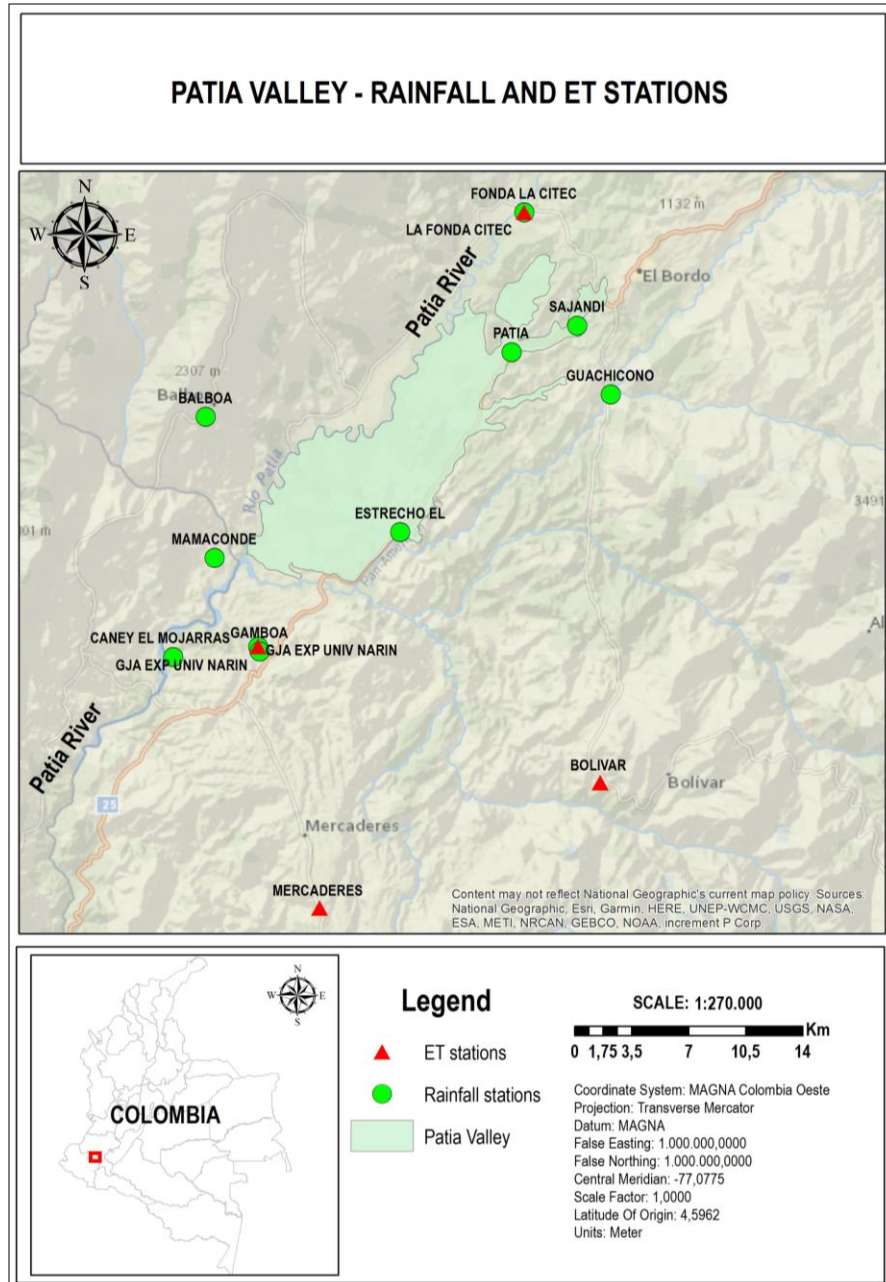


Figure 10. Rainfall and ET stations in the area

### 4.2.3 Model development

Given that lysimeter data is not publicly available, the procedure was to train a NN in order to check whether this model can match the previous LSR estimates calculated employing a water balance. Three different approaches were utilised:

- Approach I

A simple feed forward neural network was trained on a monthly basis with 60% of the data available and tested with the remaining 40% using three inputs (i.e. the three parameters measured in the region).

- Approach II

River flow was removed from model development since it is a parameter that is not available region-wide. Also, the ratio of training and testing data was adjusted i.e. 70% of the data was used for training and 30% for testing, and only the rainfall and ETc were used as inputs for the NN.

- Approach III

To check improvements in model performance, a simple NN was trained with Dropout (i.e. an approximation of a Bayesian NN) on a monthly basis. The inputs were the same as in approach II and the ratio of training and testing data was 70/30.

#### **4.2.4 Model Uncertainty**

The process for estimating model uncertainty was the same as described in 4.1.4.

## **5. RESULTS**

### **5.1 Canterbury, New Zealand (Case Study I)**

This section entails the results of upscaling point – scale groundwater recharge measurements to three groundwater management allocation zones (i.e. Rakaia/Selwyn, Chertsey and Ashburton) and it is divided into six sub-sections: (a) Results of data quality control and the generation of a “clean”/complete dataset; (b) Time series analysis; whereby the results of testing different inputs, architectures and time steps for predicting land surface recharge are provided; (c) Model development; (d) Results of the uncertainty analysis employing a Monte Carlo-based approximation; (e) Spatial analysis, where LSR predictions of the best model selected in the previous step are upscaled to a regional scale through the implementation of the ANN in a GIS environment; and (f) the determination of groundwater allocation limits.

#### **5.1.1 Data Quality Control**

This step consisted of two parts: (1) The identification of outliers, and (2) gap filling.

##### **- Dorie lysimeters (Chertsey GW allocation zone)**

No outliers were detected, however, there were gaps in the volumetric water content dataset (Figure 11). These gaps were observed for the months of November, January, February and March (spring, summer and autumn) of 2010, 2011, 2013, 2014 and 2016. Where gaps were observed, the missing value was replaced by the result of a multiple linear regressor (MLR) developed based on previous complete data from the same season where the gap was observed (i.e. three different MLR were trained for this location based on complete data from previous springs, summers and autumns). The calculation of missing values was carried out as a function of rainfall, irrigation and volumetric water content at deeper depths (only where VWC data at deeper depths was available - Figure 11).

```
In [254]: #Locate NaN values in the dataset
dorrie.loc[np.isnan(dorrie["vwc_10"]) & (dorrie.index.year == 2017)]
```

```
Out[254]:
```

	L1	L2	L3	rainplusirri	Rain	Irrigation	vwc_10	vwc_30	vwc_54
2017-01-01	0.0	0.0	0.0	0.0	0.0	0.0	NaN	24.80	18.97
2017-01-01	0.0	0.0	0.0	0.0	0.0	0.0	NaN	24.81	18.96
2017-01-01	0.0	0.0	0.0	0.0	0.0	0.0	NaN	24.92	18.92
2017-01-01	0.0	0.0	0.0	0.0	0.0	0.0	NaN	25.03	18.92
2017-01-01	0.0	0.0	0.0	0.0	0.0	0.0	NaN	25.01	18.92
2017-01-01	0.0	0.0	0.0	0.0	0.0	0.0	NaN	24.88	18.92
2017-01-01	0.0	0.0	0.0	0.0	0.0	0.0	NaN	25.02	18.92
2017-01-01	0.0	0.0	0.0	0.0	0.0	0.0	NaN	24.80	18.92
2017-01-01	0.0	0.0	0.0	0.0	0.0	0.0	NaN	24.80	18.92
2017-01-02	0.0	0.0	0.0	0.0	0.0	0.0	NaN	24.80	18.92
2017-01-02	0.0	0.0	0.0	0.0	0.0	0.0	NaN	24.80	18.97
2017-01-02	0.0	0.0	0.0	0.0	0.0	0.0	NaN	24.90	18.96

Figure 11. Example showing the gaps observed in the volumetric water content data at Dorie, “NaN” represents gaps.

- **Methven lysimeters (Ashburton-Lyndhurst GW allocation zone)**

Only two values were considered outliers and removed from the analysis since they were recorded by the soil moisture sensors as negative values. At this location, two missing values were observed in the recharge dataset and were recorded as 0, since the other two lysimeters did not record recharge on the same day either (Figure 12). The missing points in the soil moisture data were filled by averaging the values recorded by the two remaining soil moisture sensors (At this location, three soil moisture sensors were located at 10 cm depth).

```
In [25]: df_methven.loc[(np.isnan(df_methven["L1"]))]
```

```
Out[25]:
```

	L1	L2	L3	rainplusirri	Rain	Irrigation	vwc_10_1	vwc_10_2	vwc_10_3
date									
2011-05-27	NaN	0.0	0.0	0.0	0.0	0.0	42.37	44.85	44.35

```
In [26]: df_methven.loc[(np.isnan(df_methven["L2"]))]
```

```
Out[26]:
```

	L1	L2	L3	rainplusirri	Rain	Irrigation	vwc_10_1	vwc_10_2	vwc_10_3
date									
2015-05-01	0.0	NaN	0.0	0.0	0.0	0.0	35.94	36.11	35.46

Figure 12. NaN (i.e. missing) values detected in the recharge dataset at Methven.

- **Dunsandel lysimeters (Rakaia-Selwyn GW allocation zone)**

3 outliers were observed in the volumetric water content dataset (Figure 13), which are attributed to instrumental errors. These three were replaced by the average of the other two soil moisture sensors which are located at the same depth (10 cm).

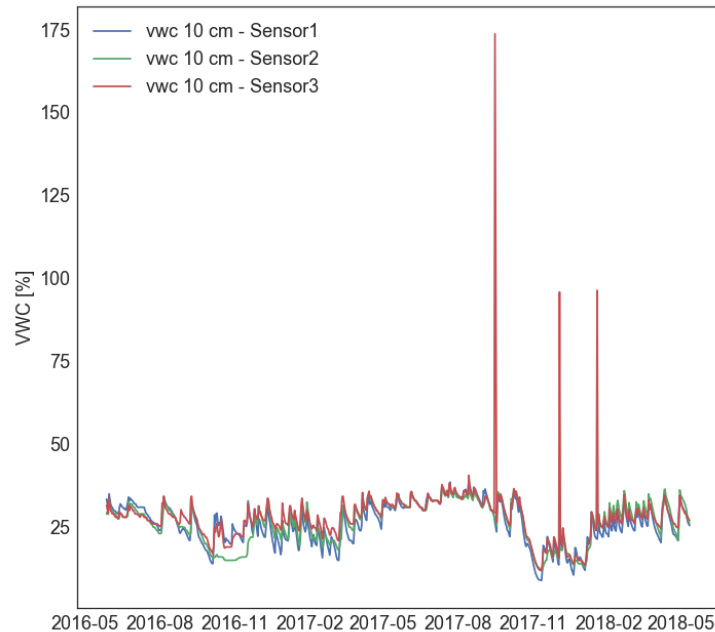


Figure 13. VWC outliers recorded by one of the soil moisture sensors at Dunsandel.

Table 3 shows an overview of the findings during the quality control procedure. In general, the dataset for all three locations was fairly complete and outliers were only observed for the Methven and Dunsandel lysimeters. The gap analysis and gap filling procedure is summarized in Table 3.

Table 3. Overview of the gaps and outliers observed in the dataset.

Parameter	Location						Gap filling method/ Replacing outliers
	Dorie	Methven	Dunsandel	Dorie	Methven	Dunsandel	
	Gaps observed?			Outliers?			
Recharge [mm]	No	2	No	No	No	No	The missing values were replaced by the average of the two remaining values recorded at the same time.
R + I [mm]	No	No	2	No	No	No	Replaced by 0
Vwc_10cm [%]	*Yes(1 2)	**Yes(62 <sup>1</sup> , 72 <sup>2</sup> , 34904 <sup>3</sup> )	No	No	**Yes	**Yes (3)	* Linear Regression **Average of measurements
Vwc_30cm [%]	Yes (307)	N/A.	N/A.	No	N/A	N/A	Linear Regression
Vwc_54cm [%]	Yes (3)	N/A.	N/A	No	N/A	N/A	Average of previous daily measurements
PET [mm/d]	No	No	No	No	No	No	-

\*\* At Methven and Dunsandel three measurements of volumetric water content were recorded by three different probes <sup>1,2,3</sup> (all of them located at the same depth – 10 cm), therefore, where gaps were observed, that value was replaced by the average of the two remaining values recorded by the other two probes. N/A: Data not available.

### 5.1.2 Time series analysis

- “Complete” data overview

Figure 14, Figure 15 and Figure 16 show a general overview of the datasets after the quality control procedure at Dorie, Dunsandel and Methven, respectively. These datasets were used for the time series analysis and the construction of different artificial neural networks. However, the recharge value used for the analysis was the result of averaging the measurements that were available at the three lysimeters at each location. In general, the behaviour of the recharge component measured at the three locations showed a similar pattern, where most of the recharge is observed during autumn and winter, followed by spring-recharge and finally, the summer season with the least amount of recharge. LSR measured at Dunsandel had the highest mean daily values, followed by Methven, and Dorie with the lowest recharge. In terms of rainfall and irrigation, the behaviour is equal to that observed for LSR, meaning that the rainfall and irrigation measured at Dunsandel had higher mean daily values when compared to the measurements at Dorie and Methven. On average, PET patterns showed a fairly equal behaviour across the sites. Volumetric water content at 10 cm depth had a higher variation at Dunsandel and Methven, being this parameter an indicator of plant water use and the changes in water content induced by precipitation events (either rainfall or irrigation).

At Dorie, from 9 July 2010 to 31 December 2017 the three lysimeters measured mean daily recharge in a range from 0 to 40.97 mm d<sup>-1</sup> and averaged 0.405 mm recharge per day (Table 4).

Table 4. Descriptive statistics of the data measured at Dorie.

	Dorie lysimeters							
	L [mm/d]	Rain and Irrigation [mm/d]	Rain [mm/d]	Irrigation [mm/d]	PET [mm/d]	vwc_10 [%]	vwc_30 [%]	vwc_54 [%]
Mean	0.405	2.575	1.808	0.773	2.286	31.594	25.362	22.067
$\sigma$	2.183	5.722	5.43	2.197	1.736	5.568	4.206	3.189
Median	0	0	0	0	1.8	32.130	24.641	22.222
Min	0	0	0	0	0	18.49	18.148	15.17
Max	40.97	71.6	71.6	17.6	9.6	45.886	41.978	38.792

\*\* L: Recharge, PET: Potential evapotranspiration, vwc\_10: Volumetric water content at 10 cm depth, vwc\_30: VWC at 30 cm depth, vwc\_54: VWC at 54 cm depth,  $\sigma$ : Standard Deviation.

Rainfall and irrigation ranged from 0 to 71.6 mm d<sup>-1</sup>, whereas the PET varied between 0 and 9.6 mm d<sup>-1</sup>. As can be seen in Figure 14, most of the recharge occurred out of the irrigation season, when the PET was lower. The highest recharge records were observed in the winter of 2013 and 2017, being triggered by rainfall events above 40 mm d<sup>-1</sup>.

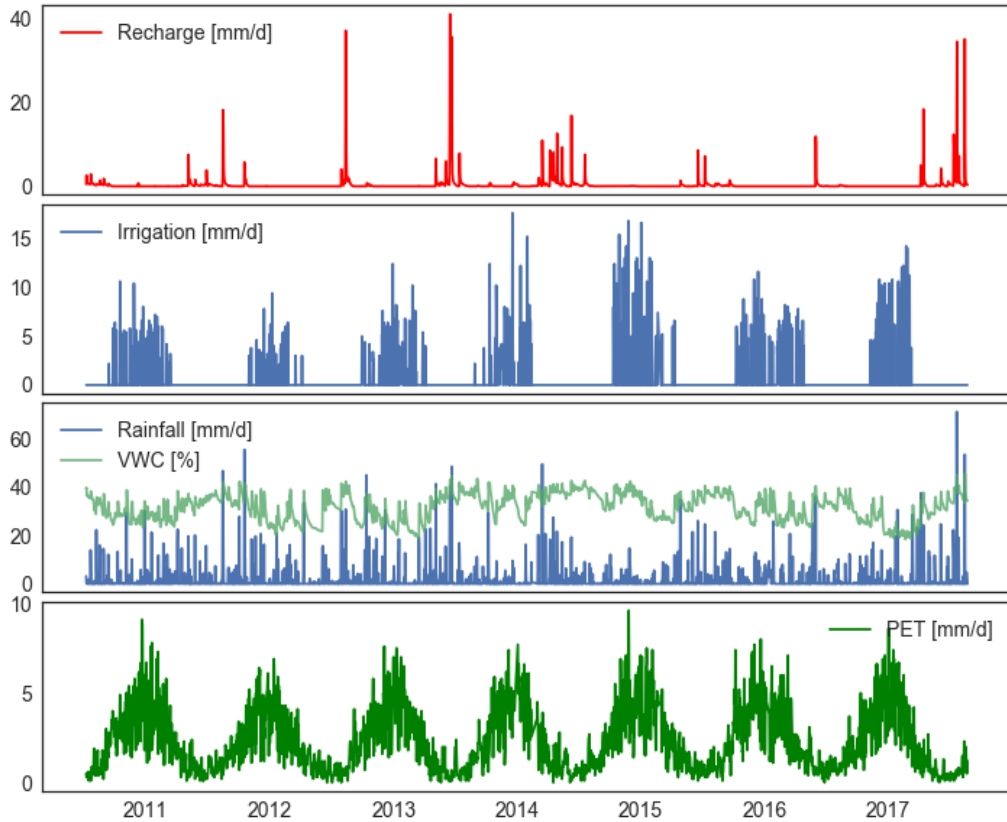


Figure 14. Dataset after the QC procedure at Dorie

At Dunsandel, from 28 May 2016 to 11 May 2018, the lysimeters measured mean daily recharge in a range of 0 to 72.62 mm d<sup>-1</sup> and averaged 2.078 mm recharge per day (Table 5).

Table 5. Descriptive statistics of the data measured at Dunsandel.

Dunsandel lysimeters						
	L	Rain and	Rain	Irrigation	PET	wvc_10
	[mm/d]	Irrigation [mm/d]	[mm/d]	[mm/d]	[mm/d]	[%]
Mean	2.078	4.07	3.459	0.61	2.427	26.955
$\sigma$	7.241	10.403	9.632	4.434	1.821	6.104
Median	0.032	0.2	0	0	2	27.604
Min	0	0	0	0	0	10.954
Max	72.618	80	80	58	8.7	75.826

\*\* L: Recharge, PET: Potential evapotranspiration, wvc\_10: Volumetric water content at 10 cm depth,  $\sigma$ : Standard Deviation.

Rainfall and irrigation ranged between 0 and 80 mm d<sup>-1</sup>, with a considerable standard deviation of 10.4 mm d<sup>-1</sup>. On the other hand, PET was on average 2.42 mm d<sup>-1</sup>, which is fairly similar to the PET observed at Dorie. 8.7 mm d<sup>-1</sup>, which was the maximum amount of water lost due to evapotranspiration. As can be observed in

Figure 15, Dunsandel lysimeters were the most responsive in terms of recharge. Infiltration was observed at this location across all seasons, during irrigated and not irrigated periods. The largest recharge event was recorded at the end of the winter of 2017. On that day, a large rainfall event was also recorded (i.e. more than 50 mm of rain).

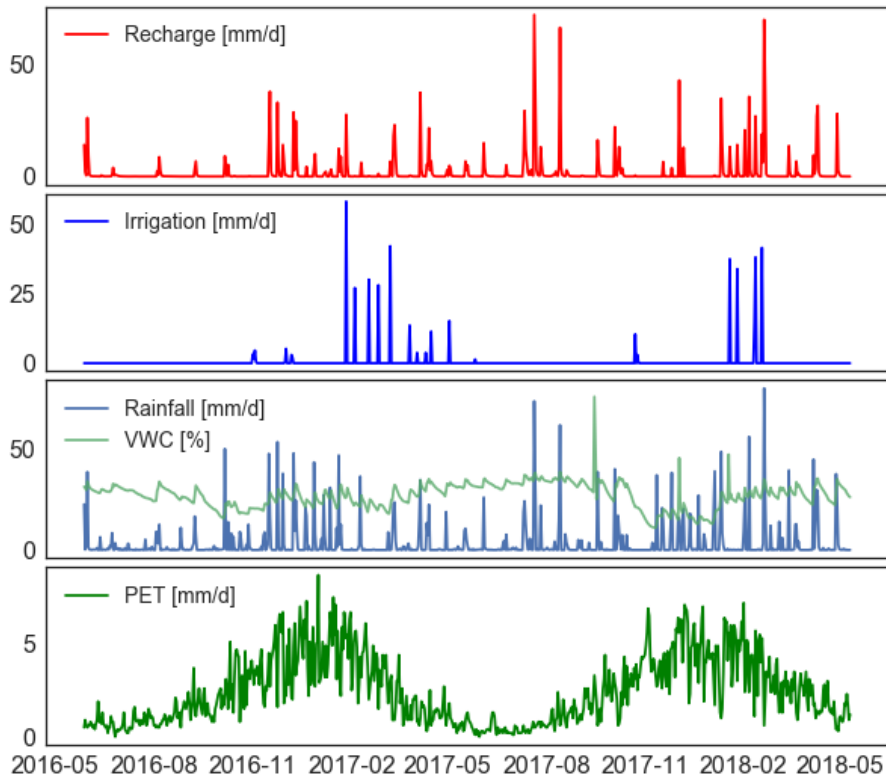


Figure 15. Dataset utilised in the analysis at Dunsandel

At Methven, from 11 January 2011 to 31 May 2018, the lysimeters averaged mean daily recharge of 0.976 mm, in a range of 0 to 94.95 mm d<sup>-1</sup> (Table 6). The largest rainfall event (134.6 mm) occurred on 21 July 2017, and triggered the largest recharge event observed across all locations. Similar to Dorie, recharge occurred mostly out of the irrigation season, although recharge was also recorded a few times during irrigation events. Evapotranspiration losses ranged from 0 to 9.2 mm d<sup>-1</sup> with the same behaviour previously observed at the other two locations. Volumetric water content measured at 10 cm depth, showed a mean daily value of 36.67% with a variation of 6.041 (%). Being both values higher than those observed at Dorie, where both irrigation and rainfall are lower both in frequency and quantity.

Table 6. Descriptive statistics of the data measured at Methven

Methven lysimeters						
	L [mm/d]	Rain and Irrigation [mm/d]	Rain [mm/d]	Irrigation [mm/d]	PET[mm/d]	vwc_10 [%]
Mean	0.976	3.028	2.792	0.217	2.201	36.672
$\sigma$	4.105	7.19	7.169	1.161	1.614	6.041

Median	0	0	0	0	1.8	37.634
Min	0	0	0	0	0	18.924
Max	94.954	134.6	134.6	12.4	9.2	47.742

\*\* L: Recharge, PET: Potential evapotranspiration, vwc\_10: Volumetric water content at 10 cm depth,  $\sigma$ : Standard Deviation.

Figure 16 shows the seasonal patterns of recharge across the study period. In general, the same behaviour previously observed at the other two locations is observed, where most of the recharge occurs during the autumn and the winter, with some spring-recharge recorded, (e.g. 2017 spring). The largest recharge event also matches both the largest rainfall event, and the winter season, where evapotranspiration losses are minimal.

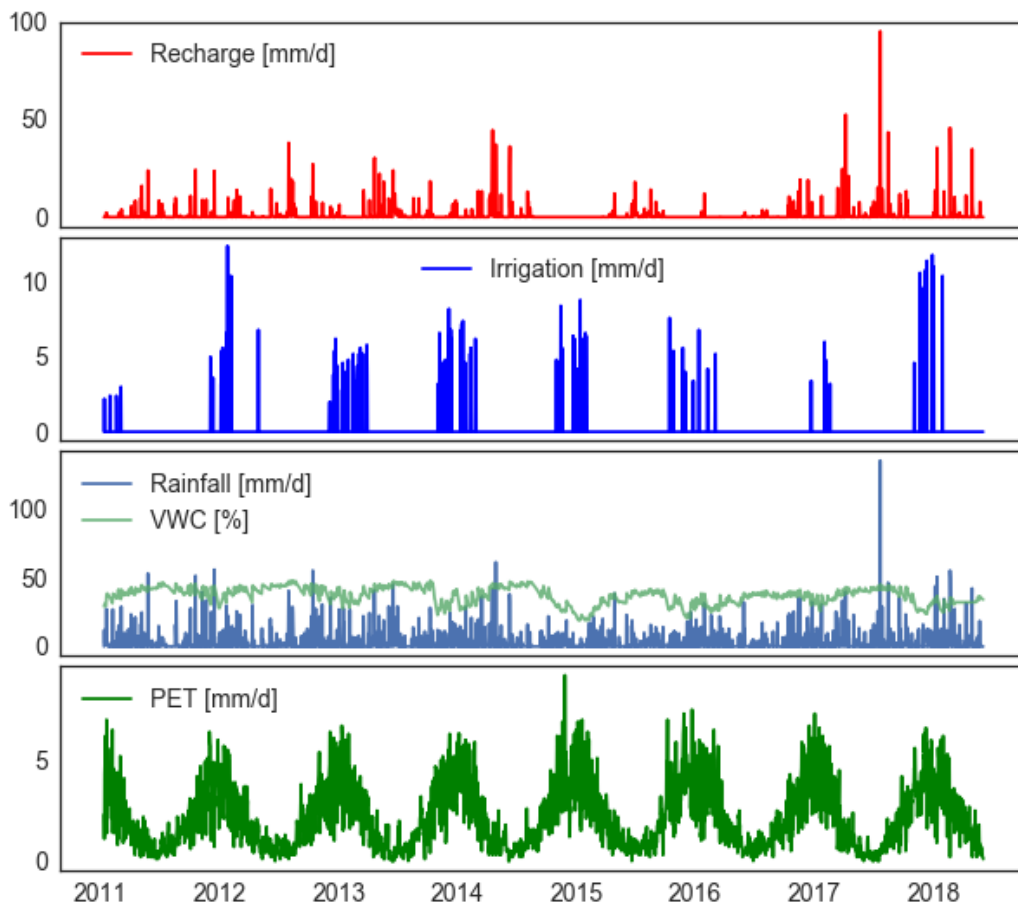


Figure 16. Dataset utilised in the analysis at Methven

- Recharge variability across sites and seasons

Table 7 shows the cumulated values for recharge, rainfall/irrigation and PET across the seasons at the three lysimeter locations. Since the stations were not set up at the same time, every measurement period was different, however, the overall patterns with regard to recharge variability are evident. At Dorie, the total amount of recharge is less than half to the one measured at Methven within a similar period of time

(approximately 7 years). Also, the Dorie site shows a total recharge lower than the one recorded at Dunsandel, even though the dataset at the latter only entails approximately two years of measurements. From a seasonal perspective, the total amount of recharge shows a clear pattern, where most of the recharge is recorded during the winter and the autumn, followed by the spring and the summer seasons. However, differences can be noticed when comparing the total amount of spring recharge at Dorie (i.e. 46.624 mm) with measured-recharge at Methven (i.e. 391.754 mm) for the same season for a similar time period. These differences may be attributed to the largest total amount of precipitation at Methven, lower PET, and more responsive soils in terms of recharge at this location.

Recharge is recorded across every season at Dunsandel. The largest amount of recharge was observed in the summer season, mainly due to the larger-than-usual amounts of irrigation applied. At this location, soils are well drained (loamy-like) with a low PAW (ranging from 53 mm to 80 mm), which reduces the availability to retain water. For this reason, irrigation occurs more frequently and in larger quantities.

In comparison, the total amount of recharge measured at the Dunsandel lysimeters account for approximately 56% of the total recharge at Methven, though the period of measurement at Dunsandel accounts for 5 years less. Also, Dunsandel measured-recharge is larger compared to the total recharge observed at Dorie. As observed in Table 7, groundwater recharge behaves differently at each location both in terms of frequency and quantity. Given that PET shows a similar behaviour across the sites, the observed differences in GW recharge across sites can be attributed to the differences in soil type and rainfall/irrigation amounts.

Table 7. Cumulated values of recharge, rainfall/irrigation and PET across the lysimeter locations for the entire study period.

<b>DORIE LYSIMETERS</b>	From	09/07/2010	to	31/07/2017	<b>Total</b>
	<b>Summer</b>	<b>Autumn</b>	<b>Winter</b>	<b>Spring</b>	
Recharge [mm]	16.053	243.915	727.671	46.624	1034.263
Rainfall + Irrigation [mm]	2017	1590.8	1476.2	1628.6	6712.6
PET [mm]	2454.6	1058.1	506.9	2159.5	6179.1
<b>METHVEN LYSIMETERS</b>	From	11/01/2011	to	02/06/2018	<b>Total</b>
	<b>Summer</b>	<b>Autumn</b>	<b>Winter</b>	<b>Spring</b>	
Recharge [mm]	422.378	860.309	960.8	391.754	2635.241
Rainfall + Irrigation [mm]	2699.6	2136.2	1606.8	1733.8	8176.4
PET [mm]	2645.7	1118.7	451.8	1725.6	5941.8
<b>DUNSANDEL LYSIMETERS</b>	From	28/05/2016	to	11/05/2018	<b>Total</b>
	<b>Summer</b>	<b>Autumn</b>	<b>Winter</b>	<b>Spring</b>	
Recharge [mm]	533.845	354.112	354.101	235.616	1477.674
Rainfall + Irrigation [mm]	1158.4	661.2	444.6	629.6	2893.8
PET [mm]	787.7	272.6	137.5	527.9	1725.7

### 5.1.3 Model development

In order to upscale the point measurements it is necessary to develop a model capable of predicting recharge to the GW allocation zone scale. For model development, two different approaches were considered.

#### 5.1.3.1 Approach 1

Step (i): One neural network for each location

Table 8 shows the results after testing the various combinations of parameters (inputs), structures (different number of hidden neurons) and different sets of data for training (i.e. data from every season; only data from previous summers; autumns only; winters only and; springs only) at Methven. One evident pattern is that using data out of every seasons tends to outperform the neural networks trained with data from every season separately, with the general exception of NNs trained with data only from previous winters. This was expected, since most of the recharge occurs during the winter, which provides the NN model with “more examples to learn” from, in comparison with a summer training dataset, where most of the measured-recharge is either zero or very low. This means that the neural network trained on summer data is capable to predict the non-occurrence of recharge i.e. it learns to predict zero values, however, since no peak recharge events occur during the summer, the network fails to predict e.g. peak events of recharge occurring during the autumn or the winter. When employing data only from previous springs the predictive performance at Methven was unsatisfactory with  $R^2$  values ranging from 0.1 up to 0.6. In terms of inputs, the inclusion of volumetric water content tends to outperform the models employing only rainfall and PET data.

Table 8. Results of developing a feed forward neural network employing data collected at Methven only.

		METHVEN									
Parameters	Structure	ALL SEASONS		SUMMER		AUTUMN		WINTER		SPRING	
		Test - $R^2$	Test MAE								
rainplusirri ; wvc_10 ; PET(mm)	3-20-1	0.685	0.796	0.416	0.8	0.584	0.99	0.715	1.242	0.032	0.811
	3-25-1	0.546	0.964	0.503	0.766	0.725	0.771	0.592	1.476	0.339	0.958
	3-30-1	0.688	0.725	0.184	0.773	0.659	0.875	0.428	1.477	0.295	0.688
	3-35-1	0.735	0.645	0.092	0.758	0.7	0.86	0.703	1.333	0.109	0.706
	3-40-1	0.678	0.765	0.07	0.864	0.606	1.02	0.644	1.313	0.171	0.866
	3-45-1	0.699	0.705	0.117	0.903	0.25	1.119	0.769	1.253	0.046	0.875
	3-50-1	0.602	0.866	0.196	0.725	0.601	1.03	0.776	1.26	0.24	0.65
	3-55-1	0.708	0.702	0.083	0.838	0.668	0.844	0.608	1.415	0.567	0.691
	3-60-1	0.736	0.652	0.465	0.789	0.227	1.096	0.693	1.22	0.544	0.736
	3-65-1	0.711	0.704	0.436	0.722	0.511	1.061	0.69	1.25	0.595	0.652
	3-70-1	0.572	0.892	0.097	0.673	0.485	0.994	0.533	1.396	0.619	0.638
3-63-1	0.738	0.627	0.465	0.776	0.63	0.962	0.409	1.53	0.562	0.697	

	3-15-1	0.698	0.678	0.43	0.794	0.511	0.933	0.462	1.263	0.554	0.777
	3-9-1	0.702	0.703	0.483	0.835	0.646	1.012	0.764	1.299	0.524	786
	3-5-1	0.712	0.704	0.408	0.941	0.709	0.922	0.765	1.362	0.576	0.732
	3-13-1	0.703	0.698	0.12	1.008	0.355	1.445	0.238	1.693	0.515	0.839
	3-20-100-1	0.734	0.603	0.439	0.798	0.678	0.877	0.566	1.429	0.384	0.764
rainplusirri ; vwc_10	2-20-1	0.686	0.743	0.352	0.763	0.653	0.855	0.626	1.422	0.508	0.752
	2-25-1	0.678	0.751	0.425	0.745	0.604	0.969	0.722	1.247	0.103	0.596
	2-30-1	0.613	0.871	0.143	0.954	0.352	1.085	0.687	1.379	0.417	0.866
	2-35-1	0.688	0.712	0.435	0.765	0.506	1.163	0.556	1.504	0.599	0.625
	2-40-1	0.676	0.698	0.364	0.872	0.67	0.878	0.794	1.237	0.586	0.624
	2-45-1	0.733	0.644	0.431	0.756	0.745	0.708	0.621	1.38	0.113	0.603
	2-50-1	0.693	0.716	0.127	0.679	0.623	1.013	0.705	1.306	0.305	0.728
	2-55-1	0.69	0.713	0.094	0.753	0.684	0.87	0.295	1.524	0.646	0.572
	2-60-1	0.678	0.744	0.167	0.795	0.656	0.959	0.621	1.368	0.638	0.599
	2-65-1	0.717	0.68	0.212	0.776	0.665	0.88	0.684	1.223	0.032	0.719
	2-70-1	0.652	0.765	0.148	0.773	0.673	0.919	0.514	1.541	0.489	0.767
	2-63-1	0.727	0.652	0.418	0.798	0.688	0.867	0.688	1.22	0.174	0.818
	2-15-1	0.664	0.791	0.41	0.822	0.608	1.087	0.762	1.372	0.545	0.739
	2-13-1	0.493	0.973	0.165	0.889	0.649	0.976	0.591	1.351	0.574	0.657
	2-20-100-1	0.453	0.919	0.426	0.734	0.546	0.958	0.63	1.413	0.568	0.677
rainplusirri ; PET (mm)	2-20-1	0.518	0.973	0.255	0.869	0.497	1.079	0.657	1.402	0.503	0.724
	2-25-1	0.569	0.894	0.404	0.87	0.518	1.022	0.761	1.31	0.066	0.691
	2-30-1	0.505	0.925	0.138	1.004	0.294	1.146	0.596	1.547	0.32	0.945
	2-35-1	0.578	0.84	0.394	0.917	0.462	1.137	0.683	1.353	0.511	0.698
	2-40-1	0.508	0.956	0.447	0.851	0.547	0.956	0.786	1.278	0.514	0.697
	2-45-1	0.581	0.829	0.399	0.88	0.509	1.045	0.647	1.381	0.091	0.584
	2-50-1	0.554	0.874	0.129	0.699	0.534	1.045	0.722	1.3	0.191	0.662
	2-55-1	0.57	0.845	0.092	0.745	0.522	0.989	0.283	1.628	0.509	0.718
	2-60-1	0.572	0.855	0.132	0.809	0.555	0.95	0.738	1.361	0.515	0.699
	2-65-1	0.586	0.828	0.216	0.859	0.515	0.984	0.606	1.371	-0.08	0.723
	2-70-1	0.57	0.857	0.133	0.834	0.527	0.991	0.555	1.596	0.379	0.821
	2-63-1	0.623	0.783	0.283	0.87	0.542	0.958	0.747	1.301	0.038	0.737
	2-15-1	0.555	0.893	0.362	0.919	0.505	1.055	0.724	1.467	0.452	807
	2-13-1	0.403	1.117	0.064	0.989	0.516	1.103	0.776	1.4	0.476	0.774
	2-20-100-1	0.26	1.059	0.453	0.819	0.457	1.057	0.786	1.239	0.472	0.754

Results of testing a NN at Dunsandel are shown in Table 9. Performance was relatively high with  $R^2$  values ranging between 0.6 and 0.8 for every set of data. However, the networks trained with data collected in previous spring seasons showed  $R^2$  values were lower than zero i.e. in this case the models failed for every prediction. Also, the NNs using the VWC at 10 cm depth as part of the inputs outperformed the ones utilising only rainfall/irrigation and PET data as inputs. At this location, model performance when training with data from the summer period was satisfactory ( $R^2 = 0.867$  and  $MAE = 1.766$ ) since there is recharge occurring at this location during the summer, which is mainly triggered by irrigation.

Table 9. Results of developing a feed forward neural network employing data collected at Dunsandel only

DUNSANDEL											
Parameters	Structure	ALL SEASONS		SUMMER		AUTUMN		WINTER		SPRING	
		Test - R^2	Test MAE	Test - R^2	Test MAE	Test - R^2	Test MAE	Test - R^2	Test MAE	Test - R^2	Test MAE
rainplusirri ; wvc_10 ; PET(mm)	3-35-1	0.801	1.29	0.627	2.852	0.598	2.259	0.816	1.666	<0	
	3-38-1	0.793	1.332	0.709	2.138	0.351	2.619	0.194	2.53	<0	
	3-37-1	0.815	1.234	0.671	2.296	0.768	1.62	-0.036	2.625	<0	
	3-36-1	0.801	1.314	0.723	2.224	0.428	2.474	0.545	2.265	<0	
	3-42-1	0.806	1.234	0.53	3.055	0.591	2.165	0.098	2.499	<0	
	3-44-1	0.8	1.26	0.867	1.766	0.348	2.532	0.932	1.177	<0	
	3-45-1	0.807	1.252	0.753	2.111	0.69	1.928	0.112	2.641	<0	
	3-10-1	0.789	1.423	0.783	2.16	0.656	2.093	0.068	2.628	<0	
	3-40-1	0.798	1.246	0.723	2.471	0.71	1.862	-0.001	2.732	<0	
	3-41-1	0.805	1.247	0.643	2.776	0.413	2.39	0.129	2.466	<0	
	3-79-1	0.813	1.237	0.099	3.159	0.747	1.711	0.596	2.076	<0	
	3-27-1	0.794	1.315	0.767	2.323	0.591	2.273	0.89	1.448	<0	1.333
	3--3-1	0.787	1.144	<0		<0		<0		<0	
	3--11-1	0.797	1.279	<0		<0		0.932	1.168	<0	
	3--13-1	0.799	1.272	<0		<0		<0		<0	
	3--5-1			<0		0.73	1.855	<0		<0	
	3--7-1			0.765	2.217	0.737	1.799	<0		<0	
	3--9-1			<0		<0		0.94	1.1	0.007	0.97
3--15-1			0.808	1.883	<0		<0		<0		
3-25-1	0.788	1.329	<0		-0.034	3.077	0.236	2.707	<0	1.007	
rainplusirri ; wvc_10	2-35-1	0.801	1.185	0.78	1.99	0.191	2.695	0.864	1.472	<0	
	2-38-1	0.802	1.203	0.554	2.964	-0.003	2.703	0.387	2.385	<0	
	2-37-1	0.802	1.19	0.761	2.214	0.324	2.398	0.528	2.202	<0	
	2-36-1	0.806	1.176	0.014	2.968	0.782	1.541	0.599	2.238	<0	
	2-42-1	0.803	1.136	0.833	1.91	0.282	2.666	0.633	2.276	<0	
	2-44-1	0.804	1.13	0.846	1.795	0.245	2.541	0.877	1.457	<0	
	2-45-1	0.81	1.091	0.806	1.868	0.469	2.369	0.568	2.177	<0	
	2-10-1	0.799	1.167	0.641	2.966	0.637	2.282	0.138	2.342	<0	
	2-40-1	0.8	1.198	0.308	3.018	0.78	1.524	0.113	2.699	<0	
	2-41-1	0.808	1.122	0.794	1.764	0.23	2.713	0.218	2.597	<0	
	2-79-1	0.796	1.244	0.22	2.953	0.811	1.444	0.71	1.957	<0	
	2-27-1	0.803	1.153	0.826	1.715	0.692	1.933	0.272	2.197	<0	
	2-25-1	0.801	1.154	0.81	1.975	<0	2.617	0.87	1.475	<0	
rainplusirri ; PET (mm)	2-35-1	0.616	1.653	0.56	2.68	-0.075	2.899	0.816	1.694	<0	0.701
	2-38-1	0.623	1.614	0.441	3.454	<0	2.735	0.818	1.671	<0	0.765

2-37-1	0.617	1.625	0.504	3.195	-0.06	2.73	0.228	2.526	<0	
2-36-1	0.616	1.648	0.184	3.237	0.504	2.359	0.45	2.363	<0	
2-42-1	0.626	1.62	0.528	2.875	0.122	2.804	0.669	1.98	0.007	0.776
2-44-1	0.627	1.58	0.387	3.56	0.322	2.512	0.785	1.747	<0	
2-45-1	0.612	1.648	0.397	3.483	0.413	2.457	0.533	2.215	<0	
2-10-1	0.61	1.709	0.484	3.584	0.49	2.501	0.087	2.602	<0	
2-40-1	0.618	1.619	0.12	3.124	0.511	2.352	0.04	2.718	<0	
2-41-1	0.627	1.616	0.535	2.758	-0.091	2.897	-0.038	2.733	0.071	0.936
2-79-1	0.619	1.614	0.025	3.115	0.519	2.345	0.726	1.827	<0	
2-27-1	0.623	1.622	0.393	3.394	0.509	2.471	0.255	2.404	<0	
2-25-1	0.616	1.687	0.37	3.53	-0.049	2.74	0.735	1.869	<0	

Table 10 shows the results of model development at Dorie. For the model using 3 inputs (i.e. rainfall/irrigation, VWC at 10 cm depth and PET) performance was unsatisfactory, with  $R^2$  values from 0.169 to 0.464 when using “all seasons”, autumn and winter data for training. The models trained using data from the summer and spring seasons failed on every prediction i.e.  $R^2 < 0$ . The same results were observed for the NNs using rainfall/irrigation and VWC as inputs. In comparison, it was observed that performance was reduced approximately 10% for the NNs using only PET and Rainfall/Irrigation data as inputs when compared to the ones using those two plus the VWC measured at 10 cm depth.

Table 10. Results of developing a feed forward neural network employing data collected at Dorie only  
DORIE - RAKAIA

Parameters	Structure	ALL SEASONS		SUMMER		AUTUMN		WINTER		SPRING	
		Test - $R^2$	Test MAE								
rainplusirri ; wvc_10 ; PET(mm)	3-20-1	0.227	0.57	<0	0.312	0.296	0.499	0.373	1.018	<0	
	3-25-1	0.24	0.641	0.006		0.325	0.48	0.388	1.095	<0	
	3-30-1	0.208	0.57	<0		0.207	0.512	0.257	0.942	<0	
	3-35-1	0.25	0.587	<0		0.023	0.473	0.407	1.05	<0	
	3-40-1	0.367	0.559	<0		0.221	0.516	0.388	1.128	<0	
	3-45-1	0.315	0.586	<0		0.252	0.479	0.386	1.078	<0	
	3-50-1	0.411	0.513	<0		0.261	0.48	0.16	0.872	<0	
	3-55-1	0.378	0.544	<0		0.266	0.522	0.392	1.035	<0	
	3-60-1	0.338	0.589	<0		0.307	0.501	0.398	1.039	<0	
	3-65-1	0.313	0.571	<0		0.177	0.433	0.256	0.902	<0	
	3-70-1	0.464	0.479	<0		0.179	0.489	0.395	1.068	<0	
	3-63-1	0.431	0.502	<0		0.212	0.47	0.316	0.96	<0	
	3-15-1	0.357	0.564	<0		0.336	0.61	0.43	1.036	<0	
	3-13-1	0.277	0.676	<0		0.194	0.556	0.238	1.053	<0	
	3-5-1	0.408	0.504	<0		0.238	0.596	0.399	1.163		
	3-20-100	0.169	0.504	<0		0.197	0.464	0.422	0.998	<0	

rainplusirri ; vwc_10	2-20-1	0.032	0.522	<0	0.118	0.493	0.267	0.977	<0
	2-25-1	0.199	0.578	<0	0.249	0.514	0.354	1.057	<0
	2-30-1	0.22	0.6	<0	0.18	0.617	0.381	1.083	<0
	2-35-1	0.333	0.581	<0	0.264	0.513	0.401	1.039	<0
	2-40-1	0.318	0.585	<0	0.205	0.53	0.349	1.134	<0
	2-45-1	0.458	0.497	<0	0.322	0.443	0.382	1.107	<0
	2-50-1	0.352	0.603	<0	0.186	0.499	0.37	1.117	<0
	2-55-1	0.352	0.574	<0	0.244	0.46	0.365	1.113	<0
	2-60-1	0.403	0.514	<0	0.11	0.428	0.119	0.899	<0
	2-65-1	0.365	0.535	<0	0.279	0.432	0.264	1.021	<0
	2-70-1	0.383	0.528	<0	0.318	0.482	0.318	1.038	<0
	2-63-1	0.366	0.538	<0	0.114	0.483	0.129	0.918	<0
	2-15-1	0.227	0.555	<0	0.244	0.465	0.38	1.093	<0
	2-13-1	0.227	0.606	<0	0.285	0.464	0.405	1.134	<0
	2-20-100	0.177	0.587	<0	0.229	0.502	0.091	0.891	<0
Rainplusirri; PET (mm)	2-20-1	0.08	0.602	<0	0.088	0.62	0.217	0.995	<0
	2-25-1	0.165	0.581	<0	0.149	0.601	0.305	1.066	<0
	2-30-1	0.304	0.573	<0	0.082	0.742	0.286	1.149	<0
	2-35-1	0.215	0.627	<0	0.153	0.57	0.297	1.153	<0
	2-40-1	0.299	0.588	<0	0.124	0.616	0.308	1.132	<0
	2-45-1	0.307	0.582	<0	0.155	0.582	0.325	1.088	<0
	2-50-1	0.296	0.586	<0	0.122	0.502	0.326	1.086	<0
	2-55-1	0.303	0.578	<0	0.125	0.567	0.31	1.116	<0
	2-60-1	0.306	0.573	<0	0.016	0.497	0.054	0.922	<0
	2-65-1	0.285	0.588	<0	0.155	0.597	0.267	1.059	0.01
	2-70-1	0.294	0.578	<0	0.146	0.592	0.169	0.991	<0
	2-63-1	0.291	0.599	<0	<0		0.07	0.951	<0
	2-15-1	0.203	0.64	<0	0.137	0.568	0.314	1.131	<0
	2-13-1	0.199	0.616	<0	0.123	0.611	0.311	1.12	<0
	2-20-100	0.114	0.602	<0	0.069	0.575	0.033	0.9	<0

Overall, the Dunsandel NN yielded the best performance, i.e. at this location recharge occurred more rapidly and frequently, followed by Methven and finally Dorie. At the latter, the higher soil water retention ability and good irrigation management induced a lower amount of lysimeter-measured recharge, which potentially induced more difficulty for the model to match measured recharge. Also, the best performance at every location was obtained by employing three inputs (rainfall/irrigation, PET and 10 cm depth soil moisture) and training data from all seasons (see Table 11). At every location the best model was selected in relation to both predictive performance and parsimony. In terms of complexity, every NN showed a different pattern, being the one developed for Dunsandel the most complex one with 11 neurons in the hidden layer, followed by the Methven NN with 9 hidden neurons and the Dorie NN with 5 hidden neurons.

Table 11. Results of testing the NN on a seasonal basis

Dorie	All seasons				Summer				Autumn				Winter				Spring			
	O.R	P.R	R2	MAE	O.R	P.R	R2	MAE	O.R	P.R	R2	MAE	O.R	P.R	R2	MAE	O.R	P.R	R2	MAE
All	-	-	0.51	0.45	6.02	29	<0	0.14	244	213	0.3	0.41	728	603	0.6	0.867	43.62	154	<0	0.29
Sum	1021	0	<0	0.44			0	0.04	244	0	<0	0.42	728	0	<0	1.099	43.62	1.39	<0	0.09
Aut	1021	668	0.3	0.65	6.02	84	<0	0.49			0.4	0.58	728	372	0.3	0.984	43.62	174	<0	0.51
Wint	1021	1114	0.3	0.97	6.02	81	<0	1	244	66.9	<0	0.91			0.6	1.004	43.62	210	<0	0.98
Spr	1021	122	0.07	0.42	6.02	11	<0	0.08	244	47.6	0.1	0.41	728	109	0	1.001			0.4	0.11

rech\_season

(aut and win) (3-4-1)	1021	1161	0.59	0.43	6.02	31	<0	0.15	244	251	0.4	0.36	728	685	0.7	0.805	43.62	194	<0	0.32
-----------------------	------	------	------	------	------	----	----	------	-----	-----	-----	------	-----	-----	-----	-------	-------	-----	----	------

Methven	All seasons				Summer				Autumn				Winter				Spring			
	O.R	P.R	R2	MAE	O.R	P.R	R2	MAE	O.R	P.R	R2	MAE	O.R	P.R	R2	MAE	O.R	P.R	R2	MAE
All	-	-	0.7	0.7	422	432	0.6	0.68	860	750	0.7	0.84	961	1036	0.8	1.111	391.8	478	0.7	0.57
Sum	2635	4011	0.56	1.3			0.5	0.84	860	1109	0.6	1.37	961	1669	0.6	2.063	391.8	767	0.6	0.98
Aut	2635	3790	0.68	1.1	422	721	0.6	0.86			0.7	0.92	961	1332	0.7	1.584	391.8	819	0.5	0.92
Wint	2635	2868	0.66	0.97	422	465	0.5	0.8	860	775	0.6	1.03			0.8	1.362	391.8	605	0.7	0.76
Spr	2635	1799	0.62	0.9	422	416	0.6	0.71	860	387	0.6	1.06	961	599	0.7	1.19			0.6	0.73

Dunsandel	All seasons				Summer				Autumn				Winter				Spring			
	O.R	P.R	R2	MAE	O.R	P.R	R2	MAE	O.R	P.R	R2	MAE	O.R	P.R	R2	MAE	O.R	P.R	R2	MAE
All	-	-	0.8	1.28	534	513	0.9	1.1	354	422	0.8	1.25	354	312	1	1.053	235.6	244	0.6	1.02
Sum	1478	2932	0.5	3.15			0.8	1.88	354	812	0.4	3.46	354	1120	0.4	4.99	235.6	453	<0	2.25
Aut	1478	1615	0.67	1.63	534	536	0.8	1.86			0.7	1.8	354	407	0.8	1.726	235.6	332	<0	1.59
Wint	1478	888	0.75	1.88	534	220	0.8	2.74	354	327	0.7	1.69			0.9	1.1	235.6	4.34	0.2	2.23
Spr	1478	737	0.07	2.42	534	265	0.1	3.47	354	143	0	2.33	354	165	0.1	2.169			0	0.97

\*\* O.R: Observed recharge; P.R: Predicted recharge; MAE: Mean absolute error

#### Step (ii): Transfer to other locations

The best NN for each location was tested with data collected at the other two locations. This was done in order to check whether the predictive ability of a given neural network is transferable to a different location where both precipitation amount and soil type are different. It is worth mentioning that an additional approach was considered at Dorie, where an extra NN was trained with data collected during the season with comparably high recharge at this site, thereby using data only from previous autumns and winters. From Table 12 it can be noticed that only the Methven NN was capable of predicting recharge at Dorie and Dunsandel with adequate accuracy ( $R^2 = 0.55$  and  $R^2 = 0.59$  respectively). The Dunsandel NN was not able to predict recharge when tested with data from Dorie ( $R^2 < 0$ ) and Methven ( $R^2 = 0.21$ ). Finally, the Dorie NN trained with data from the recharge season showed a reduction in performance of approximately 12% when compared to the NN trained with data from all seasons. Furthermore, the Dorie NN performance was

adequate when predicting recharge at Methven ( $R^2 = 0.61$ ), however, it showed a fairly poor performance ( $R^2 = 0.18$ ) predicting the high amounts of recharge measured at Dunsandel.

Table 12. Results of checking whether a NN developed with data from one location was able to predict recharge at a different location.

Location	Training	Dorie				Methven				Dunsandel			
		Test Period	01/01/2016	to	22/08/2017	Test Period	01/01/2017	to	02/06/2018	Test Period	01/01/2017	to	11/05/2018
		Test R2	Test MAE	O.R.	P.R.	Test R2	Test MAE	O.R.	P.R.	Test R2	Test MAE	O.R.	P.R.
Dorie	R.S. (3-4-1)	0.71	0.398	268.6	204.193	0.61	1.382	818	724.125	0.18	2.21	1164	192.692
	A.S. (3-5-1)	0.62	0.427	268.6	170.113	0.57	1.256	818	575.105	0.30	2.057	1164	200.776
Methven	A.S. (3-9-1)	0.55	0.618	268.6	204.722	0.80	0.95	818	607.341	0.59	1.79	1164	401.914
Dunsandel	A.S. (3-11-1)	<0	1.887	268.6	1056.587	0.21	3.378	818	1980.507	0.89	1.2	1164	1273.231

In order to check whether performance can be improved the training and testing datasets were switched (i.e. the NN were now trained with what used to be the testing set, and tested with what was used for training). The results (Table 13) show a percentage decrease in NN predictive performance of 22, 10 and 2 at Dorie, Methven and Dunsandel respectively. This reduction is likely due to the smaller amount of data now used for training. However, the results exhibit the same behaviour observed in Table 12, meaning that a NN developed at one location does not have the ability to predict groundwater recharge at a different location.

Table 13. Results of checking whether a NN developed with data from one location was able to predict recharge at a different location, after switching the training and testing datasets.

Location	Model	Dorie				Methven				Dunsandel			
		Test Period	09/07/2010	to	22/08/2017	Test Period	11/01/2011	to	02/06/2018	Test Period	28/05/2016	to	11/05/2018
		Test R2	Test MAE	O.R	P.R	Test R2	Test MAE	O.R	P.R	Test R2	Test MAE	O.R	P.R
Dorie	R.S. (3-4-1)	0.588	0.425	1021	1161.144	0.441	1.549	2635	5082.261	0.16	1.969	1478	202.602
	A.S. (3-5-1)	0.509	0.445	1021	999.421	0.563	1.124	2635	3435.912	0.281	1.85	1478	213.115
Methven	A.S. (3-9-1)	0.297	0.624	1021	983.729	0.719	0.801	2635	2695.978	0.565	1.596	1478	478.62
Dunsandel	A.S. (3-11-1)	<0	2.41	1021	5598.755	<0	3.526	2635	9180.68	0.875	1.102	1478	1491.033

\*\*R.S.: Recharge season, A.S.: All seasons, O.R.: Observed recharge, P.R.: Predicted Recharge

### 5.1.3.2 Approach 2: Step (i)

The next step was to evaluate a single neural network, testing its performance with data from the three locations, in order to assess whether one single model was capable to predict the spatial variability of recharge on a monthly basis. The inputs considered for analysis were rainfall/irrigation, PET, dominant soil texture and topsoil stoniness and results are shown in Table 14.

The NNs using the rainfall, PET and dominant soil texture as inputs, and 4 hidden neurons showed a high predictive performance, with an  $R^2$  of 0.86, 0.76 and 0.79 when tested at Methven, Dunsandel and Dorie respectively. However, they showed high values of MAE ranging between 12.27 and up to 20.51. Furthermore, the NNs employing the same three parameters plus the topsoil stoniness yielded a higher accuracy when matching monthly recharge observations with  $R^2$  values of 0.90, 0.75 and 0.88 when tested at Methven, Dunsandel and Dorie respectively. Though the increase in performance is less than 10% for a more complex model i.e. number and of hidden neurons increased from 4 to 10. Though NN predictive performance was higher on a monthly time scale, the mean absolute error (MAE) was high in every case, with values ranging from 12.46 up to 20.51 for the NN using 3 inputs, and from 8.94 up to 20.02 for the NN using the same 3 inputs plus the topsoil stoniness. These high values may be attributed to the effect of aggregating (i.e. adding up) the climatic parameters on a monthly basis, which led to consider a daily basis as the preferred way to carry on with the analysis.

Table 14. Results of testing one NN on a monthly basis, the dataset employed for training included information from the three locations.

Training Period:		2010-07-31 to 2016-12-31		Testing period:		2017-01-31 to 2018-05-31	
Inputs	Arch	R2 Methven	MAE Methven	R2 Dunsandel	MAE Dunsandel	R2 Dorie	MAE Dorie
rainfall, PET, soil dominant texture	3--3-1	0.45	23.43	0.11	39.40	0.66	13.16
	3--4-1	0.86	12.46	0.76	20.51	0.79	12.27
	3--5-1	0.71	16.51	0.57	27.36	0.75	13.03
	3--6-1	0.17	29.30	<0	45.08	0.48	15.18
	3--7-1	0.84	12.95	0.43	32.47	0.80	12.8
	3--8-1	0.89	11.83	0.69	24.36	0.81	11.39
	3--9-1	0.03	32.55	0.06	29.92	0.42	15.17
	3--10-1	0.89	11.98	0.26	40.36	0.82	11.36
rainfall, PET, soil dominant texture, topsoil stoniness	4--3-1	0.77	14.89	0.61	26.66	0.74	11.11
	4--4-1	0.44	23.23	0.34	34.30	0.47	14.52
	4--7-1	0.86	12.48	0.52	30.59	0.83	11.1
	4--8-1	0.89	11.33	0.64	25.37	0.86	9.47
	4--9-1	0.88	11.80	0.71	23.81	0.86	9.21
	4--10-1	0.90	10.93	0.75	20.02	0.88	8.94
	4--11-1	0.87	11.73	0.75	19.76	0.85	9.95
	4--12-1	0.86	12.33	0.45	30.14	0.81	10.97

Table 15 shows the results of testing different NN architectures and different inputs on a daily time scale. Different soil characteristics were considered as inputs for the model in order to check which one had a significant effect on the prediction of land surface recharge. As expected, the performance decreased 25%, 23% and 31% in comparison to the results from Table 14 when tested at Methven, Dunsandel and Dorie respectively. This variation can be attributed to the higher variability when testing the model with daily measures. Overall, the accuracy ( $R^2$ ) of the model ranged from 0.50 to 0.65 across the three sites, with the general pattern of showing the best performance at Methven, and the worst at Dorie. From Table 15, the best two structures are: the model having inputs of rainfall, PET and dominant soil texture and; the NN having the same inputs plus the topsoil stoniness. Although there was an increased accuracy of 3% when testing the latter at Methven, the performance decreased at Dorie and Dunsandel when compared to the results of the model having three inputs only (i.e. rainfall, PET and dominant soil texture). Also, the MAE increased when compared to the model with three inputs across all the locations.

Table 15. Results of testing one NN on a daily basis, the dataset employed for training included information from the three locations.

Inputs	Arch	R2	MAE	R2	MAE	R2	MAE
		Methven	Methven	Dunsandel	Dunsandel	Dorie	Dorie
rainfall, PET	2-3-1	0.37	1.58	0.27	2.20	0.37	0.98
	2-4-1	0.45	1.56	0.34	2.24	0.41	1.01
	2-5-1	0.63	1.29	0.48	1.97	0.52	0.88
	2-6-1	0.42	1.52	0.32	2.14	0.39	0.96
	2-7-1	0.32	1.61	0.23	2.28	0.34	0.94
	2-8-1	0.56	1.40	0.43	2.06	0.47	1.00
	2-9-1	0.47	1.49	0.36	2.14	0.44	0.97
	2-10-1	0.30	1.52	0.22	2.19	0.31	0.86
	2-11-1	0.53	1.43	0.40	2.08	0.47	0.96
	2-12-1	0.51	1.45	0.38	2.09	0.46	0.97
rainfall, PET, dominant soil texture	3-3-1	0.37	1.63	0.31	2.6	0.36	1.06
	3-4-1	0.65	1.23	0.58	2.13	0.54	0.29
	3-5-1	0.41	1.41	0.37	2.88	0.41	0.85
	3-6-1	0.60	1.31	0.50	2.24	0.51	0.8
	3-7-1	0.25	1.60	0.24	2.883	0.27	0.88
	3-8-1	0.13	1.62	0.11	3.19	0.18	0.83
	3-9-1	0.53	1.46	0.40	2.36	0.46	1.00
	3-10-1	0.59	1.33	0.45	2.36	0.49	0.92
	3-11-1	0.47	1.45	0.39	2.49	0.43	0.93
	3-12-1	0.55	1.43	0.43	2.35	0.47	0.99
rainfall, PET, dominant soil texture, topsoil stoniness	4-3-1	0.38	1.59	0.32	2.77	0.36	0.80
	4-4-1	0.43	1.64	0.37	2.85	0.38	0.90
	4-5-1	0.67	1.28	0.55	2.09	0.53	0.78
	4-6-1	0.52	1.52	0.42	2.46	0.45	0.89
	4-7-1	0.33	1.73	0.19	2.73	0.31	0.85
	4-8-1	0.46	1.56	0.40	2.45	0.42	0.92
	4-9-1	0.49	1.48	0.41	2.38	0.44	1.01
	4-10-1	0.59	1.47	0.46	2.17	0.49	0.93
	4-11-1	0.50	1.45	0.44	2.32	0.44	0.89
	4-12-1	0.63	1.30	0.51	2.00	0.50	0.82
rainfall, PET, soil dominant texture, topsoil stoniness, PAW	5-3-1	0.62	1.38	0.50	2.85	0.51	0.82
	5-4-1	0.34	1.79	0.29	2.30	0.35	0.84
	5-5-1	0.24	1.62	0.21	2.94	0.22	0.80
	5-6-1	0.37	1.64	0.22	3.01	0.32	0.82
	5-7-1	0.53	1.56	0.41	2.41	0.45	0.92
	5-8-1	0.31	1.63	0.29	2.72	0.31	0.89
	5-9-1	0.53	1.52	0.43	2.43	0.45	0.78
5-10-1	0.27	1.73	0.14	2.48	0.26	0.85	

	5--11-1	0.68	1.25	0.57	1.95	0.54	0.78
rainfall,	6--3-1	0.32	1.67	0.25	3.44	0.32	0.92
PET, soil	6--4-1	0.65	1.33	0.57	2.05	0.51	0.73
dominant	6--7-1	0.38	1.66	0.32	2.58	0.32	0.87
texture,	6--8-1	0.43	1.63	0.27	2.64	0.40	0.88
topsoil							
stoniness,	6--9-1	0.65	1.29	0.53	2.07	0.52	0.74
PAW,	6--10-1	0.62	1.39	0.47	2.13	0.51	0.81
drainage	6--11-1	0.47	1.58	0.40	2.50	0.42	0.91
class	6--12-1	0.32	1.82	0.27	2.73	0.35	0.87

### 5.1.3.3 Approach 2: Step (ii)

The NN having inputs of rainfall/irrigation, PET and dominant soil texture size with one hidden layer (and 4 hidden neurons) showed a balance regarding both predictive power and parsimony. However, the accuracy ( $R^2$ ) of the NN was not yet satisfactory with values of 0.653, 0.582 and 0.545 when matching the recharge observations at Methven, Dunsandel and Dorie, respectively. Given these findings, the challenge was to evaluate different ways to increase performance of the model, by keeping in consideration that gathering more data was not possible. This was achieved through two steps: (1) Switching to a more customisable programming environment (i.e. Keras) and (2) Increasing the amount of data used during training (i.e. the training set ended originally on 31 December 2016, and was extended to 31 July 2017). In general, the model showed a positive response to the increased amount of data for training (Table 16), but also to switching to a more customisable language where epochs and dropouts (to avoid overfitting) are more manageable. The NN that showed the best performance has one hidden layer with 5 hidden neurons. Comparing the latter to the previous NN, the accuracy ( $R^2$ ) increased by 13%, 12% and 58%, whereas the mean absolute error decreased by 19%, 18% and 49.6% at Methven, Dorie and Dunsandel, respectively. Therefore, this was the final NN selected, and the one that was implemented into a GIS environment for the upscaling analysis.

Table 16. Results of testing different architectures of a NN with 3 inputs, and an increased training dataset on a daily basis.

Arch	Epochs	Dropout (P)	R <sup>2</sup> Methven	MAE Methven	R <sup>2</sup> Dunsandel	MAE Dunsandel	R <sup>2</sup> Dorie	MAE Dorie
3--4-1	400	0.1	0.68	0.90	0.56	1.82	0.80	0.30
3--4-1	500	NO	<0		<0		<0	
3--4-1	500	0.1	0.73	1.01	0.64	1.89	0.85	0.43
3--4-1	600	0.1	0.72	1.01	0.65	1.82	0.86	0.43
3--4-1	700	0.1	0.72	1.01	0.65	1.80	0.85	0.43
3--4-1	2000	0.1	0.72	1.01	0.65	1.79	0.85	0.43
<b>3--5-1</b>	<b>500</b>	0.1	<b>0.74</b>	<b>0.99</b>	<b>0.65</b>	<b>1.75</b>	<b>0.86</b>	<b>0.41</b>
3--5-1	500	0.15	0.73	1.04	0.64	1.77	0.85	0.43
3--5-1	500	0.2	0.70	1.08	0.60	1.90	0.82	0.49
3--5-1	600	0.1	0.68	0.90	0.56	1.82	0.80	0.34
3--6-1	300	0.1	0.65	0.92	0.54	1.82	0.75	0.35
3--6-1	400	0.1	0.71	0.92	0.64	1.72	0.84	0.36
3--6-1	500	0.1	0.71	0.91	0.61	1.78	0.81	0.36
3--7-1	300	0.1	0.72	0.89	0.61	1.77	0.82	0.36
3--8-1	100	0.1	0.61	0.95	0.50	1.86	0.67	0.39
3--8-1	200	0.1	0.70	0.89	0.58	1.77	0.81	0.33
3--8-1	300	0.1	0.72	0.97	0.60	1.76	0.81	0.40
3--9-1	100	0.1	0.68	1.03	0.57	1.90	0.75	0.48
3--10-1	100	0.1	0.69	0.89	0.58	1.79	0.78	0.35
3--11-1	100	0.1	0.67	0.90	0.56	1.81	0.76	0.36
3--12-1	100	0.1	0.64	0.93	0.51	1.84	0.72	0.37
3--13-1	100	0.1	0.68	0.90	0.57	1.80	0.77	0.35
3--13-1	200	0.1	0.72	0.88	0.62	1.73	0.83	0.32

#### 5.1.4 Neural Network Uncertainty

Monte Carlo dropout (Y Gal & Ghahramani, 2016b) was employed to estimate model uncertainty (the relevant python code is shown in Appendix E). 10,000 stochastic forward passes were computed in order to calculate the uncertainty associated to the NN model. As the dropout randomly switches off 10% (dropout rate) of the hidden units in the hidden layer, the predicted values varied across the 10,000 simulations. Model uncertainty is estimated as the standard deviation of the predictions after passing stochastically through the network. The mean recharge uncertainty lies between 0 and 10 mm d<sup>-1</sup>(Figure 17), with a mean uncertainty value of 0.21 mm d<sup>-1</sup> and a mean daily percentage uncertainty of 6%, however, maximum values occur up to 9 mm d<sup>-1</sup>.

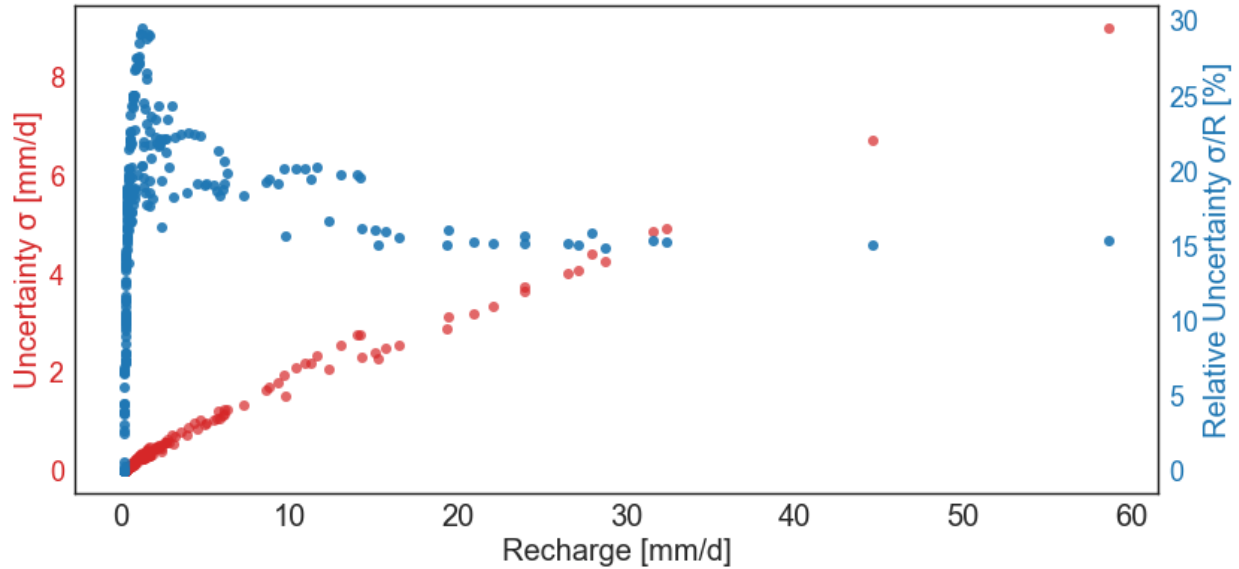


Figure 17. The behaviour of mean daily recharge uncertainty, plotted on two axes: [1] In  $\text{mm d}^{-1}$  (left axis, red); and [2] as a percentage of recharge (right axis, blue).

Figure 18, Figure 19 and Figure 20 show the behaviour of mean daily recharge and mean daily uncertainty associated with each input used for model prediction (Rainfall/Irrigation, PET and dominant soil texture respectively). Overall, rainfall/irrigation plays a dominant role for both recharge and uncertainty. Daily uncertainty seems to be more sensitive to precipitation, in particular for precipitation events (i.e. either rainfall or irrigation) greater than 10 mm. The behaviour of daily recharge uncertainty exhibits a linear pattern, with a tendency to increase as rainfall or irrigation increase. Although PET and the soil dominant texture class have a lower influence on uncertainty, they still play a significant role, e.g. for PET between 0 and 3  $\text{mm d}^{-1}$ , both daily recharge and recharge uncertainty show a considerable variation, with a tendency to stabilize as PET increases. Perhaps the most challenging part of the uncertainty analysis is to evaluate the effect of soil dominant texture on recharge uncertainty, since only two soil classes are observed at the testing set (i.e. silty soils for Methven and Dorie, and loamy soils at Dunsandel). Overall, the effect of the dominant soil texture class on model uncertainty tends to be low, becoming slightly higher when testing the model at loamy soils. This may be attributed to the well-drained nature of loamy soils, which enhances recharge and therefore, more uncertainty is observed (consistent with the results displayed in Figure 17).

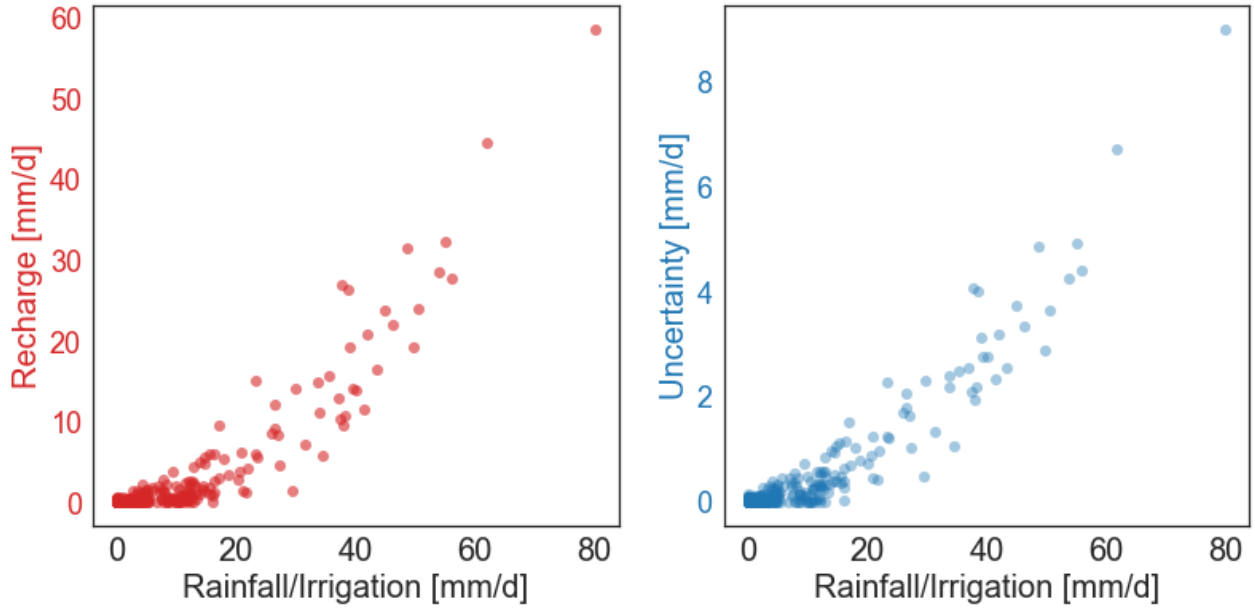


Figure 18. Rainfall/irrigation plotted against daily recharge (left, red) and daily uncertainty (right, blue).

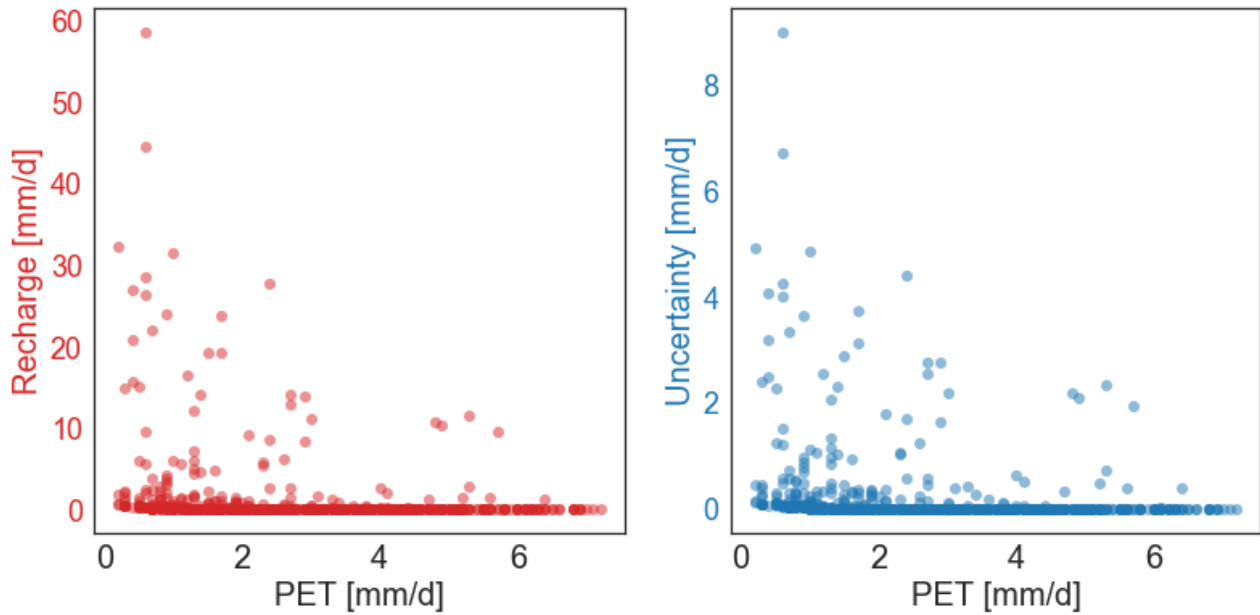


Figure 19. Potential Evapotranspiration plotted against daily recharge (left, red) and daily uncertainty (right, blue).

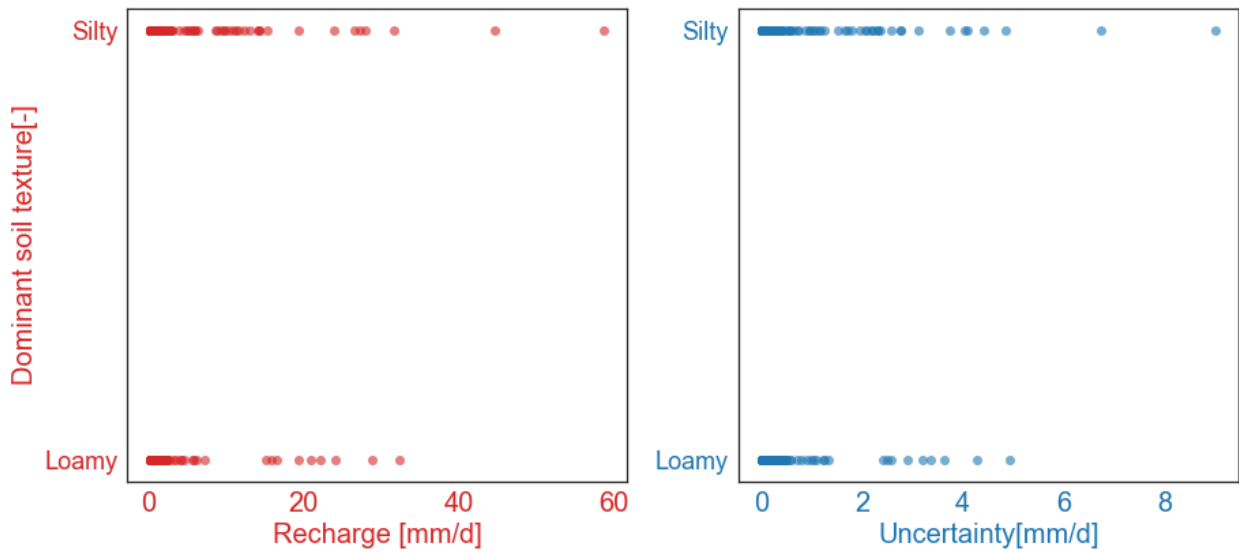


Figure 20. Soil particle dominant size plotted against daily recharge (Left axis, red) and daily uncertainty (right axis, blue).

### 5.1.5 Spatial analysis - Upscaling

For the spatial analysis, the model (NN) selected in section 5.1.3 - 5.1.3.3, was transferred into a GIS environment (i.e. the matrix of weights and biases which describe the best NN (Appendix B), was introduced into a GIS). Figure 21 shows the way the GIS software handles the data to predict land surface recharge for each pixel, to finally produce a map showing LSR on a larger area. The code for modelling land surface recharge within a GIS environment is shown in Appendix C.

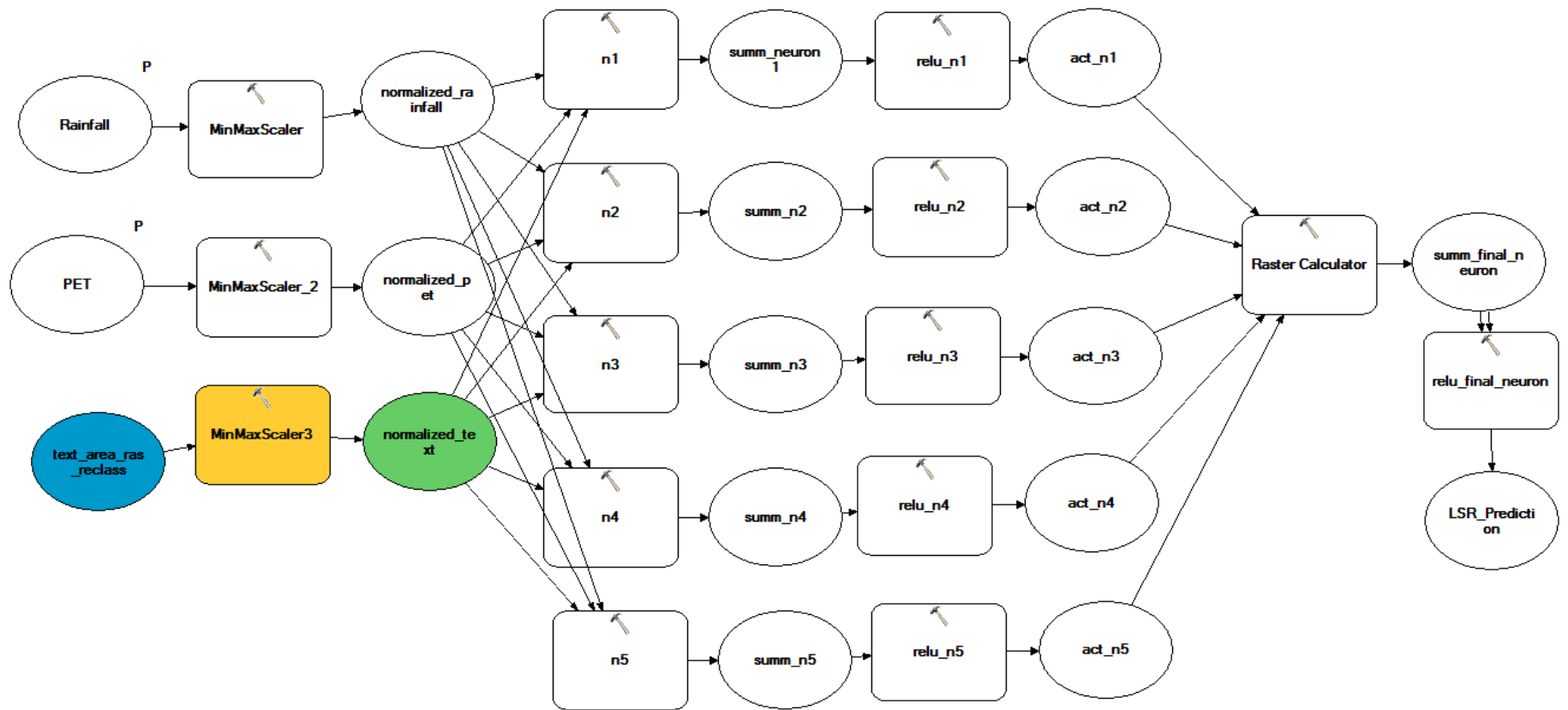


Figure 21. GIS tool for predicting land surface recharge in a larger area.

The NN-model estimates a single value of land surface recharge (LSR) on every pixel of a raster grid. Therefore, raster layers of the inputs were required to run the model (i.e. at least, one raster layer of rainfall, one of PET and one showing the dominant soil texture of each pixel). An example of a model run is shown in Figure 22, where the rainfall (top left) and PET (top right) from 11 July 2017, together with a map showing the dominant soil texture (lower left), were introduced into the GIS tool (based on the NN), in order to produce a map of LSR (lower right) for the three allocation zones. The result shows an expected pattern, where most of the recharge occurs in Sandy, Loamy and Peaty soils, but also where higher rainfall events are observed. LSR predicted for this day shows values ranging from 0 up to 42 mm d<sup>-1</sup>, being the highest values observed mostly in the Rakaia-Selwyn zone, especially in the presence of well-drained soils and large rainfall events ranging from 20 to 35 mm d<sup>-1</sup>. High LSR values are also observed close to Te Waihora/Lake Ellesmere, where sandy soils are present. The PET shows a fairly equal pattern across the three allocation zones, being at its lower range due to the winter season. The Rakaia River flows between the Rakaia-Selwyn allocation zone and Chertsey, and given that the model was not developed to estimate the interaction between aquifers and rivers, LSR is not calculated for this area.

# DAILY LAND SURFACE RECHARGE PREDICTION

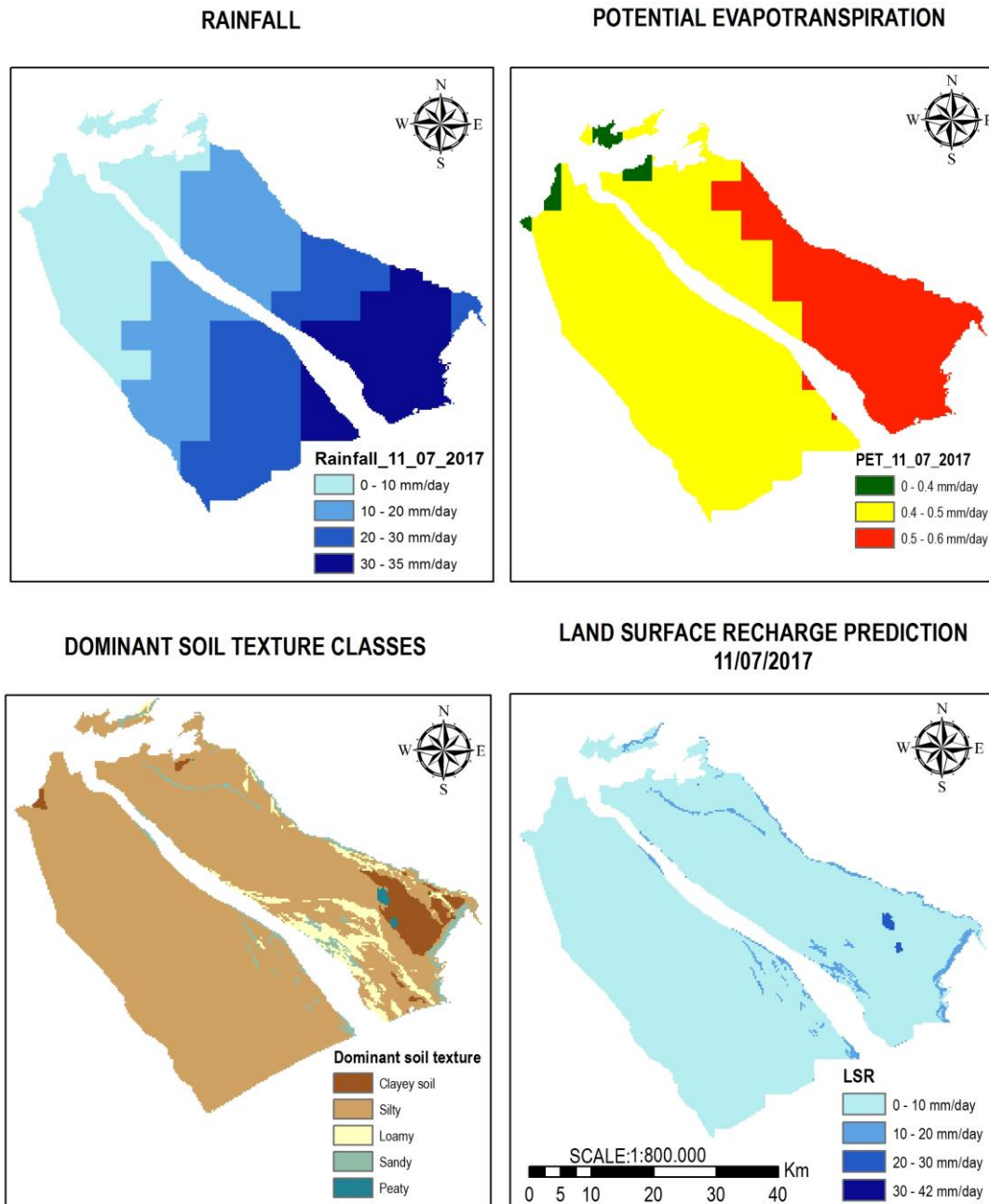


Figure 22. Sample model output. The NN trained on point scale data now transferred into a GIS software calculates land surface recharge for the three GW allocation zones on a daily basis (here recharge was calculated for 11 July 2017 as an example). Data Source: NIWA, grid size: 280 m x 280 m pixels.

### 5.1.6 Groundwater allocation limits calculated employing the NN model

To automate calculation of LSR on a daily basis a Python script for predicting recharge from 1 April 2017 to 1 September 2017 was developed (see Appendix D). An example application is shown in Figure 23, where a considerable amount of LSR is observed across the three allocation zones. The highest values of recharge are observed in the Rakaia-Selwyn region, where the Dunsandel lysimeter station is installed. At Chertsey, a fair amount of recharge was also predicted, with values ranging from 100 mm up to 1500 mm. Contrarily, at Ashburton, the lowest values of total recharge for the period evaluated were predicted, in a range of 100 - 500 mm. Table 17 shows the total values of land surface recharge estimated by the model for each zone, but also, the allocation limit based on LSR occurring in the previously mentioned period of the year. The highest amount of GW available for allocation is estimated to be approximately  $650 * 10^6 \text{ m}^3 \text{ year}^{-1}$  for the Rakaia-Selwyn allocation zone (Including Little Rakaia). An allocation limit of  $284.41 * 10^6 \text{ m}^3 \text{ year}^{-1}$  and  $332.45 * 10^6 \text{ m}^3 \text{ year}^{-1}$  was estimated for Ashburton and Chertsey respectively. Although these two zones show similar conditions, a higher LSR was estimated for the Chertsey, mainly attributed to the most frequent presence of Sandy and Loamy soils in this area.

Table 17. LSR predicted for each allocation zone (\*Rakaia –Selwyn and Little Rakaia comprehend the same allocation zone)

GW Allocation zone	Lysimeter Station	Total LSR [mm]	Total LSR [ $10^6 \text{ m}^3 \text{ year}^{-1}$ ]
Rakaia – Selwyn*	Dunsandel	3003074.378	$558.02 \pm 19.5\%$
Little Rakaia*	Dunsandel	498095.9218	$92.55 \pm 18\%$
Ashburton	Methven	1530588.66	$284.41 \pm 12.5\%$
Chertsey	Dorie	1789113.528	$332.45 \pm 5\%$

## LAND SURFACE RECHARGE PREDICTION TO ASSIST WATER ALLOCATION

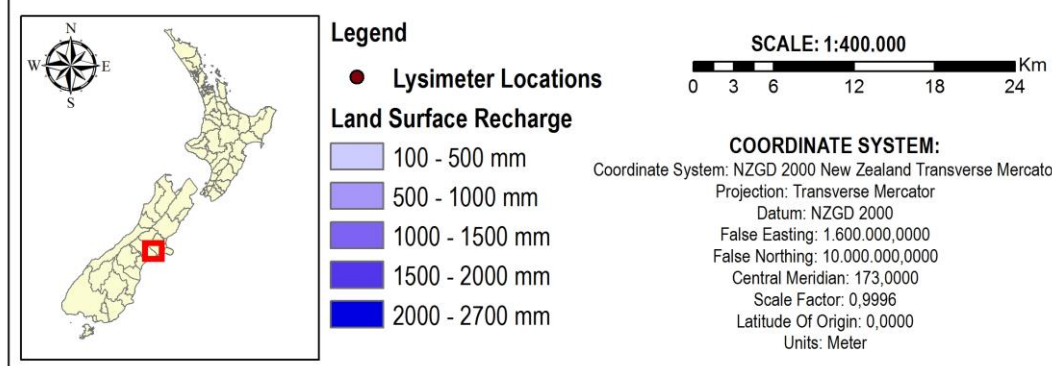


Figure 23. Land surface recharge predicted with the NN model for three GW allocation zones.

## **5.2 Patia Valley, Cauca, Colombia (Case Study II)**

Initially, the aim was to transfer the upscaling procedure developed in New Zealand to a data scarce region in Colombia, where groundwater is used as a source for irrigation and domestic use. Although lysimeter data may be available in the area, it is proprietary data which ended up not being available for this study. However, a rainfall, evapotranspiration and runoff dataset was obtained. The goal was to explore how machine learning techniques (e.g. neural networks) could assist in water allocation decisions with limited data. To achieve this a similar approach to the one tested in the three GW allocation zones (Canterbury) was applied for estimating regional recharge in a region of South-West Colombia.

### **5.2.1 Overview of available data**

#### **- Rainfall, ET and river flow data**

The open pan evaporation sites to measure ET are located outside the model boundary, however, this is the only data available in the region. In general, annual evapotranspiration shows a fairly equal behaviour across the area, with minimum values of approximately 1,065 mm per year which go up to 1,250 mm year<sup>-1</sup> towards the southern part of the Valley as shown in Figure 24. The ET has been measured on a monthly basis for approximately 30 years by the regional council. The raw data for creating the average scenario of ET is shown in Appendix F.

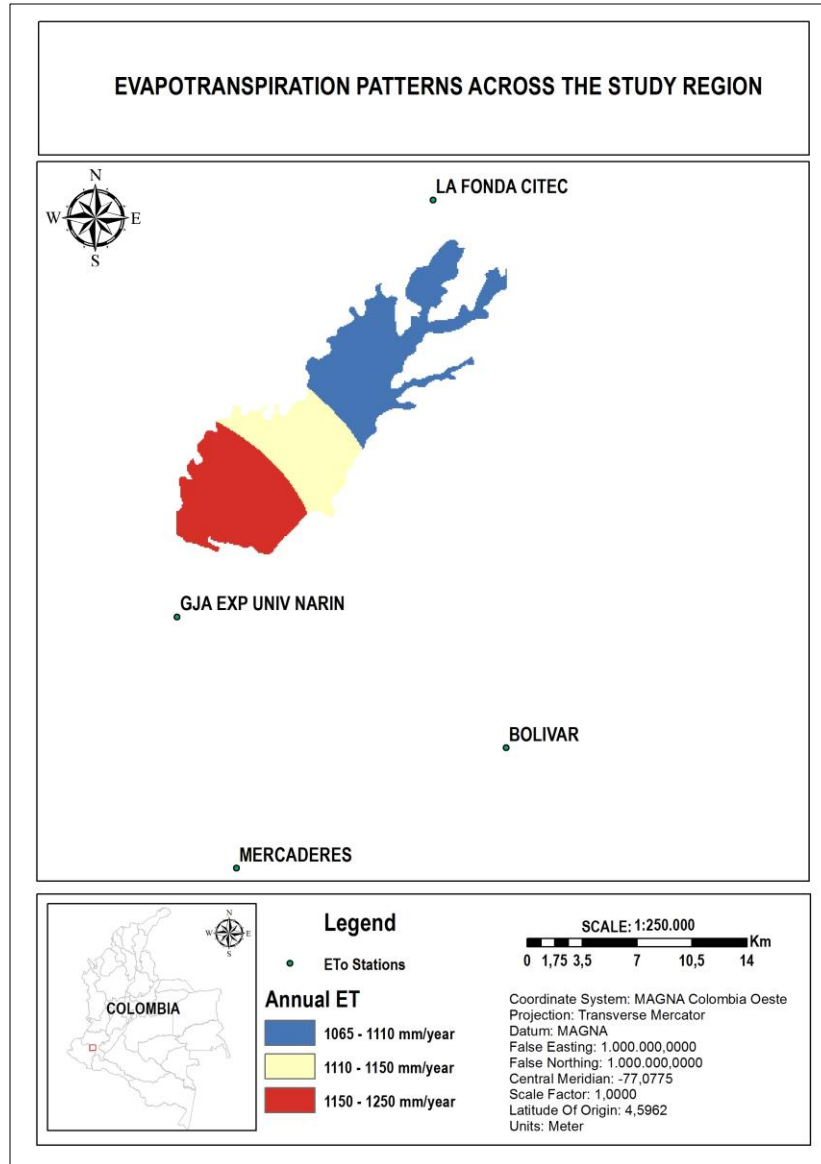


Figure 24. Evapotranspiration patterns in a small region of Colombia, units are in mm year<sup>-1</sup>.

Rainfall shows a much larger variation, with maximum yearly rainfall values ranging from 2,000 to 2,100 mm towards the upper parts of the catchment. Minimal rainfall amounts are registered downstream where measures with a range of 1,200 to 1,600 mm per year are recorded (Figure 25). Seasons-wise, the valley shows a bimodal distribution (i.e. 2 dry seasons and 2 rainy seasons). The first part of the year is characterised for dry periods which go usually from January to the end of February. The first wet season of the year starts in March and reaches its peak during April and May and ends around July. The second wet season usually starts in October and end around mid-December. The rainfall data records are shown in Appendix G.

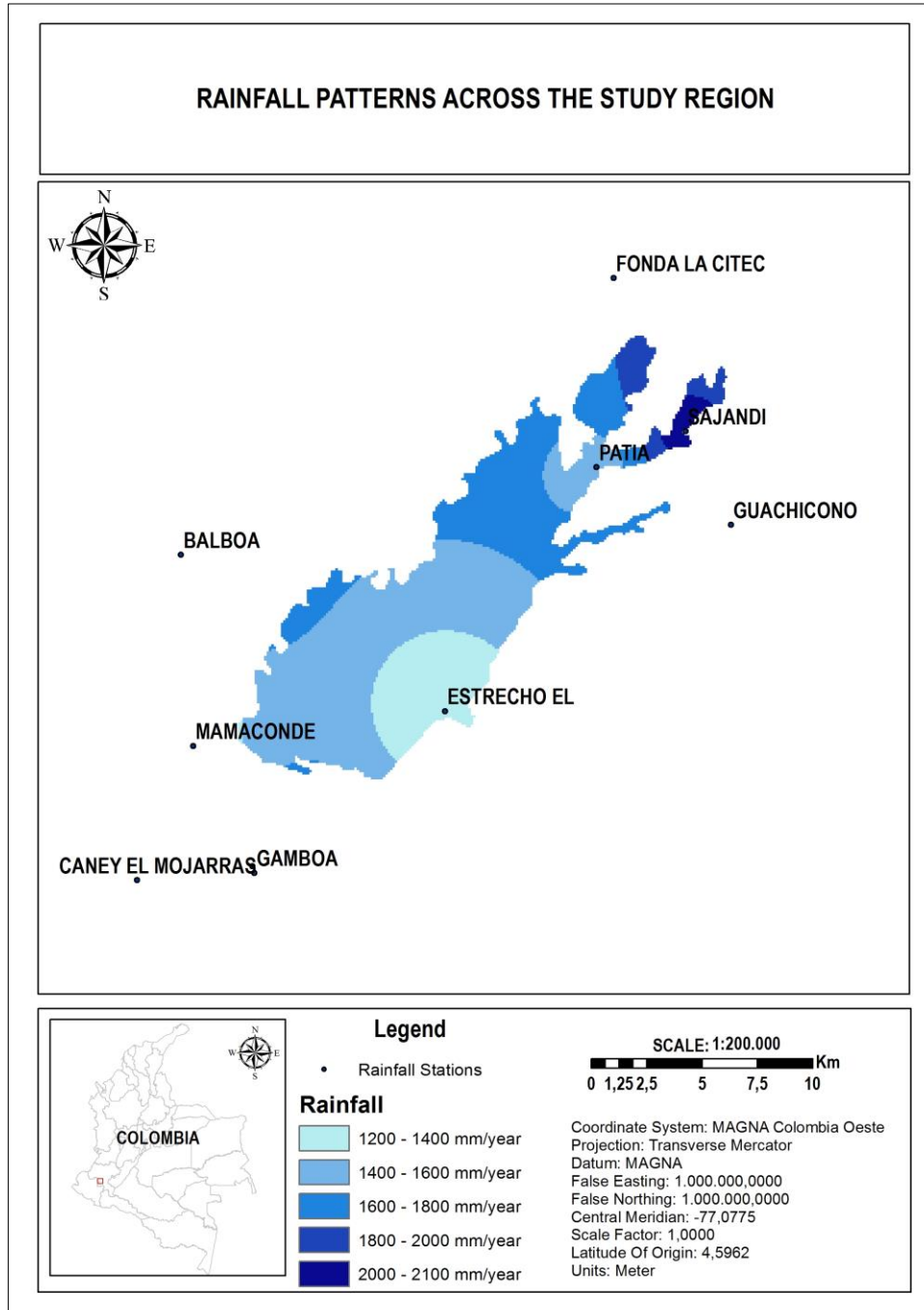


Figure 25. Yearly rainfall patterns in the area of interest inside Colombia, units are in mm year<sup>-1</sup>.

Figure 26 describes the average monthly behaviour of river flow through the period of records (Approximately 16 years). The highest values are 110.10 m<sup>3</sup> s<sup>-1</sup>, 130.60 m<sup>3</sup> s<sup>-1</sup> and 162.40 m<sup>3</sup> s<sup>-1</sup> observed downstream in April, November and December respectively. The bimodal nature of river flow matches the two rainy seasons that characterise the study area. Records for catchment runoff (river flow) in two stations located upstream (“La Fonda”) and downstream (“Loma Alta”) the study area are shown in Appendix , and the river flow gauges locations are shown in the methodology, section 4.2.1.

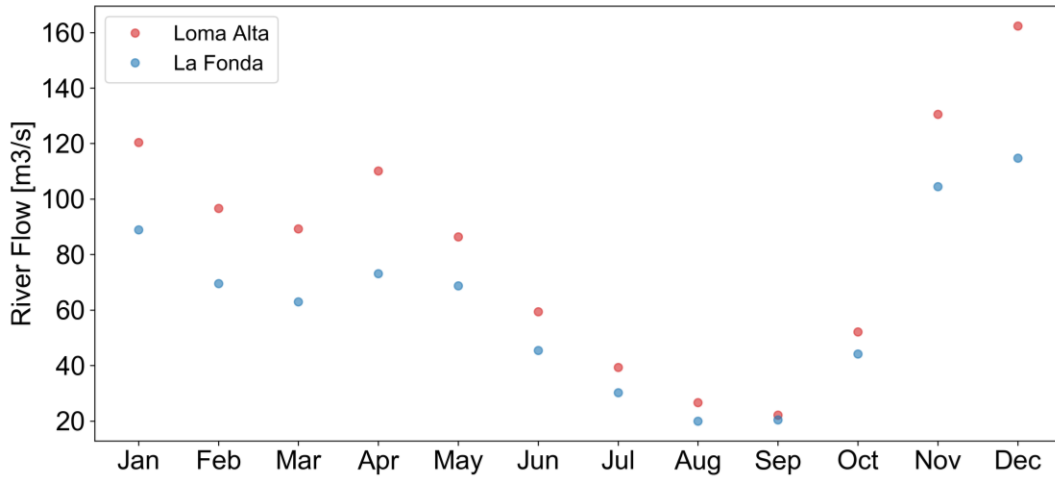


Figure 26. Mean flow measured upstream (La Fonda) and downstream (Loma Alta).

After generating a spatial mapping of the data, the available LSR estimates from a water balance analysis were fed into the Python with the assistance of Pandas (McKinney, 2010) as shown in Figure 27.

```
In [13]: col_df[["rain", "runoff", "ET", "LSR"]]
```

```
Out[13]:
```

	rain	runoff	ET	LSR
0	197.300000	88.200000	82.90	26.223646
1	125.900000	98.800000	79.00	0.000000
2	199.300000	107.000000	84.20	8.062896
3	198.900000	127.700000	77.30	0.000000
4	160.600000	69.300000	76.20	15.126608
5	56.400000	59.700000	81.10	0.000000
6	28.300000	43.400000	92.20	0.000000
7	25.100000	26.400000	103.00	0.000000
8	88.200000	8.400000	121.30	0.000000
9	240.900000	51.700000	87.70	101.539699
10	263.100000	140.100000	73.40	49.593386

Figure 27. Overview of a portion of the data employed for training and testing a NN in the Patia Valley. Runoff represents river flow in the python code.

### 5.2.2 Model Development

- Approach I

The monthly dataset was divided in a proportion of 60% for training and 40% testing and was fed into a simple feed forward NN. Rainfall, evapotranspiration and river flow were considered as model inputs. Table 18 shows the results after testing whether this NN was able to predict the previous LSR values calculated in this

area employing a water balance. Model accuracy tends to either fail every prediction ( $R^2 < 0$ ) or to be low, with values ranging from 0.32 to 0.56 and MAE values ranging from 6.2 to 7.2.

Table 18. Results of testing a NN on a monthly basis, employing a ratio of 60% of data for training and 40% for testing.

Arch	Iterations	Dropout	R2 - Test	MAE - Test
3--9-1	6000	No	0.569	7.133
3--10-1	6000	No	<0	
3--18-1	6000	No	0.325	6.285
3--4-1	6000	No	0.225	6.88
3--5-1	6000	No	<0	
3--5-1	6000	No	0.448	7.011
3--3-1	6000	No	<0	
3--4-1	6000	No	<0	
3--6-1	6000	No	<0	
3--7-1	6000	No	<0	
3--8-1	6000	No	<0	
3--9-1	6000	No	<0	
3--10-1	6000	No	<0	
3--11-1	6000	No	<0	

- Approach II

The results (Table 19) show a MAE increment and a reduction in  $R^2$  values in comparison with the results observed in Table 18, meaning no improvements in model performance. Although model complexity was increased in terms of hidden neurons (i.e. from 5 to 14) and more hidden layers (i.e. from 1 to 2), no improvements were observed when testing against the previously LSR estimations made by the regional council.

Table 19. Results of testing a NN on a monthly basis, employing a ratio of 70% of data for training and 30% for testing.

Arch	Iterations	Dropout	R2 - Test	MAE - Test
2--5-1	6000	No	<0	
2--3-1	6000	No	<0	
2--4-1	6000	No	<0	
2--6-1	6000	No	<0	
2--7-1	6000	No	<0	
2--8-1	6000	No	<0	
2--9-1	6000	No	<0	
2--10-1	6000	No	<0	
2--11-1	6000	No	0.528	11.441
2-6-3-1	6000	No	0.483	12.42
2--12-1	6000	No	0.268	12.893
2--13-1	6000	No	<0	
2-14-1	6000	No	<0	

- Approach III

Table 20 shows the results of applying this technique and no significant improvements (i.e. predictive performance only increased 1.5%) are observed in comparison with findings from the previous two approaches. However the NN with 10 hidden neurons, trained only based on rainfall and ET data showed an  $R^2$  greater than 0.6 and a 6% reduction of the MAE when compared to the other networks. Furthermore, increasing complexity, both in terms of hidden neurons and hidden layers, did not increase NN predictive performance either. Two different networks with 20 hidden neurons and 100 hidden neurons failed on matching every recharge estimation ( $R^2 > 0$ ). On the same manner, the networks with two hidden layers (i.e. Arch 2-6-6-1, and Arch 2-6-3-1) failed at every estimation (i.e.  $R^2 > 0$ ). Lastly, increasing the number of times the training data “teaches” the NN (epochs) did not increase performance either.

Table 20. NN trained with 70% of data, on a Keras environment (employing dropout)

Arch	Number of Epochs	Dropout	R <sup>2</sup> - Test	MAE - Test
2--2-1	4500	Yes (0.1)	0.54	11.08
2--8-1	2000	Yes (0.1)	0.51	11.76
2--9-1	2000	Yes (0.1)	0.54	11.46
2--10-1	800	No	0.37	11.54
2--10-1	800	Yes (0.1)	0.40	11.20
2--11-1	800	Yes (0.1)	0.25	11.92
2--10-1	2000	Yes (0.1)	0.61	10.72
2--10-1	3000	Yes (0.1)	0.32	12.13
2--12-1	3000	Yes (0.1)	0.36	11.74
2-20-1	4500	Yes (0.1)	<0	
2-20-1	4500	No	<0	
2-50-1	4500	Yes (0.1)	<0	
2-100-1	4500	Yes (0.1)	<0	
2-6-6-1	2000	No	<0	
2-6-6-1	2000	Yes (0.1)	<0	
2-6-3-1	2000	Yes (0.1)	<0	

### 5.2.1 Model Uncertainty

As observed in Figure 28, monthly recharge uncertainty tends to increase linearly with increased recharge. The model showed a mean monthly uncertainty of 41%. Mean monthly recharge uncertainty is up to 20 mm month<sup>-1</sup>. Recharge uncertainty, relative to recharge (right axis - Figure 28), is highest for low values of recharge. It is also observed that mean uncertainty for low values of recharge, ranging between 0 and 10 mm month<sup>-1</sup>, can be higher than the recharge value itself. As a matter of fact, 10% of recharge values ranging in between 0 and 1 mm month<sup>-1</sup> had an uncertainty of around 200% higher than their recharge value. With increasing recharge, uncertainty reduces to approximately 20% of the recharge estimation.

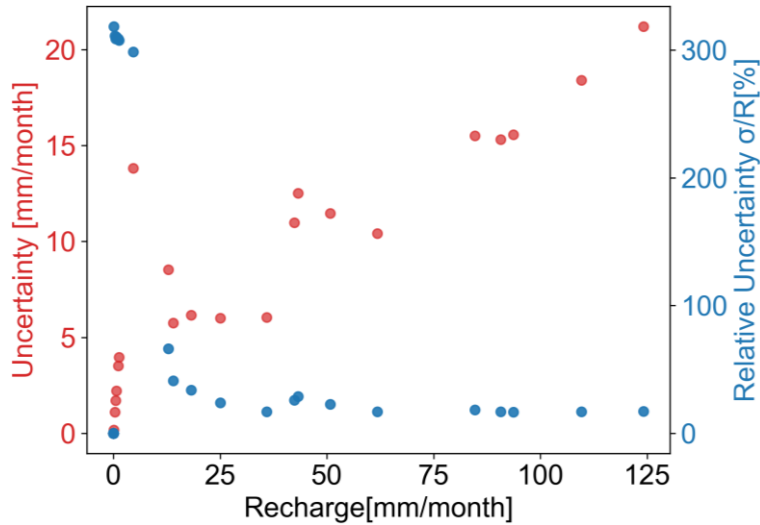


Figure 28. The behaviour of mean monthly recharge uncertainty, plotted on two axes: [1] In mm month<sup>-1</sup> (left axis, red); and [2] as a percentage of recharge (right axis, blue).

## 6. DISCUSSION

### 6.1 Canterbury, New Zealand – Case study I

#### 6.1.1 Data quality control

In general, the presence of outliers was attributed to small disturbances in the devices employed for measurements i.e. the tipping buckets and the soil moisture sensors. Regarding the recharge measurements, zero values were recorded on different conditions; which means, they were either noticed during, or after precipitation events. This may be attributed to the effect of preferential flow, which affects the distribution of water in the soil column (Li et al., 2018), but also to the nonlinearities associated to the GW recharge process, as noted by Lorenz & Delin (2007). Also, given that the lysimeters are installed on irrigated farms, water quality could also have an effect on infiltration volumes. Borselli et al. (2001) demonstrated how silty-like soils are more prone to be affected by water quality with regard to infiltration. However, this is an issue that was not considered in this thesis and remains as a recommendation for future research.

Recharge was also recorded with no rainfall/irrigation recorded. This may be attributed to the to the effect of delayed infiltration (Graham et al. 2018). Same findings were reported by Duncan et al. (2016) who mentioned how recharge was measured even three days after precipitation events at Methven. Also, the underestimation of low-intensity precipitation events may explain the differences in the records of recharge and rainfall. Gebler et al. (2015) mentioned that tipping buckets rain gauges are known to underestimate precipitation events, such as fog and dew, which may also be responsible for an underestimation of the amount of rainfall/irrigation availability for recharge. However, the lysimeters are 70 cm depth, so the effect of fog or dew on recharge seems negligible. Furthermore, a different response of the lysimeters to rainfall events at the same locations was observed as well. However, the seasonal behaviour was in general rather similar, which is supported by findings of Duncan et al. (2016).

### 6.1.2 Time Series analysis

The analysis of the three lysimeter stations considered in this study revealed how each location responded differently to precipitation events. In general, land surface recharge measured at the lysimeter locations showed that most of the recharge is either occurring during the day of the precipitation event, or in some cases one day or two days after, which is consistent with previous findings by Duncan et al. (2016). At Dorie, the largest recharge events were observed during the winters of 2013 and 2017, being triggered by rainfall events larger than  $40 \text{ mm d}^{-1}$ . This also matches the observations of Duncan et al. (2016), where the authors mentioned that daily rainfall in excess of  $45 \text{ mm}$  was required to trigger recharge. In general, the Dunsandel lysimeters recorded the largest mean daily recharge, which may be attributed to a higher stone content in the soil profile (also noted by White et al., 2003) and its higher response to precipitation events and large irrigation applications.

Figure 29, Figure 30, Figure 31 show the 2017 data recorded at Dorie, Dunsandel and Methven respectively. This year was selected for comparison since it was the only part of the data where all three sites have data available i.e. this is the only part of the dataset where all the time series overlap and therefore allow comparison.

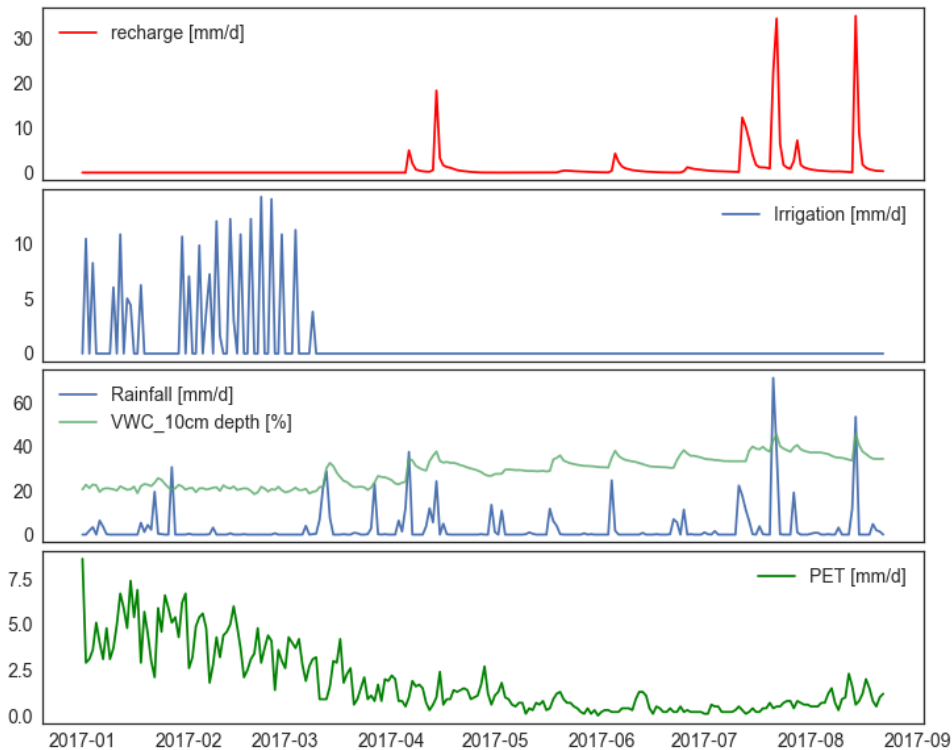


Figure 29. Recharge behaviour - Dorie 2017

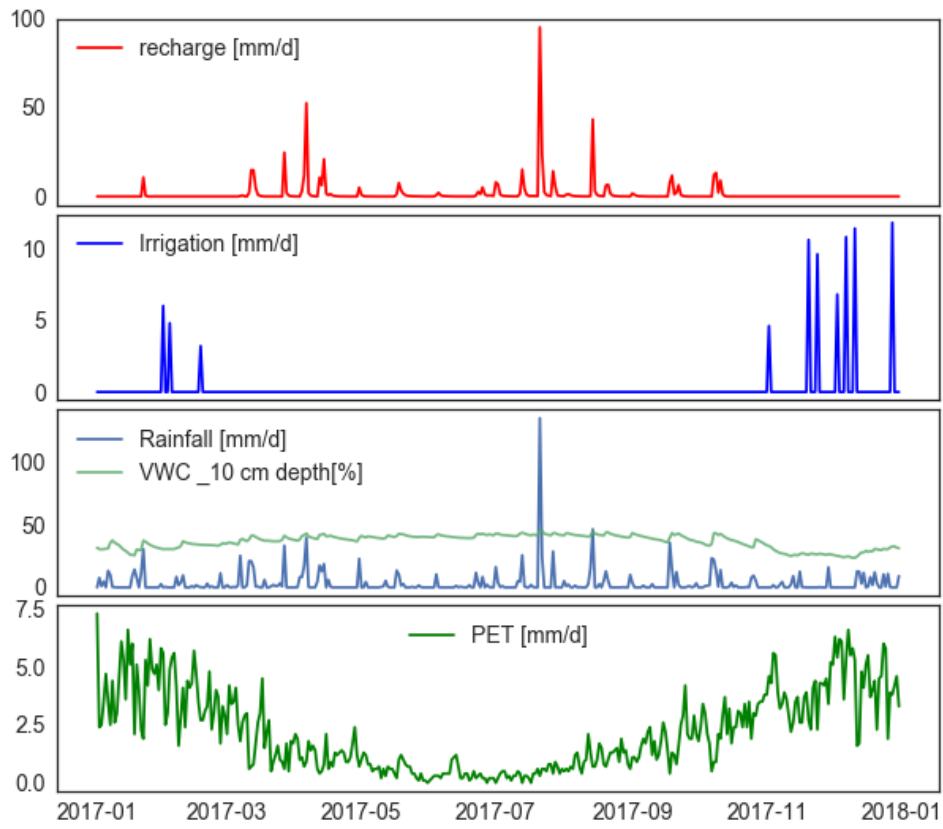


Figure 30. Recharge behaviour - Methven 2017

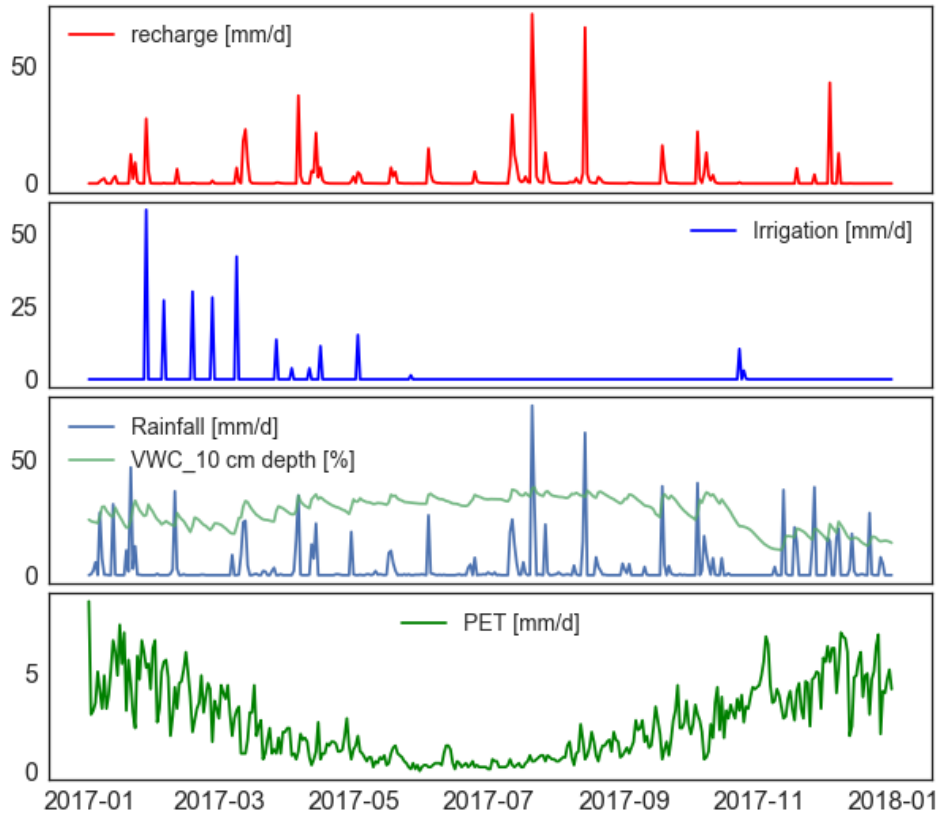


Figure 31. Recharge behaviour - Dunsandel 2017

The Dunsandel lysimeters, installed in the Rakaia-Selwyn allocation zone, recorded the highest amount of recharge in 2017 with an amount of 658.452 mm (Table 21); whereas the Dorie lysimeters (Chertsey allocation zone) measured the least amount of recharge with a total of 235.36 mm. From Figure 29, Figure 30 and Figure 31 it can be observed that extreme recharge events occurred during the winter, however, at Dunsandel and Methven recharge frequency was much higher compared to records at Dorie. From a seasonal perspective, all the locations show a similar behaviour i.e. a lower proportion of rainfall converted into recharge during the spring and summer seasons, and a higher proportion during autumn and winter. For instance. On average, there are differences in seasonal recharge between sites which reflect both the rainfall amount, irrigation management and differences in soil texture. These variations may be attributed to the amount of grass covering the lysimeters, though, and in line with Duncan et al. (2016) and White et al. (2003), the differences in soil type and stone content in the soil profile are more likely to be the reasons which explain the differences in recharge patterns.

Table 21. Seasonal recharge behaviour across locations in 2017.

2017						
Location	Parameter	Summer	Autumn	Winter	Spring	Total
Dorie	Recharge [mm]	0.032	40.832	194.528	N.A	235.36
	Rainfall and Irrigation [mm]	266.4	271.8	326.4	N.A	864.6
	PET [mm]	259.2	125.4	47	N.A	431.6
Dunsandel	Recharge [mm]	76.65	175.797	318.005	88	658.452
	Rainfall and Irrigation [mm]	335.4	318.2	349.6	290	1293.2
	PET [mm]	263.7	128.1	60.5	270.1	722.4
Methven	Recharge [mm]	11.285	201.824	270.56	72.25	555.92
	Rainfall and Irrigation [mm]	168.8	339.4	397.8	256.2	1162.2
	PET [mm]	235.6	116.9	55.7	243.1	651.3

### 6.1.3 Model development

From a regional point of view, approach 1 (Section 5.1.3.1) yielded unsatisfactory results  $R^2$  values ranging from 0.1 up to 0.6 at Methven, 0.17 to 0.46 at Dorie and 0.6 up to 0.8 at Dunsandel. These were expected, as the variation in recharge patterns in the region has been shown in the past by Duncan et al. (2016) and approximating that variation with a NN trained based on data collected at one location only seemed challenging. However, White et al. (2003) developed a single NN to successfully predict lysimeter-measured recharge under dryland conditions in Canterbury. The authors only used data collected from the Christchurch Airport site for training the NN model. The data from three monitoring sites (i.e. Lincoln, Winchmore, and Hororata sites) were used to test the White's model. In that study, irrigation did not have an effect on recharge, and the unsatisfactory results showed in this thesis for developing a NN based on a single location may be attributed to the differences induced by irrigation management. This is supported by Porhemmat et al. (2018), who showed how differences in irrigation schemes (i.e. drip and sprinkler) had a noticeable different effect on deep recharge. Nevertheless, assuming that the aim was to upscale from a point-scale to a farm-scale, the results based on approach 1 show how the inclusion of VWC, jointly with local recharge observations seems promising for modelling recharge estimates at the farm scale, as has been previously mentioned for stony Canterbury soils (Graham et al., 2018).

An approximation of a Bayesian NN was developed in approach 2 by adding a dropout layer during the training phase (Srivastava et al., 2014). The main challenge of this approach was, to some extent, approximate the differences in soil texture that could potentially enhance infiltration. The results showed how the model generalization ability increased i.e. higher  $R^2$  and lower MAE, however, it tends to underestimate the daily peak recharge values. This could be attributed to: the simple representation of the soil column as a class describing the dominant soil texture. In reality, soil water content varies with soil depth (Graham et al., 2018). Thus, a dominant soil texture class that do not incorporate this variation in soil water storage, could potentially alter the predictive performance of the model to match lysimeter-measured recharge. Similarly, Carrick et al. (2017) showed how lysimeter soil profiles can have different patterns in terms of pore size distribution and continuity, which consequently influences soil water dynamics. In general, the variation of

the hydraulic properties of a soil column based on soil texture are recognized, however, the dominant soil texture classification shown here demonstrates how a simple conceptualization provides useful results when coupled with lysimeter-measured data.

Furthermore, the model may not cope well with the effect of preferential flow. When preferential flow occurs a portion of the soil is not involved in the transport of water, which reduces storage capacity and increases flow rate. Previously, preferential flow has been shown in stony soils of Canterbury (McLeod et al., 2014) and its effect has also been analysed with lysimeter experiments (Greve et al., 2010). It was observed that the model performed worst at Dunsandel, where the highest daily values of recharge were recorded. This location also showed the highest irrigation intensity and frequency, which has been proven to have a significant effect on preferential flow (Cichota et al., 2016). Although macropore flow can be described through dual-porosity modelling (Simunek et al., 2003), these approaches require data describing macroporosity which are not available regionally wise (Graham et al., 2018).

Finally, the NN model is sensitive to the amount of data and the quantity of “information-rich” (peak daily values) events used for training. The longer datasets are recorded at Methven and Dorie (approximately 7 years of records for both locations) and the NN predictive performance was the highest at these two locations. At Dunsandel, a shorter dataset was available for training, and model performance at this location was the worst. For instance, model performance at Dorie decreases approximately 38% if the largest rainfall event on 21 July 2017 (which also triggered a large recharge event of approximately 30 mm d<sup>-1</sup>) is not included for training, which is consistent with findings reported by Singh et al. (2014). They mentioned how the model generalisation ability is likely to increase if the quantity of “rich” events i.e. data from critical/peak events in the dataset used for training increases as well. However, identifying these information-rich segments of data could be very challenging, especially for long time series with a large magnitude variation. Similar behaviour was observed by Heuvelmans et al. (2006), who showed how NNs have only a limited capability to predict outside the range they were trained for i.e. they tend to underestimate peak values if similar data were not used during the model training stage. Nevertheless, despite the inability of the model to perfectly match lysimeter-measured data, recharge estimation employing neural networks and lysimeter data led to a methodology that achieved very similar simulations compared to lysimeter-measured recharge. Overall, this lends some confidence in our ability to both measure and model groundwater recharge (Graham et al., 2018).

To the best of the author’s knowledge, this study represents the first attempt to predict and upscale lysimeter-measured recharge on a daily basis employing ANNs. Previous studies have presented successful results modelling lysimeter recharge on dryland conditions at a weekly (White et al., 2003) and monthly (Westerhoff et al., 2018) time steps. The results from this study do agree with previous reports, but, although the prediction performance of the NN model was higher when working on a monthly basis, the aggregation i.e. adding up daily data into a monthly basis, do not represent properly the variation of the inputs considered for the model.

Also, one of the aims was to develop a model capable of reflecting the environmental dynamics of land surface recharge on irrigated land, keeping a balance between model performance and parsimony. In terms of complexity, findings from this study agree with previous findings from Karahan & Ayvaz (2008) and Nayak et al. (2006), where the relation between model complexity (i.e. number of hidden layers and hidden neurons) and performance is not linear i.e. increasing model complexity does not imply better model predictive

performance. As observed in Table 16, increasing the number of neurons in the hidden layer, or even increasing the number of hidden layers, does not lead to a significant increase in performance (accuracy). The final model selected was composed of only one hidden layer. This simple NN architecture has been previously recommended by Maier & Dandy (2000), who mentioned that one hidden layer for a NN architecture is usually sufficient to tackle water resource issues.

The NN model developed for this project is assumed to be an approximate of the “true” model, which is much more complex, and certainly nonlinear. The approach has limitations, mostly due to its simplifications. But, in general, this simplified model aims to show a procedure for upscaling lysimeter measured recharge in the region provided a few assumptions are met. First of all, the model was not developed to predict the interaction between rivers and the aquifers. Thus the exclusion of the Rakaia’s river bed of the analysis. Secondly, the model was not developed to predict land surface recharge on steep areas, since the dataset used for training was based on measures conducted in predominately flat areas. Also, the Southern alps and steep areas are known to have low groundwater recharge potential (Singh et al., 2018). Finally, the model was not designed to predict the exact timing of recharge occurrence, meaning that the model predicts recharge the same day where precipitation occurs (i.e. does not consider changes in VWC over time). This may be a drawback for its implementation e.g. to predict nitrogen leaching. However, the cross correlation analysis by Graham et al. (2018) indicated that the strongest correlation between precipitation and measured lysimeter recharge occurred on the day of the precipitation event, which supports the way the model was developed. Also, for groundwater allocation the total LSR is meant to be estimated by the model from April to September, thus model boundaries and assumptions are still valid.

#### **6.1.4 Neural Network Uncertainty**

In general, daily uncertainty tends to increase as daily recharge increases, which has been previously observed by Westerhoff et al. (2018). Model uncertainty can be categorized into homoscedastic uncertainty which is constant for different inputs, and heteroscedastic uncertainty, which depends on model inputs, meaning that some inputs may potentially produce more noisy outputs than others (Kendall & Gal, 2017). In this study, and in relation to the NN model, rainfall/irrigation play the main role for both recharge and uncertainty. Although the PET and dominant soil texture play a less dominant role, they still influence recharge and uncertainty. For instance, and similarly to Westerhoff et al. (2018), for PET values in between 0 and 2 mm d<sup>-1</sup>, uncertainty shows the highest values. This may be attributed to the fact that most of the recharge occurs when the PET is lowest, i.e. during the winter and the spring. However, the NN model does not relate the PET to seasons i.e. the model handles a day of e.g. 3 mm PET in summer in the same way as in autumn, spring or winter.

In terms of soil type, when the soil texture limits recharge, uncertainty becomes slightly lower. This can be explained given that the percentage of sand, silt, and clay in a soil, is one of the major inherent factors affecting infiltration. Which means, water moves more quickly through the large pores in sandy soils than it does through the small pores in clayey soils. (USDA 2014). It has been observed how uncertainty in soil texture can lead to significant uncertainty in groundwater recharge estimations (Mathias et al., 2017),

however, for this thesis, the number of samples provided to the NN model for testing, may not be enough to evaluate the effect of dominant soil texture in recharge uncertainty.

Model uncertainty as a percentage of recharge shows a mean value of 6%. This value only represents how uncertain we are about the specification of model parameters. Though it does not keep in consideration the amount of noise inherent in the data generation process as explained in section 4.1.4. The uncertainty reported in this study could be explained as follows: Given that the approach here was to upscale from point scale lysimeter recharge to the GW allocation zone scale, availability of data regionally wide was a constraint, and simplifications to describe soil and recharge variations across sites had to be made e.g. representing the soil type as a dominant soil texture class. Another reason to explain it may be the data that the model was trained on i.e. lysimeter data. Different sources of error in lysimeter experiments have been mentioned in the past such as macropore flow and delayed infiltration (Graham et al., 2018), meaning that one may not have an idea of how uncertain lysimeter-measured recharge is, and that would be one of the topics to include for future research.

### **6.1.5 Upscaling and Groundwater allocation**

As explained in the methodology section, a toolbox was used to create land surface recharge maps by incorporating the neural network model architecture in GIS. Previously, the Canterbury Plains have been shown to have a high groundwater recharge potential (Singh et al., 2018), hence the LSR volumes estimated for the three GW allocation zones are valid. The model may not be capable to predict the effect of mountain groundwater recharge, however, it has been proven that groundwater recharge potential is higher at low elevated areas and flat terrain with Quaternary sediments (Singh et al., 2018; Westerhoff et al., 2018), making the upscaling scheme valid for application within the defined model boundaries. The selection of soil texture as the only landscape characteristic is a simple approach, but showed satisfactory results, as also observed by Lorenz & Delin (2007) who employed one single landscape characteristic (i.e. specific yield) to estimate regional GW recharge and White et al. (2003) who used PAW in their rainfall-recharge model to match lysimeter recharge measured on dryland. As shown in Figure 23, most of the recharge occurs in the Rakaia - Selwyn zone, with a tendency to be higher where Sandy and Peaty soils are presented. This was expected, since water is more likely to infiltrate in soils with large pores (USDA, 2014). LSR predictions tend to also be high towards the Rakaia's river bed and also the coast surrounding Te Waihora, mainly attributed to the presence of sandy soils and a high stone content. The highest prediction at this zone may be also attributed to the data used for training (i.e. recharge data collected at Dunsandel), where recharge was recorded at every season of the year, mainly due to irrigation practices.

The effect of irrigation was taken into account during training stage of the NN since all the lysimeter stations are installed on irrigated land. In irrigated areas the soil profile receives an additional and highly variable amount of water. Also, it has been observed in the past how irrigation management (i.e. timing and amount) plays a key role on groundwater recharge (Qin et al., 2011). Although inputs from irrigation were not incorporated in the procedure described in section 5.1.6 for calculating LSR in the three allocation zones, the proportion of irrigation converted into LSR is expected to be low. This is because the allocation volumes were

estimated based on the recharge occurring from April to September, where irrigation is zero or either very low, with few exceptions e.g. Dunsandel, where irrigations are applied at very high amounts.

As previously mentioned, recharge seems to be triggered more frequently during the spring and the winter, however, high amounts of recharge were recorded at Dunsandel (Rakaia-Selwyn zone) during the summer season. This is attributed to the high irrigation amounts that are required to avoid plant water stress at this location. In comparison, the irrigation amounts at Dunsandel are three to four times higher than the applications at Dorie and Methven. Since irrigation management is different on every farm, the NN model logic may not cope well with this variability, and this may have increased model uncertainty. As mentioned by Westerhoff et al. (2018), and assuming that irrigation data will become available in the future, it is necessary to re-calculate the amounts of GW available for allocation considering irrigation.

At the moment, GW allocation limits in Canterbury are set out in the Land and Water Regional Plan (ECan, 2017), and are based on calculations employing a water budget model introduced in Scott (2004). In this study, the methodology for estimating GW allocation limits was established on LSR estimations based on measurements over the preceding winter (i.e. 1<sup>st</sup> April to 1<sup>st</sup> September). Assuming a precautionary approach, allocation limits would be 50% of the LSR estimation calculated in section 5.1.6. These estimates were compared to the limits reported by Scott (2004) and are shown in Figure 32. Mean annual recharge estimates by the NN are similar to LSR estimated through a water budget model (i.e. the estimates reported in the regional plan fall within the uncertainty of the NN prediction). The differences are attributed to the input data to calculate the estimates i.e. the rainfall used as input for the NN allocation estimation was higher, and the PET was lower compared to the water budget model. Scott (2004) ran his model employing mean annual estimates of both rainfall and PET, ranging between 650 – 1000 mm and 800 – 900 mm respectively. On the other hand, for calculating LSR with the NN model, rainfall was in the range of 950 – 1150 mm and PET between 400 – 500 mm. Given that rainfall is likely to be the main driver influencing groundwater recharge, differences were expected given the variations in the input data. Also, in the model developed here, data only from the winter season was employed for LSR estimation, thus the expectation of higher infiltration volumes.

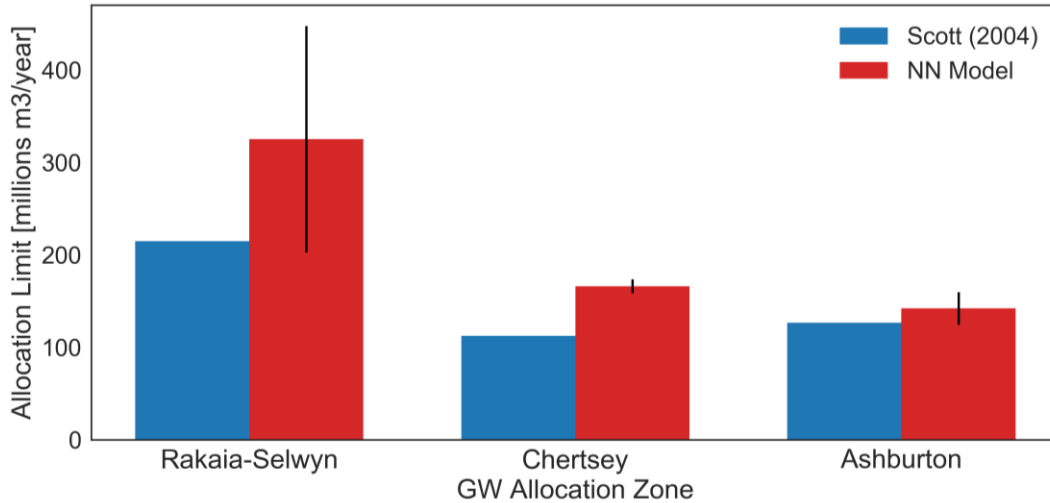


Figure 32. Groundwater allocation limits in three allocation zones in the Canterbury region. The blue bars show the limits registered in the regional plan, and the red bars show the limits calculated employing the NN model. The black error bars overlapping the NN predictions represent the uncertainty.

One major strength of the approach is its low computational costs. Once the area of interest and the minimum inputs parameters required are defined, the model can then be used to derive land surface recharge estimations. Therefore, the approach could be easily implemented for operation applications. However, this is only valid provided that the assumptions for model development remain constant with time e.g. in case of drastic changes from irrigated grasslands to a different land cover in the study area, a redefinition of model parameters would be recommended, though this is very unlikely. As mentioned by Greifeneder et al. (2016), one other reason to consider redefining the model would be the inclusion of one or more stations to the network (i.e. lysimeters), which may allow for a better and more precise upscaling of the land surface recharge process.

## 6.2 Patia Valley, Cauca, Colombia – Case study II

### 6.2.1 Model development

This project was also aiming to contribute towards development of research resources for Colombia. For this reason, the idea of employing a NN model to estimate LSR recharge was evaluated in a small region in South-West Colombia. Given that Colombia is a developing country, the availability of data is a constraint when assessing new approaches. Although lysimeter-measured recharge data was not available, training an ANN with modelled data was possible. In general, three different approaches were utilised for model development on a monthly basis, though the outcomes were not satisfactory. Based on the results in Canterbury, a better performance was expected in the model for the Patia Valley given that the model was set up with monthly data. The reduction in performance may be attributed to the simplicity in the calculation of the current recharge values. At the moment, recharge is estimated on a regional “water balance” basis, where the infiltration rate is assumed to be the input to the system (rainfall) minus the outputs (i.e.

evapotranspiration and runoff) (CRC, 2017). Given the simplicity of this approach, the NN model developed based on this LSR estimations shows many limitations in both complexity and accuracy. Also, only rainfall and ET data were assumed as the variables influencing recharge (since this was the only data available region-wide). Typically, the LSR process cannot be modelled based on a direct correlation between rainfall and ET alone because the relationship is far more complex. Similar results were reported by Greifeneder et al. (2016), who found unsatisfactory outcomes when upscaling satellite remote sensing SMC, based on a two variables relation i.e. the backscattering intensity of the radar images and in situ point scale measures of soil moisture. This behaviour suggests that the proposed model does not improve the representativeness of land surface recharge related to the previous water balance estimations. Therefore, a conclusion about the validity of the proposed LSR approach cannot be drawn in this region based solely on the correlation between rainfall and ET alone.

### **6.2.2 Model Uncertainty**

Uncertainty values greater than 100% were observed, although this is not possible from a physical point view similar results were reported by Westerhoff et al. (2018). They observed how uncertainty as a percentage of recharge for low values of recharge can be higher than their actual recharge value (i.e. mean uncertainty as percentage of recharge can exceed 200% of the actual recharge estimation). High uncertainty values were expected and can be attributed to the small proportion of rainfall and evapotranspiration data available for training the model, but also, to the simplicity of the previous LSR estimations (Based on a water balance approach) which the model was trained on (which are highly uncertain as well). With the data that was available for this case study, an artificial neural network may not be the best approach to tackle issues in water allocation in Patia Valley. Although previous reports in the region recommend groundwater allocation decisions based on water balance calculations (Pérez et al., 2015), findings in the Canterbury region have proven that the inclusion of lysimeter-measured data is useful for water allocation. Leube et al. (2012) also mentioned how providing hydrogeological data (e.g. lysimeter data) to stochastic models is likely to reduce prediction uncertainty, and consequently, decision-making processes in water allocation may be improved.

## **7. CONCLUSIONS AND RECOMMENDATIONS**

Here an artificial neural networks approach to spatially upscale point measurements of lysimeter-recharge in three groundwater allocation zones in the Canterbury Plains has been developed, tested and applied. The idea of employing a NN to estimate recharge was inspired by the approach reported by White et al. (2003) for estimating dryland recharge, with the addition that the model developed in the current study was trained to consider the effect of irrigation. The lysimeter data was thoroughly quality-checked before its use for training the model. The quality control procedure revealed outliers, unusual events and missing data time periods. Outliers themselves are points of primary interest, since they can either draw attention to unknown aspects of the data or lead to new discoveries (Hadi et al., 2009), though they can also have a break down effect in supervised learning models (Beliakov et al., 2011). While the data set used here has been thoroughly assessed and adjusted where necessary, it is recommended that in future work a refined quality control

scheme that incorporates additional measures, and new quality flags should be developed to provide the model with information-rich data from which it can learn.

To predict land surface recharge two types of neural networks were developed. A simple feed forward neural network, and an approximation to a Bayesian NN by implementing a dropout procedure during training. Both networks were constructed with different architectures. A total of 230 models were developed with different numbers of layers and neurons. The results (predicted values) were analysed for all 230 models by comparing them with the lysimeter-measured recharge at the three study locations (i.e. Dorie, Methven and Dunsandel). The models were evaluated based on their predictive performance through a suite of statistical measures. The approximation of a Bayesian NN was found to perform better compared to the feed forward NN and thus it was selected for the upscaling procedure. Future work may focus on comparing ANN prediction of land surface recharge with other machine learning techniques such as random forest regressors or recurrent neural networks.

This research also provides insights into the uncertainty on LSR prediction using an artificial neural network model. The uncertainty analysis revealed that rainfall and irrigation are the factors with the highest influence in both daily recharge and model uncertainty, followed by a less dominant contribution by the PET and the dominant soil texture, which is consistent with findings in Westerhoff et al. (2018).

Future research should look into the feasibility of reducing uncertainty through the inclusion of extreme events and “information rich” datasets, which likely expand the range of situations for which such a model implementation is valid.

The methodology developed in this study couples ANN techniques of supervised learning with a visualisation tool of spatial data, i.e. a GIS. The ArcPy module was implemented to ease the cumbersome arithmetic operations in GIS. The subjectivity issues related to weights did not arise since no prior relationship between the inputs and outputs is assumed. The regional LSR values, estimated after coupling the ANN in a GIS environment, are 650.57 million m<sup>3</sup> year<sup>-1</sup>, 332.45 million m<sup>3</sup> year<sup>-1</sup> and 284.41 million m<sup>3</sup> year<sup>-1</sup> for Rakaia-Selwyn, Chertsey and Ashburton, respectively. For the calculation of LSR in the three zones, inputs from irrigation were not considered since this information is not available region-wide. In the future, it is recommended to use the irrigable area map from the Ministry of the environment to make predictions of both irrigated area and irrigation water use in order to improve the LSR estimations calculated by the NN model. However, given that most of the recharge occurs during the winter when the irrigation is zero, the non-inclusion of irrigation in the calculations does not induce a large error, with the exception of places where irrigation is applied in high amounts e.g. Dunsandel lysimeter site.

Promising results were found by employing three key descriptors for predicting LSR: precipitation, PET and a dominant soil texture classification. Furthermore, based on the results for a single NN per location, it seems promising to include VWC jointly with lysimeter data to evaluate recharge patterns at the farm scale. Thus, it is recommended to develop a daily water balance model based on rainfall/irrigation, soil water content, PET as inputs to the ANN model in order to estimate recharge. On this regard, soil moisture sensors would improve our ability to both model and upscale groundwater recharge (Graham et al., 2018; Wang et al., 2016).

This work also aimed to prove how machine learning techniques (e.g. neural networks) could assist water allocation decisions in data scarce regions, where the access to recharge data is a constraint. However, given the results obtained for the current case study in Colombia, a conclusion about the validity of the proposed LSR approach cannot be drawn based solely on the correlation between rainfall and ET. Findings

of the study in the Canterbury region, supported by comments by Leube et al. (2012), suggest that the addition of hydrogeological data (e.g. lysimeter data), may reduce prediction uncertainty, which in turn can inform water allocation decisions. The model uncertainty was found to be high, which was mostly attributed to the lack of information to describe the recharge process in the study region in Colombia. Graham et al. (2018) proved the usefulness of a soil moisture network in modelling groundwater recharge, thus future work may investigate if the addition of this data will improve water management in that region in Colombia. However, this can only be achieved through a collaborative effort, with regional councils, research organizations and universities working towards this common goal.

Comparing the two case studies, in terms of accuracies, it was shown that in at least one case it was possible to significantly improve the representativeness of lysimeter data to a larger scale. In addition, despite the imbalance in some of the observations, the findings make a strong case for the methodology proposed here. Therefore, this method can be applied to any other region in New Zealand in order to calculate land surface recharge, given that the parameters required by the model to compute predictions are available.

## 8. APPENDIX

### 8.1 Appendix A.

Reclassified values of the soil data reported by Newsome et al. (2008).

PAW Class	PAW [mm]	Reclassified value
Very low	< 30	7
Low	30 - 59	6
Moderate to low	60 - 89	5
Moderate	90 - 119	4
Moderate to high	120 - 149	3
High	150 - 249	2
Very high	> 250	1

Drainage class	Reclassified value
Very poorly drained	1
Poorly drained	2
Imperfectly drained	3
Moderately well drained	4
Well drained	5

Soil dominant texture	Reclassified value
Peaty	5
Sandy	4

Loamy	3
Silty	2
Clayey	1

Topsoil stoniness	Reclassified value
Stoneless	0
Moderately stony	1
Stony	2

## 8.2 Appendix B

Matrix of weights and biases of the NN that showed the best performance.

```
In [274]: nn_daily.get_weights()
Out[274]: [array([[ 4.0899067 ,  3.9435768 ,  4.854136 ,  4.573645 ,  4.8157434 ],
                 [-3.674227 , -0.8574211 , -6.1246777 , -1.4302855 , -0.51860934],
                 [-0.27474046,  0.02802313,  0.5013907 ,  0.69277096,  0.94638336]],
          dtype=float32),
          array([ 0.1467431 ,  0.10605031, -0.42496523, -0.67596495, -0.9197755 ],
          dtype=float32),
          array([[4.6370482],
                 [2.9266272],
                 [5.873814 ],
                 [5.1125426],
                 [4.617172 ]], dtype=float32),
          array([0.17330451], dtype=float32)]
```

## 8.3 Appendix C

Python code to feed the NN into GIS

```
import arcpy
from arcpy import *
import arcgisscripting
import functools
import os
from arcpy import env
from arcpy.sa import *
arcpy.CheckOutExtension('Spatial')
arcpy.env.overwriteOutput = True

rws = r'C:\Users\Usuario\UNIVALLE\LINCOLN\Thesis\Data\Data_code\final_irrigated_data\rain.gdb'
arcpy.env.workspace= rws
rainrasters = arcpy.ListRasters()
```

```

petws = r'C:\Users\Usuario\UNIVALLE\LINCOLN\Thesis\Data\Data_code\final_irrigated_data\pet.gdb'
arcpy.env.workspace = petws
petrasters = arcpy.ListRasters()

#print("PET rasters are:", petrasters)

lsr = []

#outpath=r"C:\Users\Usuario\UNIVALLE\LINCOLN\Thesis\Data\Data_code\final_irrigated_data\results_loo
ping"
#arcpy.env.workspace = outpath

bws = r"C:\Users\Usuario\UNIVALLE\LINCOLN\Thesis\Data\Data_code\final_irrigated_data\bin"
arcpy.env.workspace = bws

count = 1

text_area_ras_reclass =
Raster(r"C:\Users\Usuario\UNIVALLE\LINCOLN\Thesis\Data\Data_code\final_irrigated_data\thesis_manuel
.gdb\text_area_ras_reclass")

# Process: Iterate Rasters
#for rainraster, petraster in zip(rainrasters, petrasters):

for rainraster in rainrasters:
    rainrastername = rainraster
    baserainname = rainrastername.strip("rain_")
    petrastername = "" # Initialise the variable to be populated in the inner loop
    for petraster in petrasters:
        if petraster.endswith(baserainname,4):
            petrastername = petraster
            basepetname = petrastername.strip("PET_")
            break #breaks out of the inner loop - We have a match!
    if petrastername != "": #Just to make sure

        print("The rain layer corresponds to:"+baserainname)
        print("The pet layer corresponds to:"+basepetname)

#print ("Days match")
Rainfall = (os.path.join(rws,rainrastername)) #make Raster objects from filenames

```

```

PET = (os.path.join(petws,petrastename)) #make Raster objects from filenames

# Process: MinMaxScaler
#arcpy.gp.RasterCalculator_sa("(\\\"%Rainfall%\" / 134.6)", normalized_rainfall)
normalized_rainfall = Divide(Rainfall,float(134.6))

# Process: MinMaxScaler_2
#arcpy.gp.Calculator_sa("(\\\"%PET%\" / 9.6)", normalized_pet)
normalized_pet = Divide(PET,float(9.6))

# Process: MinMaxScaler3
#arcpy.gp.Calculator_sa("(\\\"%text_area_ras_reclass%\" - 2)", normalized_text)
normalized_text = Minus(text_area_ras_reclass,2)

# Process: n1
#arcpy.gp.Calculator_sa("((0.1467431) + ((\\\"%normalized_rainfall%\" * 4.0899067) +
(\\\"%normalized_pet%\" * - 3.674227) + (\\\"%normalized_text%\" * - 0.27474046))))", summ_neuron1)
summ_neuron1 = ((0.1467431) + (((normalized_rainfall) * 4.0899067)) + ((normalized_pet) * (-
3.674227)) + ((normalized_text) * (-0.27474046)))

# Process: relu_n1
#arcpy.gp.Calculator_sa("Con(\\\"%summ_neuron1%\" > 0,\\\"%summ_neuron1%\",0)", act_n1)
act_n1 = Con((summ_neuron1 > 0), summ_neuron1, 0)

# Process: n2
#arcpy.gp.Calculator_sa("((0.10605031) + ((\\\"%normalized_rainfall%\" * 3.9435768) +
(\\\"%normalized_pet%\" * - 0.8574211) + (\\\"%normalized_text%\" * 0.02802313))))", summ_n2)
summ_n2 = ((0.10605031) + (((normalized_rainfall) * 3.9435768)) + ((normalized_pet) * (-
0.8574211)) + ((normalized_text) * 0.02802313))

# Process: relu_n2
#arcpy.gp.Calculator_sa("Con(\\\"%summ_n2%\" > 0,\\\"%summ_n2%\",0)", act_n2)
act_n2 = Con((summ_n2 > 0), summ_n2, 0)

# Process: n3
#arcpy.gp.Calculator_sa("((- 0.42496523) + ((\\\"%normalized_rainfall%\" * 4.854136) +
(\\\"%normalized_pet%\" * - 6.1246777) + (\\\"%normalized_text%\" * 0.5013907))))", summ_n3)
summ_n3 = ((-0.42496523) + (((normalized_rainfall) * 4.854136)) + ((normalized_pet) * (-
6.1246777)) + ((normalized_text) * 0.5013907))

```

```

# Process: relu_n3
#arcpy.gp.Calculator_sa("Con(!"%summ_n3%" > 0,!"%summ_n3%",0)", act_n3)
act_n3 = Con((summ_n3 > 0), summ_n3, 0)

# Process: n4
#arcpy.gp.Calculator_sa("((- 0.67596495) + (!"%normalized_rainfall%" * 4.573645) +
(!"%normalized_pet%" * - 1.4302855) + (!"%normalized_text%" * 0.69277096)))", summ_n4)
summ_n4 = ((-0.67596495) + (((normalized_rainfall) * 4.573645)) + ((normalized_pet) * (-
1.4302855)) + ((normalized_text) * 0.69277096))

# Process: relu_n4
#arcpy.gp.Calculator_sa("Con(!"%summ_n4%" > 0,!"%summ_n4%",0)", act_n4)
act_n4 = Con((summ_n4 > 0), summ_n4, 0)

# Process: n5
#arcpy.gp.Calculator_sa("((- 0.9197755) + (!"%normalized_rainfall%" * 4.8157434) +
(!"%normalized_pet%" * - 0.51860934) + (!"%normalized_text%" * 0.94638336)))", summ_n5)
summ_n5 = ((-0.9197755) + (((normalized_rainfall) * 4.8157434)) + ((normalized_pet) * (-
0.51860934)) + ((normalized_text) * 0.94638336))

# Process: relu_n5
#arcpy.gp.Calculator_sa("Con(!"%summ_n5%"> 0,!"%summ_n5%",0)", act_n5)
act_n5 = Con((summ_n5 > 0), summ_n5, 0)

# Process: Calculator
#arcpy.gp.Calculator_sa("((0.17330451) + (!"%act_n1%" * 4.6370482) + (!"%act_n2%" *
2.9266272) + (!"%act_n3%" * 5.873814) + (!"%act_n4%" * 5.1125426) + (!"%act_n5%" * 4.617172)))",
summ_final_neuron)
summ_final_neuron = ((0.17330451) + (((act_n1) * 4.6370482)) + ((act_n2) * 2.9266272) +
((act_n3) * 5.873814) + ((act_n4)*5.1125426) + ((act_n5)*4.617172))

# Process: relu_final_neuron
#arcpy.gp.Calculator_sa("Con(!"%summ_final_neuron%" > 0,!"%summ_final_neuron%",0)",
LSR_Prediction+"Day_"+str(count+1))
prws =
r"C:\Users\Usuario\UNIVALLE\LINCOLN\Thesis\Data\Data_code\final_irrigated_data\predictions.gdb"
#Predictions workspace/geodatabase
prediction = Con(summ_final_neuron > 0, summ_final_neuron, 0)

```

```

filename = "LSR_Prediction_" + basepetname
outname = os.path.join(prws, filename)
prediction.save(outname)
print("The predictions corresponds to day:" + basepetname)

lsr.append(prediction)

count += 1

print("The looping has finished.")

#Calculates the water allocation prediction
import arcpy
from arcpy import *
import arcgisscripting
import functools
import os
from arcpy import env
from arcpy.sa import *
arcpy.CheckOutExtension('Spatial')
arcpy.env.overwriteOutput = True

finalws =
r"C:\Users\Usuario\UNIVALLE\LINCOLN\Thesis\Data\Data_code\final_irrigated_data\predictions.gdb"
arcpy.env.workspace = finalws
rechargerasters = arcpy.ListRasters(",")

outCellStatistics = CellStatistics(rechargerasters, "SUM", "DATA")

# Save the output
outCellStatistics.save(os.path.join(finalws, "Water_allocation_prediction"))

print("Done")

```

## 8.4 Appendix D

```

import arcpy
from arcpy import *

```

```

import arcgisscripting
import functools
import os
from arcpy import env
from arcpy.sa import *
arcpy.CheckOutExtension('Spatial')
arcpy.env.overwriteOutput = True

finalws =
r"C:\Users\Usuario\UNIVALLE\LINCOLN\Thesis\Data\Data_code\final_irrigated_data\predictions.gdb"
arcpy.env.workspace = finalws
rechargerasters = arcpy.ListRasters(",")

outCellStatistics = CellStatistics(rechargerasters, "SUM","DATA")

# Save the output
outCellStatistics.save(os.path.join(finalws,"Water_allocation_prediction"))

print("Done")

```

## 8.5 Appendix E

Python code to calculate uncertainty employing Monte Carlo Dropout

```

from keras.models import Model

class KerasDropoutPrediction(object):
    def __init__(self,model):
        self.f = K.function(
            [nn_daily.layers[0].input,
            K.learning_phase()],
            [nn_daily.layers[-1].output])
    def predict(self,x, n_iter):
        result = []

        for _ in range(n_iter):
            result.append(self.f([x , 1]))

        #mc_pred = np.mean(result)
        #mc_unc = np.std(result)

```

```

result = np.array(result).reshape(n_iter,len(x)).T
return result#, mc_pred, mc_unc

```

```

kdp_m = KerasDropoutPrediction(nn_daily)
model_drp = kdp_m.predict(trans_model_test,n_iter=10000)
mean_model_drp = model_drp.mean(axis=1) # This is the correct axis
unc_model_drp = model_drp.std(axis=1) #Correct axis

```

### 8.1 Appendix F

Evapotranspiration data collected in stations in and surrounding the study area. All values in mm month<sup>-1</sup>.

GJA EXP UNIV NARIN													
n	P	JAN	FEB	MAR	APR	MAY	JUN	JUL	AUG	SEP	OCT	NOV	DEC
1	5	173.3	176.8	184.2	150.3	165.4	169.3	218.0	230.0	262.3	239.8	183.1	166.6
2	10	167.8	147.6	167.9	147.0	160.6	167.4	217.3	219.1	206.3	185.9	162.3	166.3
3	14	154.9	146.3	164.6	141.3	154.5	159.2	203.7	181.4	199.6	175.3	158.4	154.6
4	19	151.7	142.4	161.1	131.9	154.2	158.5	178.6	179.5	192.0	168.2	144.3	146.5
5	24	139.3	125.7	161.0	131.6	146.3	158.4	173.2	176.1	180.7	166.9	144.3	135.2
6	29	138.8	123.4	156.6	131.2	139.6	155.6	156.9	167.0	164.9	144.3	144.3	132.0
7	33	134.5	123.4	153.9	129.3	138.1	154.1	155.8	162.8	160.9	144.3	144.3	123.2
35		132.1	123.4	151.4	129.2	137.6	153.3	154.3	162.2	160.9	144.3	144.3	121.8
8	38	127.7	123.4	146.8	129.1	136.8	151.7	151.4	161.0	160.9	144.3	144.3	119.1
9	43	127.7	123.4	136.2	127.1	131.0	141.7	151.4	160.4	160.9	144.3	144.3	119.1
10	48	127.7	123.4	135.8	121.5	130.0	138.0	151.4	154.9	160.9	144.3	144.3	119.1
50		125.5	123.4	134.8	121.5	130.0	138.0	151.4	154.9	160.9	144.3	144.3	119.1
11	52	123.4	123.4	133.8	121.5	130.0	138.0	151.4	154.9	160.9	144.3	144.3	119.1
12	57	123.1	123.2	130.6	121.5	130.0	138.0	149.1	154.9	160.9	144.3	136.7	119.1
13	62	120.0	120.9	126.4	121.5	129.3	130.6	144.4	154.9	160.9	144.3	128.5	110.5
65		118.8	120.9	122.6	120.3	128.2	127.7	141.5	154.2	149.3	144.3	121.1	109.6
14	67	118.1	120.9	120.6	119.7	127.6	126.1	140.0	153.8	143.0	144.3	117.1	109.1
15	71	118.1	120.1	120.6	115.4	124.5	125.3	139.2	152.4	139.5	125.3	115.2	108.0
16	76	115.1	119.4	119.1	108.1	123.2	124.8	120.6	137.9	131.4	119.1	106.7	99.7
17	81	109.4	107.8	111.2	105.7	105.9	122.6	118.4	121.1	130.1	114.5	105.0	96.2
18	86	103.1	100.9	102.0	100.8	98.0	107.5	110.1	105.4	129.3	108.4	104.5	93.8
19	90	99.0	94.0	96.9	95.7	96.4	106.4	109.5	90.3	114.1	97.6	102.4	82.6
20	95	80.8	81.3	86.4	79.3	79.0	87.5	87.3	80.2	98.4	86.5	72.5	76.9

FONDA LA CITEC

n	P	JAN	FEB	MAR	APR	MAY	JUN	JUL	AUG	SEP	OCT	NOV	DEC
1	3	164.6	141.7	153.2	136.0	129.7	164.8	179.3	201.0	178.8	165.9	131.0	140.0
2	6	156.0	139.1	151.6	133.7	129.4	145.0	177.9	181.2	173.0	164.8	129.2	137.7
3	9	151.6	138.9	149.2	130.0	116.6	138.0	170.9	177.3	169.8	148.6	123.6	136.6
4	13	145.7	135.1	148.5	123.3	114.1	126.8	150.2	168.8	164.4	142.3	121.3	134.7
5	16	139.3	129.3	145.7	122.2	113.8	126.3	145.8	168.5	164.1	141.7	119.9	134.5
6	19	136.6	128.0	139.9	122.1	113.6	126.1	145.6	168.2	159.7	140.9	117.6	131.1
7	22	133.4	125.7	130.9	120.8	111.7	123.4	143.4	162.4	157.1	137.4	117.1	128.3
8	25	130.5	124.7	129.0	118.3	110.3	122.6	142.1	160.0	153.8	135.4	111.6	126.8
9	28	130.0	123.9	127.1	116.9	109.3	117.7	138.9	159.7	152.8	131.8	110.9	122.1
10	31	122.8	123.7	126.5	116.3	107.8	117.1	137.8	158.7	152.4	131.6	109.6	119.7
11	34	122.5	121.0	122.6	115.5	106.8	116.6	136.8	157.9	151.3	131.0	106.6	118.5
	35	122.3	120.4	122.2	115.2	106.8	116.1	135.7	156.3	150.2	130.2	106.4	117.9
12	38	121.4	117.9	120.7	114.1	106.6	114.1	131.4	149.9	145.9	127.0	105.6	115.4
13	41	118.8	117.2	119.0	111.5	105.7	113.3	131.2	145.8	137.8	125.8	105.6	112.9
14	44	118.7	113.6	118.7	110.6	105.3	111.7	129.2	145.8	133.0	123.1	105.2	112.4
15	47	118.7	113.6	118.7	110.6	103.9	111.0	125.7	145.8	133.0	123.1	105.2	110.9
16	50	118.7	113.6	118.7	110.6	103.4	111.0	124.9	145.8	133.0	123.1	105.2	110.9
17	53	118.7	111.9	118.7	110.6	103.4	109.6	124.9	145.8	133.0	123.1	105.2	110.9
18	56	115.3	111.9	118.7	110.6	103.4	109.6	124.9	145.8	133.0	123.1	105.2	110.9
19	59	112.6	109.9	113.2	110.6	102.8	106.9	123.8	144.5	133.0	123.1	105.2	110.9
20	63	110.6	107.5	112.6	110.6	101.9	106.7	121.7	144.2	133.0	119.8	104.7	106.0
	65	110.4	106.6	112.4	110.2	101.8	106.0	119.5	143.5	126.2	119.2	104.5	105.5
21	66	110.4	106.4	112.4	110.1	101.8	105.8	118.9	143.3	124.5	119.0	104.5	105.4
22	69	109.5	105.2	111.6	109.5	101.7	105.3	118.8	142.8	123.4	114.4	104.3	105.4
23	72	106.2	103.8	111.0	106.6	101.7	104.4	115.8	141.4	121.9	113.6	101.7	100.8
24	75	102.4	102.6	110.7	105.8	100.9	102.7	114.6	137.7	120.8	110.7	100.7	97.4
25	78	100.8	102.0	105.6	101.9	96.7	99.2	104.4	136.9	118.2	108.2	99.3	96.5
26	81	100.3	101.7	102.8	98.6	94.6	98.6	98.5	127.2	117.4	105.9	96.9	95.7
27	84	98.8	99.0	100.2	92.4	93.3	93.3	95.5	123.7	115.1	100.3	96.5	94.6
28	88	92.8	95.6	91.4	90.1	92.0	92.8	81.3	122.9	99.8	95.6	95.1	91.5
29	91	92.1	91.7	87.4	87.0	85.7	90.2	80.8	115.8	84.8	92.8	92.5	85.9
30	94	90.6	90.2	84.0	86.8	82.1	79.2	69.8	80.0	66.8	91.8	90.8	85.6
31	97	84.1	88.8	83.1	85.4	78.6	51.4	66.9	69.8	39.0	82.1	56.0	48.5

---

**BOLIVAR**

---

n	P	JAN	FEB	MAR	APR	MAY	JUN	JUL	AUG	SEP	OCT	NOV	DEC
---	---	-----	-----	-----	-----	-----	-----	-----	-----	-----	-----	-----	-----

1	2	156.9	127.3	155.4	138.9	123.3	165.4	186.1	238.3	200.6	161.9	126.2	127.7
2	5	140.2	123.6	145.2	121.3	120.3	143.1	182.9	234.7	177.5	154.7	125.1	120.5
3	7	131.6	123.4	126.8	117.2	116.4	139.0	177.9	209.6	175.6	152.6	122.4	119.2
4	9	131.2	118.5	125.3	115.4	116.3	134.0	177.6	202.5	174.7	150.2	120.3	117.6
5	12	130.1	116.8	124.4	109.1	115.0	132.6	172.0	195.6	168.4	149.8	115.2	115.3
6	14	128.7	115.0	122.7	108.2	112.4	131.5	168.9	193.7	159.2	139.2	111.0	112.7
7	16	128.1	112.4	121.9	106.1	112.1	131.1	168.6	192.7	157.3	126.2	106.9	111.7
8	19	127.8	112.4	120.7	106.1	111.3	123.4	166.1	185.8	154.2	124.3	101.6	111.0
9	21	127.1	110.9	115.8	103.9	110.4	121.6	165.1	185.3	153.4	121.6	100.6	110.0
10	23	126.7	110.4	114.9	103.5	108.5	119.9	164.0	173.0	150.3	121.1	99.0	109.1
11	26	123.2	110.4	114.3	101.8	107.1	119.7	155.1	170.9	149.8	119.3	98.1	107.0
12	28	121.5	106.1	113.5	101.4	106.8	111.4	152.6	165.3	148.4	118.0	96.4	106.5
13	30	115.8	106.1	112.4	97.0	105.8	108.3	152.2	157.4	138.2	117.5	95.5	105.8
14	33	115.3	104.4	111.5	96.6	104.4	107.1	150.2	156.4	133.7	116.2	91.8	103.4
15	35	114.6	102.8	108.0	96.6	103.9	106.4	147.1	154.9	131.3	116.0	91.5	102.8
16	37	111.0	102.5	107.9	96.5	103.4	106.0	146.6	150.2	130.3	115.2	89.3	102.5
17	40	108.8	102.0	107.6	95.0	102.3	106.0	146.0	150.2	128.4	114.8	88.4	102.1
18	42	108.8	100.1	104.5	94.2	102.2	106.0	140.4	150.2	128.4	114.6	88.4	102.0
19	44	108.8	99.6	104.5	94.2	101.9	106.0	139.5	150.2	128.4	110.3	88.4	101.5
20	47	108.8	99.6	104.4	94.2	101.9	106.0	138.8	148.6	128.4	110.3	88.4	101.3
21	49	108.5	99.6	103.9	94.2	101.4	106.0	138.8	146.8	126.9	110.3	88.4	100.9
	50	108.0	99.6	103.9	94.1	100.7	105.8	138.8	146.7	126.4	110.3	88.1	100.6
22	51	107.5	99.6	103.8	94.1	99.9	105.6	138.8	146.5	125.9	110.3	87.9	100.2
23	53	107.0	99.5	102.7	91.6	99.6	104.5	138.8	145.0	125.8	110.3	87.1	99.9
24	56	106.3	99.5	101.6	91.0	99.6	103.8	138.8	145.0	124.1	110.3	85.7	98.2
25	58	104.4	97.8	99.6	91.0	99.6	102.8	136.3	144.4	123.7	104.0	85.6	98.2
26	60	104.2	96.7	98.1	90.4	99.1	101.5	132.5	136.5	121.6	99.7	85.3	98.2
27	63	102.7	96.1	98.0	90.0	97.7	101.2	131.3	135.9	119.1	99.0	85.3	98.2
28	65	101.7	92.7	97.4	89.5	97.0	98.2	130.6	133.7	112.5	98.7	83.8	96.7
29	67	99.3	91.9	97.1	88.5	96.4	95.9	125.5	132.6	111.5	96.5	81.8	95.5
30	70	99.2	91.2	95.9	87.3	95.9	94.5	125.5	132.5	109.4	95.1	79.7	95.1
31	72	98.8	90.9	95.7	86.2	93.2	93.8	125.2	131.1	105.8	93.6	78.8	94.6
32	74	97.8	89.8	93.8	86.1	93.1	93.5	123.1	131.0	105.6	93.2	78.6	94.5
33	77	91.7	89.6	91.7	83.8	90.3	89.9	121.7	126.9	105.0	92.4	75.9	90.6
34	79	91.6	89.5	89.2	83.7	87.8	89.8	119.3	125.2	104.9	91.9	75.0	84.2
35	81	90.4	85.2	86.7	81.4	85.3	88.6	118.1	122.5	104.8	91.7	72.6	84.1
36	84	86.8	83.7	84.3	81.2	84.8	87.8	111.4	120.8	104.7	91.1	68.2	82.8
37	86	86.6	83.3	84.3	80.3	84.1	84.4	109.2	120.0	102.0	89.0	68.0	78.2
38	88	85.9	83.1	84.2	79.3	83.8	82.5	100.5	111.1	100.4	88.8	67.6	75.4

39	91	85.7	82.1	82.7	79.2	83.0	80.8	99.7	105.7	98.7	86.1	65.1	74.9
40	93	84.7	81.5	81.0	75.4	76.4	79.9	96.9	100.5	95.3	85.6	59.7	72.8
41	95	84.5	77.9	80.6	72.4	74.4	77.2	87.6	81.7	88.7	82.3	58.2	67.0
42	98	78.0	76.7	74.9	61.8	74.3	66.7	83.2	67.3	61.1	58.4	49.7	53.4

---

**MERCADERES**

n	P	JAN	FEB	MAR	APR	MAY	JUN	JUL	AUG	SEP	OCT	NOV	DEC
1	3	167.9	160.1	170.5	130.6	126.1	142.0	182.9	206.6	180.1	174.1	137.1	139.2
2	5	150.5	139.6	161.6	126.9	124.0	137.3	180.6	173.9	180.0	164.2	123.6	139.1
3	8	150.2	133.8	150.7	124.8	120.5	125.7	175.5	170.3	174.1	157.1	123.4	137.3
4	10	147.4	131.7	147.4	123.8	120.3	124.9	168.8	167.9	164.1	144.6	122.6	134.1
5	13	147.3	128.9	141.2	123.3	119.8	124.6	161.6	167.0	162.0	144.5	122.6	132.6
6	15	145.8	128.5	138.8	120.5	119.6	117.5	157.0	165.5	161.6	143.7	121.4	130.8
7	18	141.6	126.3	137.6	120.4	113.7	116.9	154.7	164.7	159.7	143.0	120.8	126.5
8	21	137.5	124.5	134.9	119.8	113.1	114.0	149.1	164.3	157.6	142.0	118.5	123.2
9	23	133.6	121.4	133.5	119.2	110.7	113.8	144.8	162.9	157.1	140.9	117.7	123.2
10	26	132.4	119.8	132.8	114.9	110.3	111.7	144.2	161.8	157.0	135.4	116.8	122.9
11	28	132.4	117.5	130.4	113.7	108.9	110.5	139.7	157.0	153.2	135.2	116.1	122.7
12	31	132.2	112.7	128.3	113.6	107.0	109.9	137.4	156.6	150.6	133.7	115.3	122.3
13	33	131.4	112.1	128.2	113.0	105.4	108.6	137.3	156.6	147.2	133.2	113.9	121.6
	35	131.3	111.6	127.8	111.9	104.8	108.4	134.1	154.3	147.0	131.2	113.8	121.5
14	36	131.2	111.3	127.6	111.3	104.5	108.3	132.4	153.0	146.9	130.1	113.7	121.4
15	38	128.4	111.3	123.9	110.9	104.2	108.0	131.6	151.4	145.4	130.0	110.7	121.2
16	41	127.6	111.2	122.5	110.4	102.4	107.7	131.6	145.8	138.0	128.3	110.5	119.6
17	44	125.9	110.9	121.7	104.8	102.4	106.4	131.6	145.8	137.5	125.6	108.5	119.5
18	46	124.6	110.4	119.4	103.1	102.0	106.4	131.5	145.2	137.2	125.1	107.1	118.1
19	49	124.1	110.4	119.4	101.5	101.0	104.4	130.7	143.0	135.5	123.6	106.1	118.0
	50	124.0	110.4	119.4	101.5	100.7	104.4	130.4	142.5	134.7	123.6	105.2	117.3
20	51	123.9	110.3	119.4	101.5	100.4	104.4	130.0	142.0	134.0	123.6	104.2	116.5
21	54	123.9	109.7	119.4	101.3	100.3	103.1	127.9	142.0	134.0	123.6	104.2	116.0
22	56	122.4	109.7	117.8	101.0	98.4	101.4	126.3	142.0	134.0	123.2	104.2	116.0
23	59	122.0	109.0	117.7	99.9	98.4	101.2	126.1	142.0	132.6	121.2	103.4	115.3
24	62	120.9	108.5	111.5	99.3	98.3	100.4	122.4	141.2	128.6	120.9	102.9	112.3
25	64	120.0	106.2	111.2	99.0	98.2	99.9	121.9	135.3	119.6	119.7	99.1	111.8
	65	119.9	106.2	110.9	97.7	97.6	99.7	121.7	133.5	119.6	118.8	98.6	111.6
26	67	119.6	106.2	110.2	95.3	96.6	99.4	121.4	130.1	119.5	117.1	97.8	111.1
27	69	118.3	105.4	108.9	94.3	92.9	99.0	120.5	129.0	118.3	115.0	97.3	111.1
28	72	117.2	104.6	107.8	92.9	92.1	96.9	119.7	126.3	118.0	114.3	97.2	110.1

29	74	114.4	104.3	107.5	91.3	86.0	96.1	117.4	120.8	116.4	112.6	92.8	108.9
30	77	112.0	102.3	105.6	90.2	85.2	94.7	116.2	119.5	115.5	111.5	92.4	108.8
31	79	108.6	100.5	104.4	87.4	84.6	92.8	116.1	119.2	111.8	110.4	87.2	107.3
32	82	107.0	96.1	104.3	76.0	83.3	90.7	115.3	118.5	108.0	101.9	85.2	101.5
33	85	105.4	92.5	100.1	75.3	72.5	84.2	113.0	113.6	107.9	99.2	84.9	100.7
34	87	104.6	89.7	97.8	74.1	70.4	84.0	112.7	112.0	105.4	99.0	83.8	99.2
35	90	100.5	89.5	91.4	73.4	68.5	83.7	99.0	107.6	95.6	97.2	82.3	94.1
36	92	99.0	89.3	84.6	71.2	67.4	83.4	92.9	102.9	91.2	80.8	77.2	93.9
37	95	94.7	88.8	83.0	65.1	66.8	81.2	90.5	98.3	84.3	78.8	76.7	91.0
38	97	92.1	83.8	69.7	60.3	64.6	72.7	90.0	93.7	71.6	73.1	61.2	88.6

## 8.2 Appendix G

Rainfall data collected in stations in and surrounding the study area. All values in mm month<sup>-1</sup>.

Rainfall station : 52010020 BALBOA													
n	P	JAN	FEB	MAR	APR	MAY	JUN	JUL	AUG	SEP	OCT	NOV	DEC
1	4	481	373	462	700	506	317	304	232	285	547	779	633
2	7	471	354	456	571	431	186	252	209	232	507	642	598
3	11	450	310	454	382	419	179	232	99	231	499	565	539
4	15	406	294	393	377	319	138	148	73	211	481	507	471
5	19	385	273	375	376	266	137	136	64	203	437	467	469
6	22	326	266	315	342	255	122	103	61	183	411	466	460
7	26	319	244	314	313	245	118	102	56	130	408	461	452
8	30	309	243	303	291	228	116	99	54	127	403	447	419
9	33	299	220	283	259	214	115	68	53	124	394	424	401
	35	296	220	261	259	212	111	67	51	120	386	417	376
10	37	292	219	234	258	210	106	65	49	114	376	409	346
11	41	260	209	224	242	210	100	54	40	104	368	385	312
12	44	260	187	220	235	208	97	50	38	97	348	354	300
13	48	220	157	190	223	177	47	42	31	93	313	320	294
	50	202	152	183	221	170	47	38	29	91	304	320	281
14	52	184	146	177	219	163	46	33	27	88	295	319	267
15	56	162	131	176	207	159	21	26	26	80	279	300	252
16	59	148	103	168	201	129	21	23	20	76	256	295	237
17	63	136	88	125	194	124	14	23	12	48	255	289	193
	65	113	86	124	191	108	11	18	12	44	252	281	185

18	67	95	84	123	189	96	9	14	12	40	250	275	178
19	70	91	76	103	189	91	9	13	10	40	245	254	177
20	74	88	69	83	189	86	9	12	9	40	239	232	176
21	78	71	67	64	166	76	7	11	8	29	212	196	173
22	81	64	54	41	134	70	6	3	5	24	175	148	163
23	85	62	35	39	120	57	3	1	5	22	161	75	154
24	89	43	27	36	88	47	3	0	3	18	52	50	122
25	93	41	4	19	26	31	0	0	0	15	32		38
26	2600	34	3	10	19	3	0	0	0	2			

**Rainfall station: CANEY EL MOJARRAS**

n	P	JAN	FEB	MAR	APR	MAY	JUN	JUL	AUG	SEP	OCT	NOV	DEC
1	3	288	200	258	454	233	185	123	102	221	574	466	303
2	6	224	160	239	238	225	137	109	98	214	459	368	266
3	9	175	146	212	234	204	109	89	81	159	319	340	242
4	12	166	145	185	232	187	103	87	53	126	299	313	226
5	15	152	142	184	220	186	92	85	47	125	268	305	204
6	18	149	135	168	213	175	75	80	45	121	258	290	187
7	21	144	134	163	204	156	70	76	44	116	255	261	172
8	24	140	131	156	202	152	69	63	38	115	243	260	172
9	27	137	121	155	183	150	68	53	37	111	230	238	170
10	30	122	120	152	180	146	67	49	37	93	216	230	157
11	33	114	120	140	173	130	63	47	33	81	215	219	157
	35	113	117	136	168	124	62	45	33	80	213	219	151
12	36	113	114	133	164	119	61	44	33	80	211	219	147
13	39	112	108	125	162	117	59	39	28	80	208	209	146
14	42	102	103	124	138	107	59	39	27	77	195	200	142
15	45	94	98	124	136	105	58	33	23	66	189	200	142
16	48	93	96	115	132	100	57	29	22	66	183	200	141
	50	92	93	112	130	100	51	28	22	65	182	191	133
17	52	92	90	110	127	100	46	27	21	63	181	181	125
18	55	89	85	108	120	95	44	25	20	60	164	170	123
19	58	81	74	105	119	94	37	24	20	59	161	168	122
20	61	77	73	103	116	93	37	23	20	46	157	168	121
21	64	76	66	102	116	87	33	22	17	44	153	167	110
	65	72	63	102	116	87	29	22	15	42	152	167	107
22	67	66	60	102	115	86	24	22	13	39	150	167	104
23	70	53	52	101	107	85	16	22	13	27	144	148	98

24	73	51	50	99	104	81	16	13	12	26	143	141	98
25	76	51	49	92	100	62	14	13	7	25	136	138	92
26	79	31	46	90	96	56	13	12	7	20	131	121	83
27	82	29	45	90	84	53	9	7	7	17	115	109	75
28	85	29	43	52	78	42	8	5	4	17	110	95	70
29	88	24	35	44	76	39	8	5	2	17	105	88	68
30	91	20	18	34	69	37	4	4	1	14	98	71	60
31	94	19	18	19	61	32	3	3	0	9	78	63	60
32	97	10	7	9	57	26	2	1	0	1	70	22	5

**Rainfall Station: GJA EXP UNIV NARIN**

n	P	JAN	FEB	MAR	APR	MAY	JUN	JUL	AUG	SEP	OCT	NOV	DEC
1	4	298	244	281	268	327	115	96	141	152	296	400	318
2	8	156	162	259	266	209	114	87	69	110	256	311	273
3	13	147	161	212	260	204	107	76	47	96	246	305	230
4	17	120	147	184	232	202	86	56	41	85	246	298	226
5	21	105	143	158	218	149	78	53	31	71	240	287	196
6	25	105	139	155	191	135	76	36	27	67	239	255	195
7	29	96	139	148	190	134	56	30	25	51	218	254	187
8	33	95	131	136	161	131	53	26	24	50	202	251	180
	35	91	122	136	153	131	51	26	24	49	190	241	180
9	38	84	109	136	142	131	50	26	24	48	171	226	180
10	42	79	102	136	142	119	46	19	24	48	171	196	160
11	46	79	102	128	138	111	45	18	21	48	170	192	151
12	50	79	95	120	128	106	42	18	18	48	164	174	151
13	54	66	95	112	117	93	31	14	17	43	164	172	138
14	58	65	82	109	114	86	27	12	15	40	153	163	129
15	63	63	81	109	111	84	23	9	14	36	150	150	128
	65	48	77	107	110	80	19	8	11	27	150	148	123
16	67	38	75	107	110	78	17	7	10	21	150	147	120
17	71	33	68	106	99	76	15	5	5	18	150	146	109
18	75	29	62	105	91	63	15	2	3	15	127	116	96
19	79	24	61	103	74	50	10	2	3	15	127	109	81
20	83	22	58	91	69	30	9	1	0	13	108	108	70
21	88	12	54	85	64	30	6	1	0	11	94	70	58
22	92	10	29	79	56	12	3	0	0	11	59	59	57
23	96	5	9	68	26	4	2	0	0	5	23	38	48

**Rainfall station: SAJANDI**

n	P	JAN	FEB	MAR	APR	MAY	JUN	JUL	AUG	SEP	OCT	NOV	DEC
1	3	458	416	445	446	435	386	200	224	272	561	558	508
2	6	438	371	342	415	403	262	140	188	271	528	545	488
3	9	362	293	313	388	368	200	118	140	271	405	466	473
4	12	322	280	302	347	351	186	110	102	261	401	430	437
5	15	296	272	301	316	327	148	107	94	251	363	423	378
6	18	295	266	301	302	319	131	101	88	244	337	423	362
7	21	276	238	298	298	307	128	82	83	237	336	413	355
8	24	258	228	297	290	262	118	78	77	196	323	391	354
9	27	253	207	262	280	255	117	78	66	181	318	388	335
10	30	236	184	259	279	226	110	76	56	175	304	376	321
11	33	229	179	254	270	213	108	75	55	174	301	371	283
	35	227	179	252	263	208	106	66	55	166	299	365	277
12	36	225	178	251	257	204	104	59	55	159	296	360	273
13	39	221	171	238	255	204	100	54	55	128	257	360	267
14	42	219	167	229	240	198	99	51	55	128	257	321	261
15	45	219	163	227	240	196	99	51	50	128	240	320	248
16	48	218	163	214	234	194	99	51	49	118	234	298	248
	50	210	162	214	232	192	86	51	46	116	234	293	248
17	52	202	160	214	230	190	73	51	43	114	234	288	248
18	55	199	137	214	230	190	67	51	37	110	234	287	209
19	58	176	134	213	230	182	60	39	32	91	231	284	206
20	61	159	115	209	226	179	28	27	29	89	215	253	193
21	64	150	113	200	220	174	26	24	14	83	193	249	190
	65	149	113	194	212	165	24	23	14	71	185	244	189
22	67	148	112	186	202	155	21	23	13	57	174	238	188
23	70	140	111	181	200	129	21	16	12	55	168	226	186
24	73	129	106	176	194	120	16	16	6	53	166	223	183
25	76	108	98	174	189	103	15	8	6	49	149	222	177
26	79	77	90	168	140	99	11	5	5	42	129	211	176
27	82	75	86	149	120	98	10	4	4	33	115	199	158
28	85	49	85	141	108	85	6	3	3	33	105	193	157
29	88	47	69	64	99	83	5	2	0	20	92	191	115
30	91	37	50	45	84	68	3	2	0	11	78	158	114
31	94	5	48	41	83	54	3	0	0	9	41	152	88

32      97      0    41    24    44    53    0    0    0    1    27    37    50

---

**Rainfall station: PATIA**

n	P	JAN	FEB	MAR	APR	MAY	JUN	JUL	AUG	SEP	OCT	NOV	DEC
1	5	355	306	347	301	489	152	141	109	117	362	456	501
2	9	282	271	256	266	320	136	98	55	105	280	427	413
3	14	255	179	232	265	275	126	68	52	103	271	406	391
4	18	234	173	230	232	222	109	65	38	81	251	348	391
5	23	212	165	210	226	214	101	53	37	77	248	347	372
6	27	180	164	195	209	168	99	43	33	71	246	319	299
7	32	177	149	176	184	153	99	36	31	63	238	306	288
	35	165	143	173	181	144	75	34	28	57	237	294	280
8	36	160	141	171	180	140	65	33	27	55	237	289	276
9	41	151	136	159	171	135	62	32	25	45	236	276	249
10	45	141	129	156	165	114	61	28	25	45	230	269	249
11	50	130	127	150	149	109	58	27	23	40	225	267	213
12	55	129	120	147	149	98	54	19	22	31	215	261	190
13	59	109	99	146	138	91	39	15	18	29	206	223	164
14	64	61	98	130	104	87	19	10	16	21	193	222	156
	65	60	94	127	100	85	17	10	14	21	189	221	155
15	68	59	83	119	89	79	13	10	10	20	178	219	152
16	73	36	74	98	86	56	11	8	8	14	164	169	147
17	77	23	71	82	85	20	10	5	2	12	161	167	147
18	82	22	70	79	68	19	5	5	0	9	140	138	137
19	86	21	70	29	38	17	4	1	0	3	138	84	136
20	91	17	43	25	16	15	3	1	0	2	124	30	66
21	95	13	42	23	15	9	0	0	0	1	96	19	15

---

**Rainfall station: FONDA LA CITEC**

n	P	JAN	FEB	MAR	APR	MAY	JUN	JUL	AUG	SEP	OCT	NOV	DEC
1	3	389	674	338	451	406	220	100	171	297	409	569	593
2	6	360	411	319	385	376	213	99	136	256	408	391	561
3	9	335	363	312	286	283	153	99	108	246	399	386	507
4	12	314	262	303	276	256	131	95	97	246	362	372	445
5	15	307	228	263	276	231	128	93	85	244	346	362	390
6	18	252	227	259	267	231	121	87	78	227	327	353	360

7	21	249	217	254	248	227	103	77	52	225	324	350	333
8	24	249	205	252	247	220	101	77	49	175	315	350	323
9	27	242	199	249	227	217	96	58	44	170	306	344	310
10	30	224	196	248	216	199	94	54	44	155	297	301	309
11	33	219	193	248	210	195	92	43	41	131	292	300	286
	35	217	178	239	209	184	90	42	41	129	290	294	276
12	36	216	167	231	208	175	88	42	41	128	288	289	268
13	39	212	158	211	208	175	87	38	41	118	258	268	256
14	42	211	151	202	200	173	73	36	39	114	256	267	256
15	45	189	144	201	200	161	71	34	34	112	247	262	256
16	48	168	143	196	200	160	70	34	27	96	242	256	245
	50	166	142	192	198	159	69	31	27	94	241	255	235
17	52	164	141	187	196	158	68	28	26	92	241	254	225
18	55	162	141	185	195	157	52	21	26	78	229	251	213
19	58	153	130	178	194	142	50	21	26	70	215	244	208
20	61	151	122	175	192	139	40	20	25	62	196	241	203
21	64	143	115	155	179	136	32	20	24	60	193	241	193
	65	134	115	152	178	136	28	18	23	55	192	233	189
22	67	123	114	150	176	136	22	16	22	48	191	223	184
23	70	114	95	147	171	135	21	15	18	48	188	206	174
24	73	96	75	138	167	116	20	6	16	44	187	196	170
25	76	91	61	121	166	106	20	5	8	43	183	195	157
26	79	58	60	103	142	92	18	4	6	34	178	182	153
27	82	55	59	97	123	67	14	3	4	30	171	178	139
28	85	54	55	81	113	66	8	2	1	25	170	170	138
29	88	48	54	66	96	58	8	1	1	20	157	160	136
30	91	35	53	62	91	57	7	1	0	19	121	148	124
31	94	31	47	53	84	26	6	0	0	12	105	133	112
32	97	5	35	44	42	19	4	0	0	0	100	93	92

**Rainfall station: BOCAS DE PATIA**

n	P	JAN	FEB	MAR	APR	MAY	JUN	JUL	AUG	SEP	OCT	NOV	DEC
1	3	1198	1232	1360	1358	1115	1068	1091	1227	1232	1742	1126	997
2	6	1038	860	1040	981	1090	977	908	977	1223	1177	1094	934
3	9	980	855	993	876	1067	905	796	884	1108	1125	1005	932
4	12	917	751	969	876	1043	882	755	859	1097	1083	976	921
5	15	898	736	844	850	1009	811	732	798	999	1030	961	894

6	18	824	649	839	835	1006	808	710	798	869	958	948	887
7	21	822	633	709	785	987	797	706	786	865	920	858	873
8	24	813	607	688	767	985	791	691	783	818	918	837	787
9	27	774	601	668	749	967	788	690	769	782	873	830	782
10	30	761	600	662	742	944	782	656	746	778	858	814	781
11	33	756	549	624	723	915	776	631	742	753	858	809	765
	35	748	546	609	723	896	773	627	731	750	839	795	762
12	36	741	544	596	723	881	770	624	722	748	824	784	760
13	39	728	522	544	719	855	753	617	685	693	803	734	746
14	42	708	518	533	717	855	748	593	667	692	801	685	695
15	45	680	514	525	715	831	745	588	664	691	801	683	692
16	48	656	508	519	711	828	727	582	650	685	778	679	678
	50	649	507	499	711	823	718	579	646	678	778	677	678
17	52	642	507	479	710	817	709	576	642	670	777	676	678
18	55	633	439	479	698	793	704	568	640	668	774	676	665
19	58	631	437	471	696	774	699	548	628	667	721	659	640
20	61	625	433	461	696	762	692	538	598	666	711	653	639
21	64	616	400	441	677	744	686	515	554	648	702	630	630
	65	599	399	414	671	741	682	509	554	631	673	612	621
22	67	579	398	381	663	737	678	501	554	611	637	590	609
23	70	532	393	342	656	724	667	486	518	607	606	556	593
24	73	528	372	340	652	681	604	483	510	539	605	523	575
25	76	527	357	336	643	677	603	478	501	531	600	496	545
26	79	527	354	298	583	671	563	432	474	509	577	464	533
27	82	489	350	295	536	654	530	423	468	499	539	441	523
28	85	381	336	283	463	619	518	420	461	498	533	427	463
29	88	346	311	271	437	617	499	390	396	497	516	377	412
30	91	322	298	188	388	599	498	342	376	477	442	341	374
31	94	254	263	187	363	571	472	314	331	333	408	325	368
32	97	8	259	146	339	466	323	245	207	280	287	102	291

**Rainfall station: SIERRA LA**

n	P	JAN	FEB	MAR	APR	MAY	JUN	JUL	AUG	SEP	OCT	NOV	DEC
1	3	756	588	514	402	310	209	164	173	246	591	697	650
2	6	742	519	365	363	274	148	117	163	218	549	670	644
3	9	630	403	336	346	268	140	83	101	211	476	647	640
4	12	575	334	334	339	268	131	78	84	209	473	643	557

5	15	539	324	323	333	230	130	76	76	182	431	618	535
6	18	524	321	323	296	227	124	69	71	171	415	508	519
7	21	514	302	322	285	213	123	65	69	165	413	507	475
8	24	427	301	304	273	210	122	61	68	163	404	502	469
9	27	396	292	294	258	205	117	48	57	130	404	473	462
10	30	380	266	277	257	205	102	48	56	127	403	471	440
11	33	359	265	267	255	205	96	46	55	111	363	461	428
	35	353	249	261	255	205	93	45	54	111	359	456	428
12	36	348	236	256	255	204	91	45	54	111	356	453	428
13	39	346	233	253	247	201	88	44	46	111	335	450	417
14	42	316	231	251	246	199	88	37	45	109	329	440	416
15	45	311	222	249	245	198	80	35	43	105	323	420	410
16	48	291	210	247	245	193	79	34	36	99	320	418	404
	50	287	210	245	241	193	70	34	33	97	319	416	398
17	52	283	209	244	237	192	61	33	29	95	318	414	393
18	55	269	201	219	232	185	59	30	27	92	282	352	380
19	58	216	188	210	230	183	55	30	27	86	265	341	376
20	61	211	183	203	219	183	54	28	22	73	255	334	369
21	64	203	161	193	212	183	52	27	21	71	253	331	285
	65	203	159	189	208	183	51	27	21	64	251	329	284
22	67	202	156	185	203	183	50	26	20	55	249	327	282
23	70	172	144	183	184	179	43	23	20	53	244	301	270
24	73	157	142	182	173	148	36	20	20	50	238	300	269
25	76	140	129	178	167	123	29	18	15	43	225	297	268
26	79	114	116	154	157	113	28	11	11	33	222	287	256
27	82	103	97	126	144	107	26	9	11	29	180	280	237
28	85	96	93	123	139	97	23	8	11	28	168	279	215
29	88	90	80	111	124	77	22	8	9	23	146	252	180
30	91	81	78	101	118	61	19	7	0	22	134	252	147
31	94	66	34	81	91	60	19	0	0	16	132	234	132
32	97	37	24	51	35	60	18	0	0	10	75	197	86

**Rainfall station: ESTRECHO EL**

n	P	JAN	FEB	MAR	APR	MAY	JUN	JUL	AUG	SEP	OCT	NOV	DEC
1	3	341	209	247	410	223	139	133	89	203	339	499	447
2	6	234	200	234	327	218	124	103	85	185	275	450	356
3	9	213	144	199	298	202	100	101	75	183	273	392	279

4	12	191	138	197	261	196	96	81	71	170	262	353	235
5	15	188	126	171	226	190	81	63	51	141	259	334	234
6	18	185	124	168	184	184	73	58	46	138	245	248	220
7	21	168	122	167	171	150	72	46	45	133	241	244	211
8	24	166	119	164	157	142	69	45	44	121	240	243	201
9	27	162	113	142	157	141	54	44	38	113	234	231	200
10	30	157	111	132	154	136	52	37	30	104	230	221	193
11	33	146	101	113	147	132	49	36	30	103	225	219	193
	35	145	98	113	146	132	48	35	29	102	217	219	190
12	36	144	96	113	145	132	48	34	28	102	210	218	187
13	39	137	94	110	143	130	41	31	27	94	204	210	170
14	42	135	92	106	141	129	39	27	23	84	190	205	162
15	45	119	92	106	139	115	38	26	16	66	182	203	161
16	48	106	91	105	139	112	31	23	15	55	176	203	161
	50	105	89	99	138	111	31	21	14	47	174	197	160
17	52	105	86	94	137	111	30	19	14	39	172	190	159
18	55	103	83	93	109	107	25	9	14	38	170	187	144
19	58	97	82	92	109	91	24	9	7	38	160	186	127
20	61	97	77	91	104	83	15	6	4	37	160	179	126
21	64	86	76	89	95	65	15	5	4	37	140	178	109
	65	80	75	89	95	61	13	5	4	35	137	176	109
22	67	73	74	89	94	57	12	5	4	34	134	172	108
23	70	68	55	78	81	54	11	4	3	30	127	172	104
24	73	68	54	74	78	51	10	3	2	28	123	155	86
25	76	50	40	72	77	51	3	3	2	21	123	155	83
26	79	41	40	62	56	50	2	2	1	17	109	152	83
27	82	22	38	42	52	48	2	0	0	12	109	147	74
28	85	21	36	36	49	47	1	0	0	7	101	121	60
29	88	19	36	34	44	39	1	0	0	4	86	87	58
30	91	13	18	34	34	30	0	0	0	3	86	84	47
31	94	10	16	21	33	22	0	0	0	0	68	25	38
32	97	2	14	13	14	11	0	0	0	0	12	21	26

Rainfall station: GUACHICONO

n	P	JAN	FEB	MAR	APR	MAY	JUN	JUL	AUG	SEP	OCT	NOV	DEC
1	3	410	425	514	630	556	370	176	201	229	422	670	655
2	6	387	309	398	372	532	271	170	84	228	414	545	589

3	9	366	254	387	353	380	211	139	72	192	407	481	553
4	12	347	242	320	320	272	188	139	70	145	401	465	536
5	15	346	236	313	306	271	160	132	65	141	361	379	534
6	18	336	215	302	294	235	133	115	57	140	356	370	440
7	21	324	211	289	292	230	125	106	56	132	353	363	434
8	24	301	209	279	289	222	112	75	52	130	348	355	394
9	27	266	183	251	287	218	109	67	44	130	333	349	349
10	30	236	173	247	277	216	100	60	43	119	322	339	342
11	33	224	170	246	261	216	98	59	41	114	306	321	338
	35	219	160	228	237	215	96	57	39	113	304	317	314
12	36	214	153	214	218	215	94	56	38	113	303	313	295
13	39	210	150	208	201	211	91	45	37	100	294	305	283
14	42	189	135	205	195	201	88	42	35	89	289	286	276
15	45	173	131	203	189	193	67	34	29	87	282	276	272
16	48	166	130	194	182	185	65	30	26	84	255	250	229
	50	163	122	193	182	184	55	29	25	83	246	250	228
17	52	161	114	191	182	183	45	28	25	82	236	250	227
18	55	144	110	186	181	160	41	25	20	82	234	249	222
19	58	120	105	174	171	148	40	20	15	81	228	236	218
20	61	101	102	172	161	142	30	20	15	79	227	230	193
21	64	100	97	172	158	140	25	15	14	72	222	227	188
	65	98	96	168	154	139	24	14	13	69	218	226	178
22	67	96	95	162	148	137	22	12	11	66	213	224	165
23	70	90	94	142	132	134	22	7	10	65	209	219	162
24	73	86	90	142	115	126	17	4	6	52	194	219	159
25	76	80	88	138	102	112	16	3	1	45	170	216	136
26	79	69	80	135	84	111	16	0	0	41	162	199	134
27	82	69	78	117	82	109	15	0	0	38	138	188	113
28	85	64	61	75	75	87	10	0	0	24	132	180	111
29	88	52	48	62	62	73	10	0	0	22	113	163	104
30	91	47	45	48	22	65	4	0	0	22	94	154	94
31	94	27	25	44	10	34	3	0	0	0	70	112	80
32	97	6	22	42	7	23	0	0	0	0	14	104	42

**Rainfall station: MAMACONDE**

n	P	JAN	FEB	MAR	APR	MAY	JUN	JUL	AUG	SEP	OCT	NOV	DEC
1	3	396	346	223	469	503	158	233	193	243	351	465	471

2	6	366	273	216	296	313	118	83	99	222	335	338	393
3	9	328	227	191	270	233	110	60	76	203	293	337	344
4	12	217	159	191	239	212	105	60	72	167	283	324	274
5	15	215	144	179	227	188	96	44	62	140	270	319	265
6	18	214	143	177	213	180	92	37	58	136	260	308	247
7	21	207	132	176	194	177	89	36	52	121	259	304	237
8	24	207	129	176	173	166	89	32	39	118	244	280	232
9	27	189	116	170	169	135	85	28	35	85	235	263	227
10	30	170	114	170	166	115	56	25	32	74	223	261	206
11	33	132	113	168	160	114	56	24	28	69	207	240	196
	35	131	109	162	159	110	53	23	26	67	206	237	182
12	36	130	106	157	158	107	51	23	24	66	205	235	171
13	39	129	103	152	154	103	45	20	23	65	204	230	147
14	42	128	89	140	151	96	39	20	22	52	198	223	146
15	45	125	87	126	150	96	35	19	20	51	195	220	143
16	48	117	83	123	149	96	29	18	20	50	192	214	143
	50	116	82	123	149	89	26	18	20	48	190	209	137
17	52	116	81	123	149	82	23	18	20	46	187	205	131
18	55	91	79	118	145	75	22	17	18	39	185	203	125
19	58	90	76	117	141	74	18	16	16	39	182	193	117
20	61	87	75	106	138	73	15	16	16	32	150	184	116
21	64	80	74	105	129	72	11	16	15	32	147	175	112
	65	78	70	105	123	72	10	14	15	28	144	167	106
22	67	75	66	105	115	72	10	12	14	23	141	158	99
23	70	69	63	102	104	64	9	10	13	21	140	134	93
24	73	65	58	99	97	54	7	6	11	20	135	127	73
25	76	50	57	67	78	53	7	5	5	16	126	122	72
26	79	49	50	56	74	52	6	5	4	13	118	121	67
27	82	42	47	46	72	47	4	2	3	7	102	119	61
28	85	39	39	43	69	39	2	1	1	6	97	117	59
29	88	25	39	43	64	36	2	1	0	6	86	98	51
30	91	18	35	40	60	36	0	0	0	5	84	98	46
31	94	14	18	29	43	16	0	0	0	0	76	85	37
32	97	9	13	11	27	5		0	0	0			

**Rainfall station: GAMBOA**

n P JAN FEB MAR APR MAY JUN JUL AUG SEP OCT NOV DEC

1	3	591	487	612	435	392	321	318	289	355	529	622	591
2	6	554	381	488	411	362	266	243	240	326	524	561	553
3	9	551	381	467	407	357	240	195	219	309	509	528	532
4	12	425	338	419	383	337	236	180	215	273	487	507	489
5	15	368	315	382	374	330	222	168	204	270	486	493	486
6	18	367	291	355	363	327	216	155	202	258	468	489	478
7	21	360	281	353	361	321	210	147	200	258	446	477	473
8	24	352	280	340	359	294	203	138	194	248	425	475	458
9	27	342	264	333	345	290	188	129	171	239	423	474	445
10	30	327	262	329	344	280	187	129	170	230	416	468	421
11	33	311	250	297	324	277	183	116	166	224	402	466	400
	35	309	249	292	318	274	171	115	148	224	400	464	398
12	36	307	248	288	313	272	162	115	134	224	399	463	397
13	39	306	247	280	295	272	162	113	125	223	381	444	389
14	42	305	243	274	289	266	162	113	117	223	377	433	385
15	45	271	219	255	287	257	157	111	117	201	366	428	377
16	48	258	219	243	276	252	137	99	116	192	359	419	349
	50	248	205	232	274	249	134	94	110	186	350	416	349
17	52	237	191	220	273	246	132	88	104	180	340	413	349
18	55	225	190	212	263	238	125	87	98	179	331	408	334
19	58	220	188	208	259	229	123	86	94	178	306	405	326
20	61	220	188	196	259	219	113	78	90	164	301	405	319
21	64	218	187	172	244	217	111	68	84	160	291	396	309
	65	214	187	170	243	211	107	67	83	158	287	392	300
22	67	210	187	167	242	204	102	65	81	155	281	388	289
23	70	208	181	162	239	199	98	65	74	154	280	385	287
24	73	201	173	162	236	177	98	64	62	152	266	381	286
25	76	178	168	151	230	174	86	59	55	148	265	373	254
26	79	172	124	142	209	161	83	55	41	134	250	371	244
27	82	162	115	140	205	159	56	53	20	129	249	361	239
28	85	157	108	135	174	142	38	41	18	105	244	333	224
29	88	125	100	103	135	126	32	20	15	96	201	278	213
30	91	117	95	67	65	106	31	10	12	87	167	203	155
31	94	105	67	64	64	104	17	5	1	72	156	167	140
32	97	84	59	59	53	101	16	3	0	43	142	82	51

**8.3 Appendix H**  
River Flow measures for the study area. Loma alta (downstream) and La fonda (Upstream)

<b>LOMA ALTA</b>												
<b>Year</b>	<b>JAN</b>	<b>FEB</b>	<b>MAR</b>	<b>APR</b>	<b>MAY</b>	<b>JUN</b>	<b>JUL</b>	<b>AUG</b>	<b>SEP</b>	<b>OCT</b>	<b>NOV</b>	<b>DEC</b>
1995	57.1	28.8	39.2	70.2	71.908	42.21	32.1	31.6	20.608	71.11	150.4	123.98
1996	122.1	150.9	136.28	135.2	84.701	65.2	49.5	24.8	26.7	52.7	67.8	82.508
1997	242	113	84.708	77.71	57.001	58.4	46.7	44.71	19.203	23.51	70.31	42.008
1998	19.31	20.21	18.108	57.91	91.508	61.11	24.1	17.71	13.908	21.31	150.3	146.4
1999	281	241.8	193.88	181.6	139.93	86.8	43.8	27.7	33.408	75.11	207.1	297.63
2000	200.7	171.2	178.4	164.6	110.8	78.8	52.7	22.8	25.4	24.4	68.9	54.3
2001	57.6	47.6	67.3	36.7	36.4	30.5	22.7	18.6	14.8	16.3	68.3	182
2002	104.1	29.61	28.658	104	63.058	38.55	24.58	16.48	10.421	14.56	45.6	65.728
2003	71.75	43.46	41	57.3	34.8	52.5	27.7	17.2	11.7	85.4	161	175.2
2004	57.6	47.6	66.858	155.6	123.38	75.29	38.85	28.03	10.421	85.28	152.7	141.01
2005	94.3	20.21	18.108	104	63.4	37.6	28.9	22.7	21.601	60.11	134.8	217.23
2007	71.75	43.46	66.858	155.6	123.38	75.29	38.85	28.03	17.463	81.77	165.8	274.58
2008	148.7	156.8	146.38	151.3	152.88	83.59	44.46	37.35	34.851	47.76	151	168.28
2009	148.7	110.4	115.28	106.9	63.058	38.55	24.58	16.48	10.421	14.56	45.6	65.728
2010	34.68	36.35	23.331	55.4	83.578	56.22	70.41	33.04	30.068	60.61	243.9	188.53
2011	104.4	107.6	110.88	187.9	96.558	65.5	44.14	29.65	30.001	62.31	122.1	276.48

<b>LA FONDA</b>												
<b>Year</b>	<b>JAN</b>	<b>FEB</b>	<b>MAR</b>	<b>APR</b>	<b>MAY</b>	<b>JUN</b>	<b>JUL</b>	<b>AUG</b>	<b>SEP</b>	<b>OCT</b>	<b>NOV</b>	<b>DEC</b>
1965	64.51	33.61	26.506	75.51	86.306	33.41	16.71	9.101	4.9006	38.71	100.2	103.06
1966	55.51	21.51	25.906	48.81	91.206	33.11	31.91	19.91	10.506	37.21	186.3	312.56
1967	72.31	84.01	64.906	37.91	44.306	50.71	41.41	26.41	12.406	35.21	156	76.806
1968	48.41	67.21	71.806	83.71	54.306	44.91	46.41	22.41	18.906	86.71	107	79.806
1969	43.51	61.31	24.306	84.71	69.706	34.01	27.01	18.61	30.806	74.01	79.51	104.56
1970	44.01	62.01	80.406	37.01	42.106	44.91	21.71	18.51	18.406	58.51	202.4	119.26
1971	198.6	166	141.06	127.1	111.16	77.71	55.51	28.91	28.106	53.71	125	109.66
1972	116.9	68.21	46.306	77.31	87.406	62.21	56.11	23.71	21.106	25.01	83.91	66.506
1973	27.71	20.51	16.906	36.61	35.606	37.41	29.51	30.91	40.106	84.01	144.5	150.16
1974	133.5	143.4	110.56	62.91	58.506	49.91	19.53	13.11	16.801	63.81	148	111.38
1975	58.17	99.38	90.568	52.95	91.218	64.18	62.53	29.49	26.531	56.38	157.5	202.38
1976	93.57	71.73	90.528	112.5	51.831	33.07	23.16	15.63	14.25	34.22	64.73	62.968
1977	32.29	21.58	23.041	36.61	37.491	28.13	16.78	13.55	34.708	94.49	131.5	93.49
1978	77.67	30.53	28.761	76.19	73.818	35.75	21.84	13.44	12.801	25.84	52.87	123.71
1979	59.65	30.76	52.67	46.05	79.678	91.15	35.98	16.97	31.936	46.12	74.66	50.28
1980	56.58	105	51.8	34.4	22	22	13.4	11.9	11.1	37.33	59.63	113.48

1981	58.03	54.58	83.97	83.09	105.08	60.78	36.15	20.18	17.64	24.07	160.6	141.16
1982	136.9	96.72	113.98	118.5	109.58	52.87	47.61	25.31	32.276	45.9	58.71	82.458
1983	44.88	35.92	37.258	71.4	77.006	37.15	20.73	16.26	13.02	26.52	39.62	76.728
1984	113.6	120	70.748	95.02	85.748	51.1	46.77	28.29	47.458	84.41	107.7	99.298
1985	94.98	49.52	21.598	63.25	56.148	36.79	22.39	16.8	16.356	28.57	90.28	97.208
1986	76.7	95.22	90.568	72.39	40.548	57.44	37.3	33.31	27.738	64.22	68.11	45.478
1987	38.9	22.7	19.001	20.2	62.518	21	15.1	14.7	8.3001	70.25	95.22	72.008
1988	38.3	30.5	38.806	71.54	49.776	45.75	44.21	23.01	39.816	56.51	232.3	186.38
1989	161	59.33	78.85	46.36	73.54	32.91	22.06	15.49	16.72	24.14	57.21	67.03
1990	114.1	54.35	59.13	78.18	65.478	27.5	17.35	11.47	8.303	27.54	59.41	72.658
1991	48.97	31.33	57.34	53.67	81.198	42.64	30.81	25.95	26.88	29.7	59.21	81.16
1992	49.23	46.74	34.19	33.87	29.85	28.42	24.25	17.25	15.526	20.82	47.85	98.538
1993	64.2	47.1	55	97.61	76.2	35.3	24.2	17.6	17.306	22.4	94.11	149.28
1994	105.2	83.81	76.008	97.9	70.308	43.7	25.6	20.1	18.7	42.5	62.7	69.8
1995	44	28	31.6	52	54.808	35.5	26.3	26.3	16.508	56.61	129.8	95.608
1996	96.01	112.5	112.58	108.3	63.1	47.2	30.3	23	19.5	30.5	51.61	67.9
1997	198.3	141	75.8	70.4	61	42.6	31	23.5	24.5	28.3	56.7	31
1998	14.5	14.8	13.808	37	61.7	47	16.3	11.11	9.6008	14.61	104.7	89.803
1999	224.7	186.1	161.03	129.5	93.8	58	31.2	22.7	27.1	67	176	312.83
2000	183.3	70.3	47.601	88.41	120.5	79.9	36.1	24.9	26.401	23.2	60.6	40.5
2001	36.1	25.8	39.8	18.5	17.3	11.6	6.5	4.1	24.5	28.3	71.1	123.2
2002	92.39	35.95	50.03	71.88	43.491	36.3	17.08	13.93	11.39	30.88	46.2	65.953
2003	33.6	30.7	38.901	56	37.503	39.8	26.3	17.8	17.801	40	113.5	71.003
2004	162.1	70.3	47.601	88.41	70.803	79.9	36.1	24.9	26.401	26.4	101.6	111.33
2005	76.4	84.6	90.568	72.39	49.801	31.4	22.8	20.1	21.1	51.21	133.7	182.93
2006	141.9	114	98.783	127.9	120.38	93.27	46.22	27.04	17.05	21.85	87.94	131.93
2007	80.68	43.41	46.308	127.9	73.463	54.81	20.13	13.4	9.1793	49.63	106.3	89.803
2008	163.4	156.4	106.13	98.73	131.23	60.69	22.37	16.86	13.178	23.69	141.6	181.58
2009	150.3	85.97	104.88	98.73	41.603	29.48	23.01	21.44	16.96	13.72	39.13	67.158
2010	32.92	30.7	18.678	47.32	93.648	47.43	63.32	24.7	24.308	55.56	268.9	239.38
2011	122	125	107.08	153.3	73.463	59.98	35.59	28.38	23.961	64.24	118	243.88

## 9. REFERENCES

- Abadi, M., Ashish Agarwal, Paul Barham, Eugene Brevdo, Z. C., Craig Citro, Greg S. Corrado, Andy Davis, Jeffrey Dean, Matthieu Devin, Sanjay Ghemawat, Ian Goodfellow, Andrew Harp, Geoffrey Irving, M. I., Yangqing Jia, Rafal Jozefowicz, Lukasz Kaiser, Manjunath Kudlur, Josh Levenberg, Dan Mané, Rajat Monga, Sherry Moore, Derek Murray, Chris Olah, M., Schuster, Jonathon Shlens, Benoit Steiner, Ilya Sutskever, Kunal Talwar, P., Tucker, Vincent Vanhoucke, Vijay Vasudevan, Fernanda Viégas, O. V., & Pete Warden, Martin Wattenberg, Martin Wicke, Yuan Yu, and X. Z. (2015). TensorFlow: Large-Scale Machine Learning on Heterogeneous Systems. Retrieved from <http://tensorflow.org/>
- Adamowski, J., & Chan, H. F. (2011). A wavelet neural network conjunction model for groundwater level forecasting. *Journal of Hydrology*, 407(1–4), 28–40. <http://doi.org/10.1016/j.jhydrol.2011.06.013>
- Álvarez-Villa, O. D., Vélez, J. I., & Poveda, G. (2011). Improved long-term mean annual rainfall fields for Colombia. *International Journal of Climatology*, 31(14), 2194–2212. <http://doi.org/10.1002/joc.2232>
- ASCE. (2000a). Artificial Neural Networks in Hydrology. I: Preliminary Concepts. *Journal of Hydrologic Engineering*, 5(2), 115–123. [http://doi.org/10.1061/\(ASCE\)1084-0699\(2000\)5:2\(115\)](http://doi.org/10.1061/(ASCE)1084-0699(2000)5:2(115))
- ASCE. (2000b). Artificial Neural Networks in Hydrology. II: Hydrologic Applications. *Journal Of Hydrologic Engineering*, (April), 124–137. <http://doi.org/10.5121/ijsc.2012.3203>
- Augenstein, M., Goepfert, N., & Goldscheider, N. (2015). Characterizing soil water dynamics on steep hillslopes from long-term lysimeter data. *Journal of Hydrology*, 529(P3), 795–804. <http://doi.org/10.1016/j.jhydrol.2015.08.053>
- Bastola, S., Ishidaira, H., & Takeuchi, K. (2008). Regionalisation of hydrological model parameters under parameter uncertainty: A case study involving TOPMODEL and basins across the globe. *Journal of Hydrology*, 357(3–4), 188–206. <http://doi.org/10.1016/j.jhydrol.2008.05.007>
- Beck, H. E., Dijk, A. I. J. M. Van, Miralles, D. G., Jeu, R. A. M. De, Bruijnzeel, L. A. S., Mcvicar, T. R., & Schellekens, J. (2013). Global patterns in base flow index and recession based on streamflow observations from 3394 catchments, 49, 7843–7863. <http://doi.org/10.1002/2013WR013918>
- Beck, H. E., Roo, A. De, & Dijk, A. I. J. M. Van. (2015). Global Maps of Streamflow Characteristics Based on Observations from Several Thousand Catchments. *Journal of Hydrometeorology*, 16, 1478–1501. <http://doi.org/10.1175/JHM-D-14-0155.1>
- Beliakov, G., Kelarev, A., & Yearwood, J. (2011). *Robust artificial neural networks and outlier detection. Technical report.* Retrieved from <http://arxiv.org/abs/1110.0169> <http://dx.doi.org/10.1080/02331934.2012.674946>
- Bhattacharjya, R. K., & Datta, B. (2005). Optimal Management of Coastal Aquifers Using Linked Simulation Optimization Approach, 295–320. <http://doi.org/10.1007/s11269-005-3180-9>
- Borselli, L., Torri, D., Poesen, J., & Sanchis, P. S. (2001). EFFECTS OF WATER QUALITY ON INFILTRATION , RUNOFF AND INTERRILL EROSION PROCESSES DURING SIMULATED RAINFALL, 342, 329–342.
- Brewer, K., Fogle, T., Stieve, A., & Barr, C. (2003). Uncertainty Analysis with Site-Specific Groundwater Models: Experiences and Observations. *US Department of Energy*, (865). Retrieved from <http://sti.srs.gov/fulltext/erden2003126/erden2003126.pdf>
- Camarero, L., Garcia-Pausas, J., & Huguet, C. (2009). A method for upscaling soil parameters for use in a dynamic modelling assessment of water quality in the Pyrenees. *Science of the Total Environment*, 407(5), 1701–1714. <http://doi.org/10.1016/j.scitotenv.2008.10.035>
- Carmichael, T., & Ailleres, L. (2016). Method and analysis for the upscaling of structural data. *Journal of Structural Geology*, 83, 121–133. <http://doi.org/10.1016/j.jsg.2015.09.002>

- Carrick, S., Rogers, G., Cameron, K., Malcolm, B., & Payne, J. (2017). Testing large area lysimeter designs to measure leaching under multiple urine patches. *New Zealand Journal of Agricultural Research*, 60(2), 205–215. <http://doi.org/10.1080/00288233.2017.1291527>
- Carroll, R. W. H., Pohll, G. M., Morton, C. G., & Huntington, J. L. (2015). Calibrating a Basin-Scale Groundwater Model to Remotely Sensed Estimates of Groundwater Evapotranspiration. *Journal of the American Water Resources Association*, 51(4), 1114–1127. <http://doi.org/10.1111/jawr.12285>
- Chollet, F. (2015). Keras. Retrieved from <https://keras.io>
- Cichota, R., Kelliher, F. M., Thomas, S. M., Clemens, G., Fraser, P. M., & Carrick, S. (2016). Effects of irrigation intensity on preferential solute transport in a stony soil. *New Zealand Journal of Agricultural Research*, 59(2), 141–155. <http://doi.org/10.1080/00288233.2016.1155631>
- CRC. (2017). *Evaluación Regional del Agua*.
- Crosbie, R. S., Jolly, I. D., Leaney, F. W., & Petheram, C. (2010). Can the dataset of field based recharge estimates in Australia be used to predict recharge in data-poor areas? *Hydrology and Earth System Sciences*, 14(10), 2023–2038. <http://doi.org/10.5194/hess-14-2023-2010>
- Dagan, G. (2002). An overview of stochastic modeling of groundwater flow and transport: From theory to applications. *Eos, Transactions American Geophysical Union*, 83(53), 621–625. <http://doi.org/10.1029/2002EO000421>
- Delin, G. N., Healy, R. W., Lorenz, D. L., & Nimmo, J. R. (2007). Comparison of local- to regional-scale estimates of ground-water recharge in Minnesota, USA. *Journal of Hydrology*, 334(1–2), 231–249. <http://doi.org/10.1016/j.jhydrol.2006.10.010>
- Der Kiureghian, A., & Ditlevsen, O. (2007). Aleatoric or Epistemic? Does it matter? *Special Workshop on Risk Acceptance and Risk Communication*2, 13. <http://doi.org/10.1016/j.strusafe.2008.06.020>
- Dewandel, B., Maréchal, J. C., Bour, O., Ladouche, B., Ahmed, S., Chandra, S., & Pauwels, H. (2012). Upscaling and regionalizing hydraulic conductivity and effective porosity at watershed scale in deeply weathered crystalline aquifers. *Journal of Hydrology*, 416–417, 83–97. <http://doi.org/10.1016/j.jhydrol.2011.11.038>
- Duncan, M. J., Srinivasan, M. S., & McMillan, H. (2016). Field measurement of groundwater recharge under irrigation in Canterbury, New Zealand, using drainage lysimeters. *Agricultural Water Management*, 166, 17–32. <http://doi.org/10.1016/j.agwat.2015.12.002>
- ECan. (2017). *Canterbury Land and Water Regional Plan* (Vol. 1). Christchurch, New Zealand. Retrieved from [www.ecan.govt.nz](http://www.ecan.govt.nz)
- F. Pedregosa, G. Varoquaux, A., Gramfort, V., Michel, B., Thirion, O., Grisel, M., Blondel, P., ... Duchesnay. (2011). Scikit-learn: Machine Learning in Python. *Journal of Machine Learning Research*, 12, 2825–2830.
- Gal, Y., & Ghahramani, Z. (2016a). A Theoretically Grounded Application of Dropout in Recurrent Neural Networks. *Advances in Neural Information Processing Systems*, 29.
- Gal, Y., & Ghahramani, Z. (2016b). Dropout as a Bayesian Approximation: Representing Model Uncertainty in Deep Learning. *Ultrasonic Imaging*, 3982(x), 315–324. <http://doi.org/10.1109/TKDE.2015.2507132>
- Gal, Y., Mcallister, R. T., & Rasmussen, C. E. (2016). Improving PILCO with Bayesian Neural Network Dynamics Models.
- Gebler, S., Hendricks Franssen, H. J., Pütz, T., Post, H., Schmidt, M., & Vereecken, H. (2015). Actual evapotranspiration and precipitation measured by lysimeters: A comparison with eddy covariance and tipping bucket. *Hydrology and Earth System Sciences*, 19(5), 2145–2161. <http://doi.org/10.5194/hess-19-2145-2015>
- Graham, S. L., Kochendorfer, J., Mcmillan, A. M. S., Duncan, M. J., Srinivasan, M. S., & Hertzog, G. (2016). Effects of agricultural management on measurements , prediction , and partitioning of evapotranspiration in irrigated grasslands. *Agricultural Water Management*, 177, 340–347.

- <http://doi.org/10.1016/j.agwat.2016.08.015>
- Graham, S. L., Srinivasan, M. S., Faulkner, N., & Carrick, S. (2018). Soil Hydraulic Modeling Outcomes with Four Parameterization Methods: Comparing Soil Description and Inverse Estimation Approaches. *Vadose Zone Journal*, 17(1), 0. <http://doi.org/10.2136/vzj2017.01.0002>
- Greifeneder, F., Notarnicola, C., Bertoldi, G., Niedrist, G., & Wagner, W. (2016). From Point to Pixel Scale: An Upscaling Approach for In Situ Soil Moisture Measurements. *Vadose Zone Journal*, 15(6), 0. <http://doi.org/10.2136/vzj2015.03.0048>
- Greve, A., Andersen, M. S., & Acworth, R. I. (2010). Investigations of soil cracking and preferential flow in a weighing lysimeter filled with cracking clay soil. *Journal of Hydrology*, 393(1–2), 105–113. <http://doi.org/10.1016/j.jhydrol.2010.03.007>
- Groenendijk, P., Heinen, M., Klammler, G., Fank, J., Kupfersberger, H., Pinaras, V., ... Trevisan, M. (2014). Performance assessment of nitrate leaching models for highly vulnerable soils used in low-input farming based on lysimeter data. *Science of the Total Environment*, 499, 463–480. <http://doi.org/10.1016/j.scitotenv.2014.07.002>
- Guerra, E., Ventura, F., & Snyder, R. L. (2016). Crop Coefficients: A Literature Review. *Journal of Irrigation and Drainage Engineering*, 142(3), 06015006. [http://doi.org/10.1061/\(ASCE\)IR.1943-4774.0000983](http://doi.org/10.1061/(ASCE)IR.1943-4774.0000983)
- Hadi, A. S., Rahmatullah Imon, A. H. M., & Werner, M. (2009). Detection of outliers. *Wiley Interdisciplinary Reviews: Computational Statistics*, 1(1), 57–70. <http://doi.org/10.1002/wics.6>
- Healy, R. W. (2010). *Estimating groundwater recharge*. Cambridge University Press. Retrieved from <https://ebookcentral.proquest.com>
- Heuvelmans, G., Muys, B., & Feyen, J. (2006). Regionalisation of the parameters of a hydrological model: Comparison of linear regression models with artificial neural nets. *Journal of Hydrology*, 319(1–4), 245–265. <http://doi.org/10.1016/j.jhydrol.2005.07.030>
- Hill, M., & Tiedeman, C. (2007). *Effective groundwater model calibration: with analysis of data, sensitivities, predictions, and uncertainty*. Wiley.
- Hingray, B., Picouet, C., & Musy, A. (2014). *Hydrology: A Science for Engineers*. CRC Press. Retrieved from <https://ebookcentral.proquest.com/lib/lincoln-ebooks/detail.action?docID=1591671>.
- Huang, G., & Weinberger, K. Q. (2018). Densely Connected Convolutional Networks.
- Hunter, J. D. (2007). Matplotlib: A 2D graphics environment. *Computing In Science & Engineering*, 9(3), 90–95. <http://doi.org/https://doi.org/10.1109/MCSE.2007.55>
- IGRAC. (2017). Report on Assessing Groundwater Stress published by IGRAC. Retrieved 10 April 2018, from <https://www.un-igrac.org/news/report-assessing-groundwater-stress-published-igrac>
- Ioffe, S., & Szegedy, C. (2015). Batch Normalization : Accelerating Deep Network Training by Reducing Internal Covariate Shift.
- Jackson, T. J. (2002). Remote sensing of soil moisture: Implications for groundwater recharge. *Hydrogeology Journal*, 10(1), 40–51. <http://doi.org/10.1007/s10040-001-0168-2>
- Jain, A., Varshney, A. K., & Joshi, U. C. (2001). Short-term water demand forecast modelling at IIT Kanpur using artificial neural networks. *Water Resources Management*, 15(5), 299–321. <http://doi.org/10.1023/A:1014415503476>
- Josset, L., Ginsberg, D., & Lunati, I. (2015). Functional error modeling for uncertainty quantification in hydrogeology. *Water Resources Research*, 4840–4847. <http://doi.org/10.1002/2015WR017273>.Received
- Karahan, H., & Ayvaz, M. T. (2008). Simultaneous parameter identification of a heterogeneous aquifer system using artificial neural networks. *Hydrogeology Journal*, 16(5), 817–827. <http://doi.org/10.1007/s10040-008-0279-0>
- Kasiviswanathan, K. S., & Sudheer, K. P. (2017). Methods used for quantifying the prediction uncertainty of artificial neural network based hydrologic models. *Stochastic Environmental Research and Risk*

- Assessment*, 31(7), 1659–1670. <http://doi.org/10.1007/s00477-016-1369-5>
- Kendall, A., & Gal, Y. (2017). What Uncertainties Do We Need in Bayesian Deep Learning for Computer Vision? In *Conference on Neural Information Processing Systems*. Long Beach, California.
- Kingma, D. P., & Ba, J. (2015). Adam: A Method for Stochastic Optimization (pp. 1–15). <http://doi.org/http://doi.acm.org.ezproxy.lib.ucf.edu/10.1145/1830483.1830503>
- Krishna, B., Satyajai Rao, Y. R., & Vijaya, T. (2008). Modelling groundwater levels in an urban coastal aquifer using artificial neural networks. *Hydrological Processes*, 22(8), 1180–1188. <http://doi.org/10.1002/hyp.6686>
- Krizhevsky, A., Sutskever, I., & Hinton, G. (2012). ImageNet Classification with Deep Convolutional Neural Networks, 12, 04015009. [http://doi.org/10.1061/\(ASCE\)GT.1943-5606.0001284](http://doi.org/10.1061/(ASCE)GT.1943-5606.0001284)
- Lecun, Y., Bengio, Y., & Hinton, G. (2015). Deep learning. <http://doi.org/10.1038/nature14539>
- Lee, S., An, H., & Yu, S. (2014). Creating an advanced backpropagation neural network toolbox within GIS software, 3111–3128. <http://doi.org/10.1007/s12665-014-3216-7>
- Leube, P. C., Geiges, A., & Nowak, W. (2012). Bayesian assessment of the expected data impact on prediction confidence in optimal sampling design. *Water Resources Research*, 48(2), 1–17. <http://doi.org/10.1029/2010WR010137>
- Li, B., Pales, A. R., Clifford, H. M., Kupis, S., Hennessy, S., Liang, W., ... Darnault, C. J. G. (2018). Preferential flow in the vadose zone and interface dynamics : Impact of microbial exudates. *Journal of Hydrology*, 558, 72–89. <http://doi.org/10.1016/j.jhydrol.2017.12.065>
- Lorenz, D. L., & Delin, G. N. (2007). A regression model to estimate regional ground water recharge. *Ground Water*, 45(2), 196–208. <http://doi.org/10.1111/j.1745-6584.2006.00273.x>
- Lovett, A., & Payne, J. (2014). *Installation of the Waipounamu lysimeter monitoring site , Waimea Plains , Southland.*
- Lubczynski, M. W., & Gurwin, J. (2005). Integration of various data sources for transient groundwater modeling with spatio-temporally variable fluxes - Sardon study case, Spain. *Journal of Hydrology*, 306(1–4), 71–96. <http://doi.org/10.1016/j.jhydrol.2004.08.038>
- Maier, H. R., & Dandy, G. C. (2000). Neural networks for the prediction and forecasting of water resources variables: A review of modelling issues and applications. *Environmental Modelling and Software*, 15(1), 101–124. [http://doi.org/10.1016/S1364-8152\(99\)00007-9](http://doi.org/10.1016/S1364-8152(99)00007-9)
- Mathias, S. A., Sorensen, J. P. R., & Butler, A. P. (2017). Soil moisture data as a constraint for groundwater recharge estimation. *Journal of Hydrology*, 552, 258–266. <http://doi.org/10.1016/j.jhydrol.2017.06.040>
- McKenzie, N. J., & Ryan, P. J. (1999). Spatial prediction of soil properties using environmental correlation. *Geoderma*, 89(1–2), 67–94. [http://doi.org/10.1016/S0016-7061\(98\)00137-2](http://doi.org/10.1016/S0016-7061(98)00137-2)
- McKinney, W. (2010). Pandas: Data Structures for Statistical Computing in Python. In *9th Python in Science Conference* (pp. 51–56). Retrieved from <http://conference.scipy.org/proceedings/scipy2010/mckinney.html>
- McLeod, M., Aislabie, J., McGill, A., Rhodes, P., & Carrick, S. (2014). Leaching of from Stony Soils after Effluent Application. *Journal of Environment Quality*, 43(2), 528. <http://doi.org/10.2134/jeq2013.06.0256>
- Meissner, R., Rupp, H., & Schubert, M. (2000). Novel lysimeter techniques - A basis for the improved investigation of water, gas, and solute transport in soils. *Journal of Plant Nutrition and Soil Science*, 163(6), 603–608. [http://doi.org/10.1002/1522-2624\(200012\)163:6<603::AID-JPLN603>3.0.CO;2-K](http://doi.org/10.1002/1522-2624(200012)163:6<603::AID-JPLN603>3.0.CO;2-K)
- Minns, A. W., & Hall, M. J. (1996). Artificial neural networks as rainfall-runoff models. *Hydrological Sciences Journal*, 41(3), 399–417. <http://doi.org/10.1080/02626669609491511>
- Molz, F. J. (2017). The Amazingly Rapid Birth, Growth, and Maturing of Digital Computer Modeling in Hydrogeology. *Groundwater*, 55(2), 281–285. <http://doi.org/10.1111/gwat.12498>
- Muthusamy, M., Schellart, A., Tait, S., & Heuvelink, G. B. M. (2017). Geostatistical upscaling of rain gauge data to support uncertainty analysis of lumped urban hydrological models. *Hydrology and Earth System*

- Sciences*, 21(2), 1077–1091. <http://doi.org/10.5194/hess-21-1077-2017>
- Nayak, P. C., Satyajji Rao, Y. R., & Sudheer, K. P. (2006). Groundwater level forecasting in a shallow aquifer using artificial neural network approach. *Water Resources Management*, 20(1), 77–90. <http://doi.org/10.1007/s11269-006-4007-z>
- Newsome, P. F. J., Wilde, R. H., & Willoughby, E. J. (2008). Land and resource information system spatial data layers: Data dictionary, 75. <http://doi.org/10.7931/DL1V88>
- Pérez, C. F., Echeverri-Sánchez, A., & Urrutia-Cobo, N. (2015). Aproximación de la recarga de agua subterránea en el norte Estimating groundwater recharge in the geographical valley of the Cauca River , north of the Cauca Department. *Revista Ciencias Técnicas Agropecuarias*, 25(2), 51–57.
- Pérez, F., & Granger, B. (2007). IPython: A System for Interactive Scientific Computing. *Computing In Science & Engineering*, 9, 21–29. <http://doi.org/10.1109/MCSE.2007.53>
- Poeter, E., & Anderson, D. (2005). Multimodel ranking and inference in ground water modeling. *Ground Water*, 43(4), 597–605. <http://doi.org/10.1111/j.1745-6584.2005.0061.x>
- Porhemmat, J., Nakhaei, M., Altafi Dadgar, M., & Biswas, A. (2018). Investigating the effects of irrigation methods on potential groundwater recharge: A case study of semiarid regions in Iran. *Journal of Hydrology*, 565(August), 455–466. <http://doi.org/10.1016/j.jhydrol.2018.08.036>
- Qin, D., Qian, Y., Han, L., Wang, Z., Li, C., & Zhao, Z. (2011). Assessing impact of irrigation water on groundwater recharge and quality in arid environment using CFCs, tritium and stable isotopes, in the Zhangye Basin, Northwest China. *Journal of Hydrology*, 405(1–2), 194–208. <http://doi.org/10.1016/j.jhydrol.2011.05.023>
- Ramirez, B., Solarte, V., & Ramírez, P. (2018). Mosses of the dry valley of Patía , southwestern Colombia : Richness , ecology and biogeography. *Biota Colombiana*, 19(2), 2–11. <http://doi.org/10.21068/c2018.v19n02a01>
- Refsgaard, J., R, J., AL, H., AL, H., AJ, Z., K, R., ... Morén I. (2016). *Upscaling methodologies*. Copenhagen. Retrieved from [www.Soils2Sea.eu](http://www.Soils2Sea.eu)
- Reszler, C., & Fank, J. (2016). Unsaturated zone flow and solute transport modelling with MIKE SHE: model test and parameter sensitivity analysis using lysimeter data. *Environmental Earth Sciences*, 75(3), 1–13. <http://doi.org/10.1007/s12665-015-4881-x>
- Rowan, A. (2017). Bayesian Deep Learning with Edward (and a trick using Dropout). In *PyData*. London, England. Retrieved from <https://pydata.org/london2017/schedule/presentation/33/>
- Scanlon, B. R., Reedy, R. C., Stonestrom, D. A., Prudic, D. E., & Dennehy, K. F. (2005). Impact of land use and land cover change on groundwater recharge and quality in the southwestern US. *Global Change Biology*, 11(10), 1577–1593. <http://doi.org/10.1111/j.1365-2486.2005.01026.x>
- Scott, D. (2004). *Groundwater allocation limits: land-based recharge estimates* (Vol. U04/97). Christchurch, New Zealand. Retrieved from [www.ecan.govt.nz](http://www.ecan.govt.nz)
- Siebert, S., Burke, J., Faures, J. M., Frenken, K., Hoogeveen, J., Döll, P., & Portmann, F. T. (2010). Groundwater use for irrigation - A global inventory. *Hydrology and Earth System Sciences*, 14(10), 1863–1880. <http://doi.org/10.5194/hess-14-1863-2010>
- Simunek, J., Jarvis, N., van Genuchten, M. T., & Gardenas, A. (2003). Review and comparison of models for describing non-equilibrium and preferential flow and transport in the vadose zone, 272, 14–35. [http://doi.org/10.1016/S0022-1694\(02\)00252-4](http://doi.org/10.1016/S0022-1694(02)00252-4)
- Singh, S., Jain, S., & Bárdossy, A. (2014). Training of Artificial Neural Networks Using Information-Rich Data. *Hydrology*, 1(1), 40–62. <http://doi.org/10.3390/hydrology1010040>
- Singh, S. K., Zeddies, M., Shankar, U., & Griffiths, G. A. (2018). Potential groundwater recharge zones within New Zealand. *Geoscience Frontiers*, 1–9. <http://doi.org/10.1016/j.gsf.2018.05.018>
- Sophocleous, M. (1992). Groundwater recharge estimation and regionalization: the Great Bend Prairie of central Kansas and its recharge statistics. *Journal of Hydrology*, 137(1–4), 113–140.

- [http://doi.org/10.1016/0022-1694\(92\)90051-V](http://doi.org/10.1016/0022-1694(92)90051-V)
- Sophocleous, M. (2012). On Understanding and Predicting Groundwater Response Time. *Ground Water*, 50(4), 528–540. <http://doi.org/10.1111/j.1745-6584.2011.00876.x>
- Sorensen, J. P. R., Finch, J. W., Ireson, A. M., & Jackson, C. R. (2014). Comparison of varied complexity models simulating recharge at the field scale. *Hydrological Processes*, 28(4), 2091–2102. <http://doi.org/10.1002/hyp.9752>
- Srivastava, N., Hinton, G., Krizhevsky, A., Sutskever, I., & Salakhutdinov, R. (2014). Dropout: A Simple Way to Prevent Neural Networks from Overfitting. *Journal of Machine Learning Research*, 15, 1929–1958. <http://doi.org/10.1214/12-AOS1000>
- Stoffregen, H., Yaramanci, U., Zenker, T., & Wessolek, G. (2002). Accuracy of soil water content measurements using ground penetrating radar: comparison of ground penetrating radar and lysimeter data. *Journal of Hydrology*, 267, 201–206. [http://doi.org/10.1016/S0022-1694\(02\)00150-6](http://doi.org/10.1016/S0022-1694(02)00150-6)
- USDA. (2014). Soil Infiltration (Soil Health-Guide For Educator).
- van der Walt, S., Colbert, C., & Varoquax, G. (2011). The NumPy array: a structure for efficient numerical computation. *Computing In Science & Engineering*, 13(2), 22–30.
- van Leeuwen, B. (2012). *Artificial neural networks and geographic information systems for inland excess water classification*.
- Vergara Varela, H. (2015). Vegetation patterns and land use types in the Patia valley, 18(1), 25–45. <http://doi.org/10.14483/udistrital.jour.colomb.for.2015.1.a02>
- Wang, T., Franz, T. E., Yue, W., Szilagyi, J., Zlotnik, V. A., You, J., ... Young, A. (2016). Feasibility analysis of using inverse modeling for estimating natural groundwater recharge from a large-scale soil moisture monitoring network. *JOURNAL OF HYDROLOGY*, 533, 250–265. <http://doi.org/10.1016/j.jhydrol.2015.12.019>
- Weaver, L., Karki, N., Mackenzie, M., Sinton, L., Wood, D., Flintoft, M., ... Close, M. (2016). Microbial transport into groundwater from irrigation: Comparison of two irrigation practices in New Zealand. *Science of the Total Environment*, 543, 83–94. <http://doi.org/10.1016/j.scitotenv.2015.09.075>
- Webster, R., & Oliver, M. A. (2007). *Geostatistics for environmental scientists* (Second Edi). John Wiley & Sons, Ltd, West Sussex, England.
- Wegehenkel, M., Zhang, Y., Zenker, T., & Diestel, H. (2008). The use of lysimeter data for the test of two soil-water balance models: A case study. *Journal of Plant Nutrition and Soil Science*, 171(5), 762–776. <http://doi.org/10.1002/jpln.200700244>
- Weibull, W. (1939). A statistical study of the strength of material. *Ing. Vetenskaps Akad*, 151, 15.
- Westerhoff, R., White, P., & Rawlinson, Z. (2018). Incorporation of satellite data and uncertainty in a nationwide groundwater recharge model in New Zealand. *Remote Sensing*, 10(1), 1–25. <http://doi.org/10.3390/rs10010058>
- White, P. A., Hong, Y. S., Murray, D. L., Scott, D. M., & Thorpe, H. R. (2003). Evaluation of regional models of rainfall recharge to groundwater by comparison with lysimeter measurements, Canterbury, New Zealand. *Journal of Hydrology New Zealand*.
- Wohling, D. L., Leaney, F. W., & Crosbie, R. S. (2012). Deep drainage estimates using multiple linear regression with percent clay content and rainfall. *Hydrology and Earth System Sciences*, 16(2), 563–572. <http://doi.org/10.5194/hess-16-563-2012>
- Wong, W. K., Xia, M., & Chu, W. C. (2010). Adaptive neural network model for time-series forecasting. *European Journal of Operational Research*, 207(2), 807–816. <http://doi.org/10.1016/j.ejor.2010.05.022>
- Xu, C. Y., & Chen, D. (2005). Comparison of seven models for estimation of evapotranspiration and groundwater recharge using lysimeter measurement data in Germany. *Hydrological Processes*, 19(18), 3717–3734. <http://doi.org/10.1002/hyp.5853>
- Yoon, H., Jun, S. C., Hyun, Y., Bae, G. O., & Lee, K. K. (2011). A comparative study of artificial neural

- networks and support vector machines for predicting groundwater levels in a coastal aquifer. *Journal of Hydrology*, 396(1–2), 128–138. <http://doi.org/10.1016/j.jhydrol.2010.11.002>
- Zaidel, J., Markham, B., & Bleiker, D. (2010). Simulating seepage into mine shafts and tunnels with MODFLOW. *Ground Water*, 48(3), 390–400. <http://doi.org/10.1111/j.1745-6584.2009.00659.x>
- Zeng, X., Wu, J., Wang, D., Zhu, X., & Long, Y. (2016). Assessing Bayesian model averaging uncertainty of groundwater modeling based on information entropy method. *Journal of Hydrology*, 538, 689–704. <http://doi.org/10.1016/j.jhydrol.2016.04.038>
- Zhang, G. P., & Qi, M. (2005). Neural network forecasting for seasonal and trend time series. *European Journal of Operational Research*, 160(2), 501–514. <http://doi.org/10.1016/j.ejor.2003.08.037>
- Zhang, L., Heerink, N., Dries, L., & Shi, X. (2013). Water users associations and irrigation water productivity in Northern China. *Ecological Economics*, 95, 128–136. <http://doi.org/10.1016/j.ecolecon.2013.08.014>
- Zhu, J., & Mohanty, B. P. (2002). Upscaling of soil hydraulic properties for steady state evaporation and infiltration. *Water Resources Research*, 38(9), 17-1-17–13. <http://doi.org/10.1029/2001WR000704>
- Zirlewagen, D., & Von Wilpert, K. (2010). Upscaling of environmental information: Support of land-use management decisions by spatio-temporal regionalization approaches. *Environmental Management*, 46(6), 878–893. <http://doi.org/10.1007/s00267-010-9468-4>
- Zirlewagen, D., & Wilpert, K. (2004). Using model scenarios to predict and evaluate forest-management impacts on soil base saturation at landscape level. *European Journal of Forest Research*, 123(4), 269–282. <http://doi.org/10.1007/s10342-004-0039-1>